

UNIVERSITY OF ALBERTA

**Extent of Dolomite Recrystallization along the Rimbey-
Meadowbrook Reef Trend, Western Canada Sedimentary Basin,
Alberta, Canada**

by

Erinn Kathleen Horrigan



A thesis submitted to the Faculty of Graduate Studies and Research in partial fulfillment of the requirements for the degree of Master of Science.

DEPARTMENT OF EARTH AND ATMOSPHERIC SCIENCES

Edmonton, Alberta
Fall 1996



National Library
of Canada

Acquisitions and
Bibliographic Services Branch

395 Wellington Street
Ottawa, Ontario
K1A 0N4

Bibliothèque nationale
du Canada

Direction des acquisitions et
des services bibliographiques

395, rue Wellington
Ottawa (Ontario)
K1A 0N4

Your file Votre référence

Our file Notre référence

The author has granted an irrevocable non-exclusive licence allowing the National Library of Canada to reproduce, loan, distribute or sell copies of his/her thesis by any means and in any form or format, making this thesis available to interested persons.

L'auteur a accordé une licence irrévocable et non exclusive permettant à la Bibliothèque nationale du Canada de reproduire, prêter, distribuer ou vendre des copies de sa thèse de quelque manière et sous quelque forme que ce soit pour mettre des exemplaires de cette thèse à la disposition des personnes intéressées.

The author retains ownership of the copyright in his/her thesis. Neither the thesis nor substantial extracts from it may be printed or otherwise reproduced without his/her permission.

L'auteur conserve la propriété du droit d'auteur qui protège sa thèse. Ni la thèse ni des extraits substantiels de celle-ci ne doivent être imprimés ou autrement reproduits sans son autorisation.

ISBN 0-612-18273-8

Canada

UNIVERSITY OF ALBERTA

Library Release Form

Name of Author: **Erinn Kathleen Horrigan**

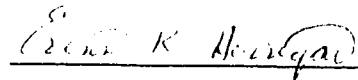
Title of Thesis: **Extent of Dolomite Recrystallization along the Rimbey-Meadowbrook Reef Trend, Western Canada Sedimentary Basin, Alberta, Canada.**

Degree: **Master of Science**

Year This Degree Granted: **1996**

Permission is hereby granted to the University of Alberta Library to reproduce single copies of this thesis and to lend or sell such copies for private, scholarly, or scientific research purposes only.

The author reserves all other publication and other rights in association with the copyright in the thesis, and except as herinbefore provided, neither the thesis nor any substantial portion thereof may be printed or otherwise reproduced in any material form whatever without the author's prior written permission.



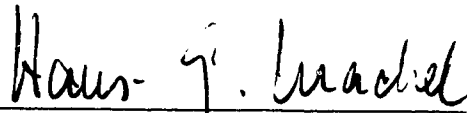
Erinn K. Horrigan
23 Thackeray Road
Wellesley, Massachusetts
02181
United States of America

Date: 15th October 1996

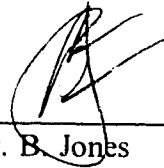
UNIVERSITY OF ALBERTA

Faculty of Graduate Studies and Research

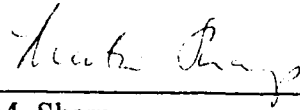
The undersigned certify that they have read, and recommend to the Faculty of Graduate Studies and Research for acceptance, a thesis entitled "**Extent of Recrystallization along the Rimbey-Meadowbrook Reef Trend, Western Canada Sedimentary Basin, Alberta, Canada**" by **Erinn Kathleen Horrigan** in partial fulfillment of the requirements for the degree of **Master of Science**.



Dr. H. G. Machel (Supervisor)



Dr. B. Jones



Dr. M. Sharp

Date: 15th October 1996

ABSTRACT

Dolomite formed by burial replacement is often not affected by later "significant" structural, textural, or chemical changes from dolomite recrystallization, whereby "significant" is "a modification via recrystallization of the original isotope composition that is larger than the original range." The pervasively dolomitized Upper Devonian Rimbey-Meadowbrook Reef Trend is one example of burial dolomitization where the extent and effects of matrix dolomite recrystallization are suggested to be minor. The objectives of this study are to identify the existence of dolomite recrystallization along a selected interval of the Rimbey-Meadowbrook Reef Trend through geochemical and petrographic techniques.

Petrography and stable isotope chemistry of matrix dolomites along the southwest dipping reef trend identified several dolomite samples that may have been "significantly recrystallized." Only one matrix dolomite sample is suggested to be "significantly recrystallized," exhibiting a relatively depleted stable isotope ($\delta^{18}\text{O}$) value of -9.9‰ PDB, with respect to the rest of the matrix dolomites in this study which range between -5.3 and -6.7 ‰ PDB $\delta^{18}\text{O}$. Ostwald-ripening may have occurred in the deep southwest of the reef trend and the northeast Morinville reef, possibly "significantly recrystallizing" fine grained (R1) dolomite textures to coarser grained (R3) dolomite textures. Petrographic analysis identified some dolomitized echinoderm fragments also possibly "significantly recrystallized" through Ostwald-ripening, exhibiting bimodal crystal fragments. Although "significant recrystallization" may have affected the chemistry of at least one sample, the textures of about fifteen matrix samples, and the sparse echinoderms, it is suggested to be a minor event, and not *extensive* in the reef trend.

ACKNOWLEDGEMENTS

The author wishes to thank the following people for their help and encouragement with this project. I would like to thank AMOCO Canada for awarding me the Graduate Student Fellowship which supplied two years of funding. Thank you also to Hans Machel for the thesis project and supervision, as well as funding. Special thanks go to Pat Cavell for her assistance with sample preparation, radiogenic strontium analysis, thesis editing, clarification of ideas, and general support. Thank you to Diane Caird, Bob Davidson, George Baybrook, and Brad Gorham for their assistance with sample analyses. I would like to acknowledge the Faculty of Graduate Studies and Research and the Vice-President (Research) for supplying travel assistance to the 1995 Annual GSA conference through the Mary Louise Imrie Graduate Student Award. Thanks to Don Resultay for thin section preparation, and Qiang Ning for the use of hand samples and thin sections from his own thesis. I would like to thank Karlis Muhlenbachs for the use of the geochemistry laboratory, and Rob Creaser for the use of the clean lab and radiogenic isotope facility. I would also like to thank Eric Mountjoy as well as Matthias Grobe and Mark Hearn for many useful discussions. And I would like to give special thanks to Steve Grant for always listening.

TABLE OF CONTENTS

CHAPTER 1: Introduction and Objectives	1
Introduction	1
Definitions	6
Objectives	8
CHAPTER 2: Geologic Setting and Background Information	10
Geologic setting	10
Diagenetic regime and paragenetic sequence	13
Matrix dolomite types and lithofacies	14
General hydrogeologic regime	19
CHAPTER 3: Dolomite Diagenesis	22
Replacement dolomitization	22
Echinoderm fragments	24
Recrystallization	25
CHAPTER 4: Methods	27
Sample Selection and Preparation	27
Petrography	30
X-ray diffraction	31
Major and trace element analysis	34
Stable isotope analysis	35
Radiogenic strontium analysis	35
CHAPTER 5: Petrographic Observations	36
Matrix	36
Matrix R1	36
Matrix R2	42
Matrix R3	45
Matrix R4	45
Cathodoluminescent properties	45
Matrix R1 zoning	45
Partial dolomite replacement of calcite cement	50
Biochems	50
General observations	50
Echinoderm fragments	53
CHAPTER 6: Chemistry Results and Discussion	63
X-ray diffraction data	63
Unit cell parameters	63
Cation ordering	63
Major elements, magnesium and calcium	68
Trace elements	69
Aluminum and silica	69

Iron	76
Manganese	76
Rubidium and Strontium, Rubidium	79
Strontium	80
Stable isotopes, $\delta^{13}\text{C}$	83
$\delta^{18}\text{O}$	87
Radiogenic strontium isotopes	88
CHAPTER 7: Extent of Dolomite Recrystallization in the Reef Trend	94
Petrographic trend	94
Geochemical trends	100
Inter-matrix type variations	100
Variations with location	105
Bimodal Crystal Echinoderm Fragments	106
Possible Fluid Sources	108
Matrix	108
Echinoderm fragments	109
CHAPTER 8: Conclusions	110
REFERENCES	112
APPENDIX A	124
APPENDIX B	134
APPENDIX C	135
APPENDIX D	136

LIST OF TABLES

TABLE 1	Location of wells and thin sections studied	29
TABLE 2	X-ray diffraction data	64 to 65
TABLE 3	Selected major and trace element data	70 to 73
TABLE 4	Stable and radiogenic isotope data	84
TABLE A1	ICP-MS running conditions	125
TABLE A2	ICP-MS external and internal standard compositions	126 to 127
TABLE A3	Complete major and trace element results	128 to 133

LIST OF FIGURES

FIGURE 1	General location map of study area	3
FIGURE 2	Township and range location map of study area	5
FIGURE 3	Burial history of the Rimbey-Meadowbrook Reef Trend	9
FIGURE 4	Upper Devonian stratigraphic sequence	11
FIGURE 5	Previous paragenetic sequence	16
FIGURE 6	Previous illustration of dolomite matrix types	18
FIGURE 7	Illustration of oil migration in reef trend	21
FIGURE 8	Compilation of isotopic data from previous studies of the reef trend	28
FIGURE 9	Township and range location map of selected samples	38
FIGURE 10	Revised illustration of dolomite matrix types	41
FIGURE 11	Plot of unit cell parameters a_0 and c_0 for all matrix types	67
FIGURE 12	Plot of major elements Ca and Mg	67
FIGURE 13	Plot of trace elements Al and Si	75
FIGURE 14	A. Plot of trace elements Fe and Al, B. Plot of trace elements Fe and Si	75 78
FIGURE 15	Plot of trace elements Fe and Mn	78
FIGURE 16	A. Plot of trace elements Rb and Sr, B. Plot of trace elements Rb and Si	82
FIGURE 17	Plot of $\delta^{13}\text{C}$ and $\delta^{18}\text{O}$ for dolomites of matrix types R1 and R2	86
FIGURE 18	$\delta^{13}\text{C}$ variations during organic matter diagenesis	86
FIGURE 19	Plot of radiogenic strontium isotopes and $\delta^{18}\text{O}$	90
FIGURE 20	Plot of radiogenic strontium isotopes and trace element Rb	90
FIGURE 21	Plot of radiogenic strontium isotopes and trace element Sr	93
FIGURE 22	Map of matrix type abundances along the reef trend	96
FIGURE 23	Illustration of Cl mottled textures	99
FIGURE 24	Revised burial history	102
FIGURE 25	Revised paragenetic sequence	104

LIST OF PLATES

PLATE 1	Photomicrograph illustrations of typical Matrix R1	40
PLATE 2	Photomicrograph illustrations of typical Matrix R2	44
PLATE 3	Photomicrograph illustrations of typical Matrix R3	47
PLATE 4	Photomicrograph illustrations of typical Matrix R4	49
PLATE 5	Photomicrograph illustration of partially dolomitized limestones	52
PLATE 6	Photomicrograph illustrations of echinoderm fragments	55
PLATE 7	Photomicrograph illustrations of echinoderm fragments	57
PLATE 8	SEM photomicrograph of echinoderm fragment	59
PLATE 9	Photomicrograph illustration of stylolites adjacent to echinoderm fragments	61

CHAPTER ONE

INTRODUCTION AND OBJECTIVES

INTRODUCTION

This study attempts to determine the extent of dolomite neomorphism / recrystallization along one depth interval of the deeply buried Rimbey-Meadowbrook Reef Trend which may have resulted from variations in paleo fluid flow patterns and compositions. The process of dolomite neomorphism / recrystallization is important because it may have affected the porosity, permeability, and, hence, the oil- and gas-bearing potential of this reef trend (Figures 1 and 2). Understanding this process will aid the understanding of reservoir development.

The exact timing and fluid sources affecting the Rimbey-Meadowbrook Reef Trend during burial replacement dolomitization and later dolomite neomorphism / recrystallization are the subjects of continuing discussions, despite numerous prior studies of this reef trend. Also under discussion are the total extent and timing of subsequent dolomite diagenesis including neomorphism and/or recrystallization and its effects on the dolomite crystallography, porosity and permeability of the reef trend.

For this study, which is focused primarily on neomorphism / recrystallization of the dolomitized reef trend, the definitions of the terms replacement, neomorphism, and recrystallization are particularly important. Replacement involves major element and mineralogic changes such as CaCO_3 (calcite) to $\text{CaMg}(\text{CO}_3)_2$ (dolomite) or $\text{CaMg}(\text{CO}_3)_2$ (dolomite) to $\text{Ca}(\text{MgFe})(\text{CO}_3)_2$ (ankerite). Neomorphism as defined by Folk (1964, 1965) is the process of minor chemical and crystal size change through inversion, recrystallization, and strain-recrystallization of sedimentary carbonate crystals. Sibley and Gregg (1987), and Sibley (1990) further defined neomorphism as a transformation from nonstoichiometric to stoichiometric dolomite, with an associated increase in crystal size, through a dissolution-reprecipitation process, *i.e.*, in the presence of fluids. In the case of the neomorphism of an unordered or calcian dolomite to an ordered dolomite,

Figure 1. Generalized location map of the study area with respect to Canada, Alberta, and latitude and longitude. The enclosed study area contains the dolomitized Rimbey-Meadowbrook Reef Trend.

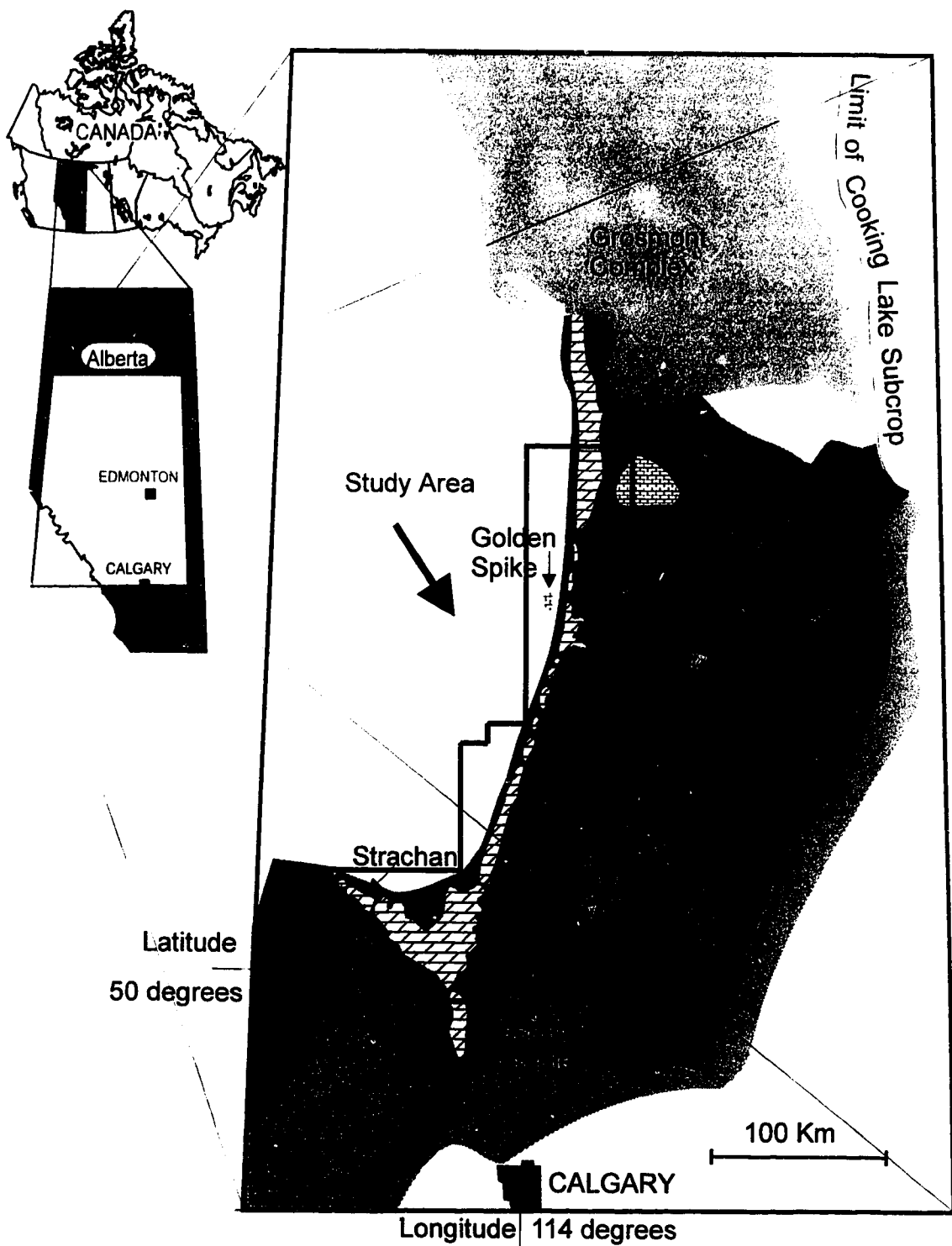
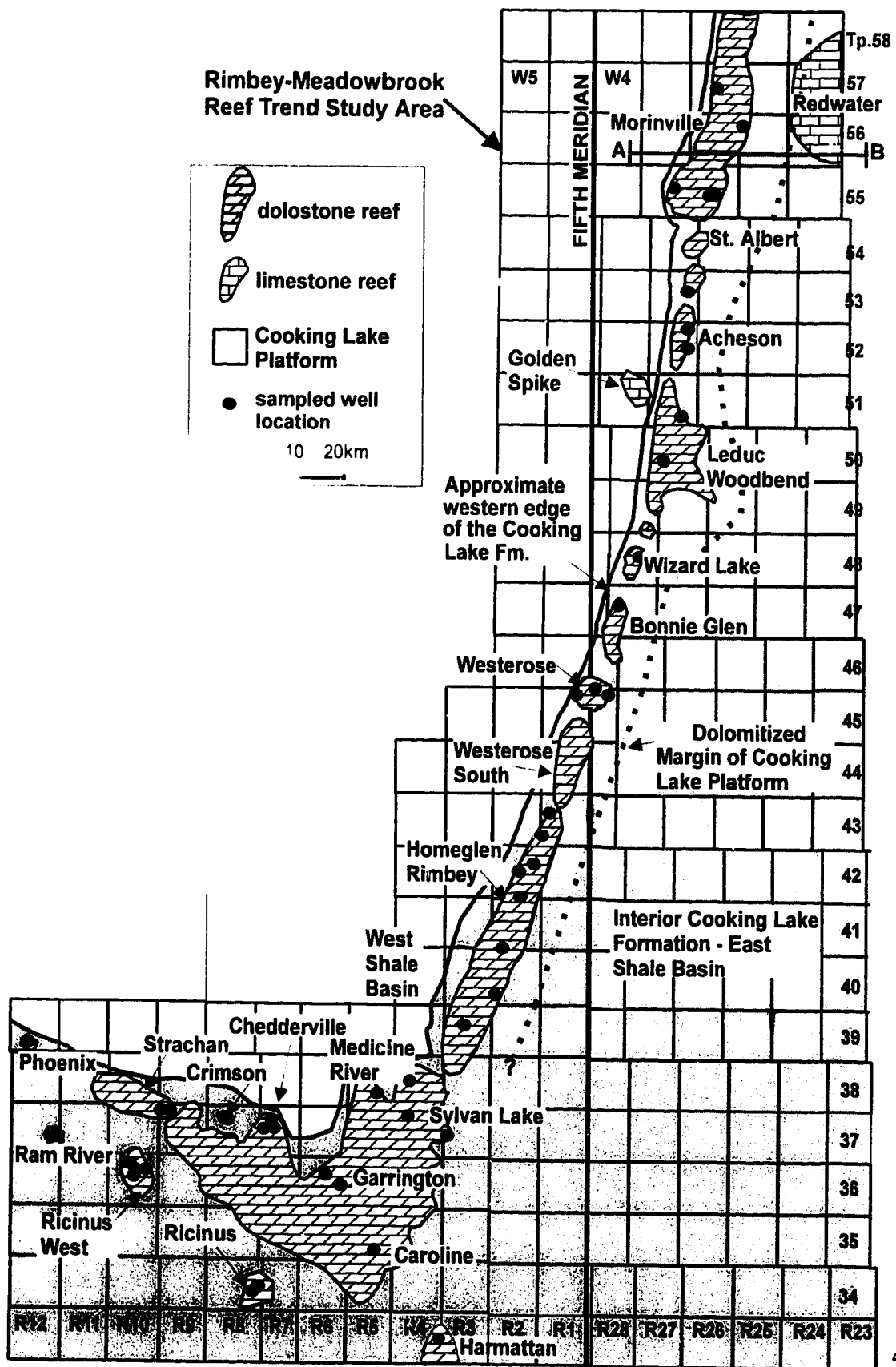


Figure 2. Township and range map of study area. The black circles represent sampled well locations with either one, two, or three samples per core. The number of samples per core is indicated in Table 1. Line A-B at the north end is the location of cross section Figure 4. Tp. = township, R = range.



neomorphism may then also include a mineralogic change (Sibley and Gregg 1987), similar to the term replacement. In contrast, Sibley and Gregg (1987), and Sibley (1990) define recrystallization as a chemical and textural, but non-mineralogic dolomite transformation in the presence of fluids. For the purposes of this study, which focuses on the minor, non-mineralogic, modification of burial dolomite resulting from temperature, fluid chemistry, and pressure variations, "recrystallization" is redefined within the parameters of common usage in sedimentary, igneous, and metamorphic geology, as follows.

Definitions

"Recrystallization" involves the breaking down and reforming of chemical bonds, without a mineralogical change, in the presence of fluids, to cause one or more of the following;

structural change, e.g., the change from poorly ordered to well ordered, or nonstoichiometric to stoichiometric;

trace element and/or isotopic chemical change, e.g., the change of a strontium concentration from >600 ppm to <200 ppm (Land 1980, Banner 1995), or the enrichment or depletion of $\delta^{13}\text{C}$ values (Malone *et al.* 1994);

textural change, most commonly the change from fine crystal size to coarse crystal size, e.g., Ostwald-ripening, or change from planar to nonplanar textures (Gregg and Sibley 1984, Sibley and Gregg 1987).

Recrystallization occurs in the presence of a fluid through a dissolution-reprecipitation process (Sibley and Gregg 1987, and Sibley 1990).

Establishing that recrystallization has occurred then requires that the extent of structural, chemical, and textural changes be significant enough to be detectable through geochemical and petrographic techniques. A new term, "significant recrystallization" has been coined by Machel *et al.* (1996) and is defined as follows.

"Significant recrystallization," is defined by Machel *et al.* (1996) as "a modification via recrystallization of the original isotope composition that is larger than

the original range." In other words, it requires that the isotopic and trace element alteration is sufficient to change the geochemical signature (greater than the error of the applied method) of the affected dolomite to represent the composition and timing of the dolomite recrystallization fluids (the term "significant recrystallization" is thus used as defined in Machel *et al.*, 1996). In keeping with the above redefinition of recrystallization, textural change is also added to the list of requirements for "significant recrystallization," *e.g.*, a dolomite sample can be classified as "significantly recrystallized" where either a chemical change, Ostwald-ripening, or both are recognized. Conversely, recrystallization is deemed "*insignificant*" "if the extent of isotopic and trace element alteration was so small that the geochemical signature of these rocks is still representative of the dolomitizing fluids," as defined by Machel *et al.* (1996).

There are specific driving forces for recrystallization. These include (1) the thermodynamic drive with elevated temperature and pressure to form stable crystals, *i.e.*, poorly ordered and nonstoichiometric to well ordered and stoichiometric; this drive is common for 'protodolomite' diagenesis (Land 1985, Sibley and Gregg 1987, Gao and Land 1991, Malone *et al.* 1994); (2) pressure-induced crystal strain resulting in crystal growth (strain-recrystallization) (Folk 1965); and (3) significant changes in trace element and isotopic fluid compositions compared to the fluids present during original dolomite formation (Land 1980, Gregg *et al.* 1992, Montanez and Read 1992, Banner 1995).

The process of dolomite recrystallization in the Rimbey-Meadowbrook Reef Trend during burial diagenesis was considered by Drivet (1993), Amthor *et al.* (1993), and Mountjoy and Amthor (1994). These authors derived the preliminary interpretation that recrystallization is not a fully recognizable process and it is probably not widespread in the Rimbey-Meadowbrook Reef Trend. If recrystallization is more widespread than has been previously identified, then the conditions for the initial replacement dolomitization may have been obscured and/or obliterated (Land 1980, Land 1985, Gregg and Shelton 1990, Gao and Land 1991, Montanez and Read 1992, Malone *et al.* 1994).

Most of the matrix dolomite of this reef trend are seemingly indistinguishable petrographically and geochemically from one end of the trend to the other (Machel and

Mountjoy 1987, Amthor *et al.* 1993, Drivet 1993, Marquez 1994, Mountjoy and Amthor 1994). It is this uniformity of the reef trend dolostones that has led to the preliminary suggestions that recrystallization, if it has occurred in the reef trend, is "minor" (Amthor *et al.* 1993, Drivet 1993, Marquez 1994, Mountjoy and Amthor 1994), *i.e.*, "insignificant" as defined above.

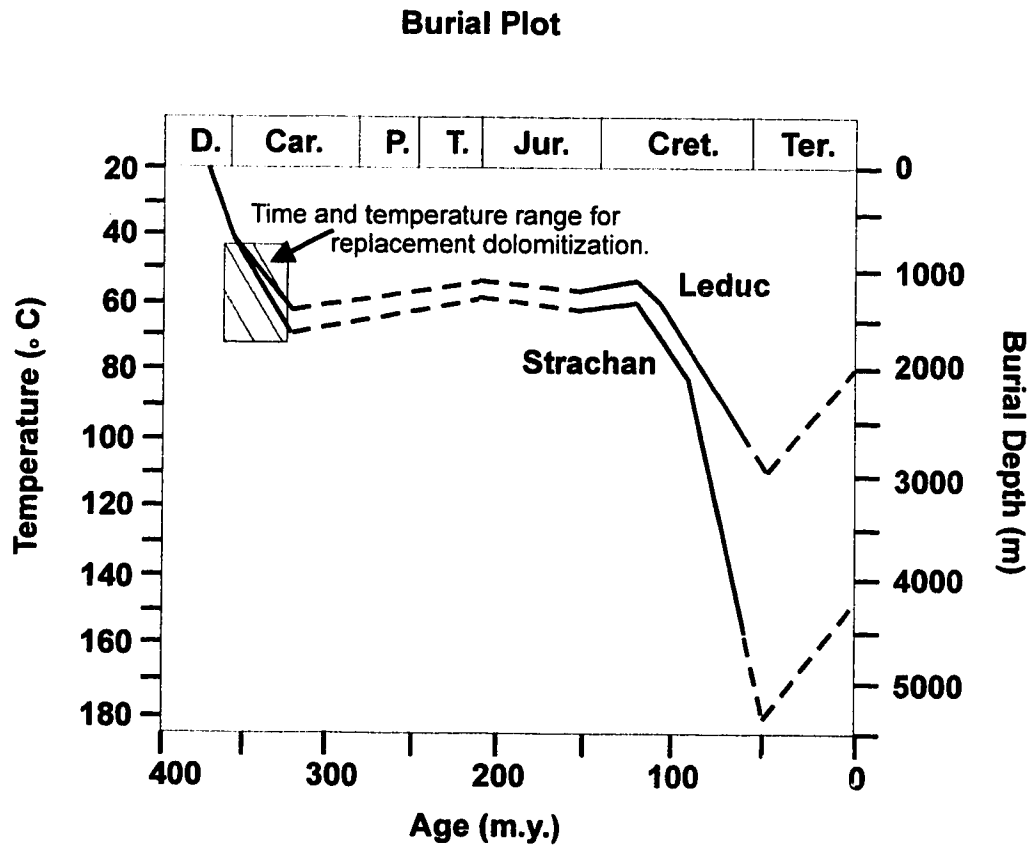
OBJECTIVES

Previous studies on the Rimbey-Meadowbrook Reef Trend have interpreted the petrographic and geochemical data to indicate that dolomite recrystallization has not "significantly" affected the reef trend. The main objective of this study is to identify evidence of dolomite recrystallization along a selected interval of the Rimbey-Meadowbrook Reef Trend. Evidence of dolomite recrystallization is determined using petrographic and geochemical techniques, with the ultimate goal of finding criteria that can be successfully used to identify dolomite recrystallization.

Matrix dolomite is the first dolomite phase and the most abundant dolomite type in the reef trend. If reef trend dolomite is pervasively recrystallized, the indicators of this diagenetic process will be found in matrix dolomite samples because of their abundance and relatively early position in the burial history (Figure 3). Analysis of matrix dolomites of the reef trend by thin section transmitted light petrography, cathodoluminescence, blue-light epifluorescence microscopy, X-ray diffraction analysis, trace element geochemistry, stable isotope geochemistry, and strontium isotope geochemistry should reveal possible indicators of dolomite recrystallization.

In the event that the above criteria, data, and methods show that at least some of the matrix dolomites of the Rimbey-Meadowbrook Reef Trend are "significantly recrystallized" (which does not necessarily imply extensive recrystallization along the reef trend), logic dictates that their geochemical compositions would be representative of dolomite recrystallization fluid compositions and timing, rather than replacement dolomitization fluids. Previous interpretations of dolomitization for the reef trend would then have to be reevaluated to incorporate recrystallization into its diagenetic history.

Figure 3. Burial history diagram for the Rimbey-Meadowbrook Reef Trend. The two curves represent the shallow northeast (Leduc) and the deep southwest (Strachan) areas of the reef trend. Included is the interpreted time and temperature range for replacement dolomitization. Based on Amthor *et al.* (1993) and Marquez (1994). Assumed 30°C/Km geothermal gradient.



CHAPTER TWO

GEOLOGIC SETTING AND BACKGROUND INFORMATION

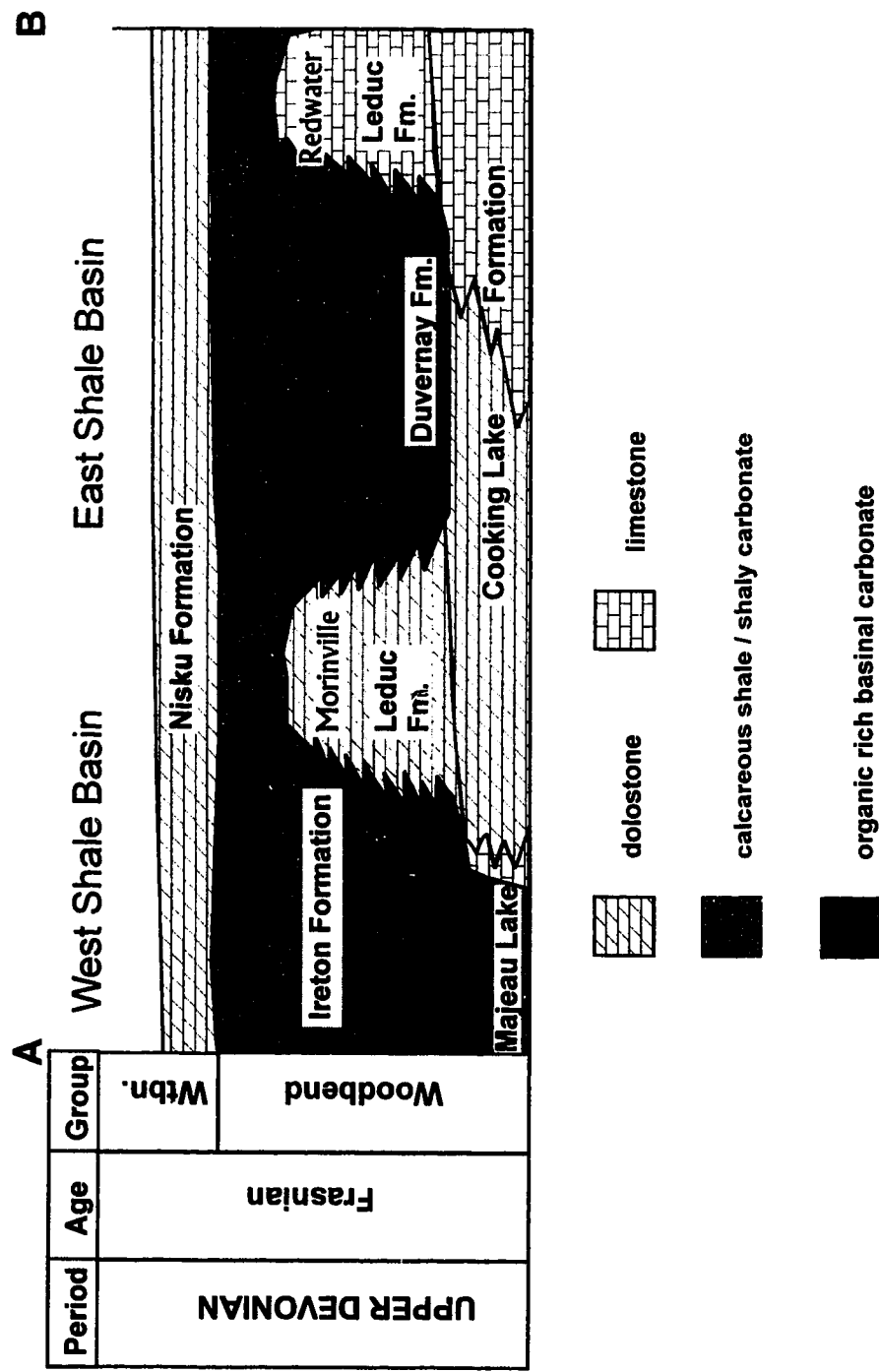
GEOLOGIC SETTING

The dolomitized Upper Devonian Rimbey-Meadowbrook Reef Trend extends for about 560 km in the subsurface of Alberta from the NE near Athabasca slightly dipping 1° to the southwest towards the Canadian Rockies (Figures 1 and 2) (Drivet 1993, Switzer *et al.* 1994). The reef trend is part of the Upper Devonian, Frasnian, Leduc Formation in the Woodbend Group and lies on top of Cooking Lake Platform carbonates (Figure 4) (Allan and Creaney 1991, Weissenberger 1994). The sedimentary rocks that comprise the Woodbend Group were deposited in the Western Canada Sedimentary Basin at a time when epeirogenic seas dominated the cratonic platform (Porter *et al.* 1982, Wright *et al.* 1994). During Frasnian time, Alberta was at a latitude of about 30°N in a subtropical climate (Moore 1989).

The Upper Devonian Woodbend Group contains about 32% of initial established conventional oil and gas in place in Alberta, with the Rimbey-Meadowbrook Reef Trend containing $577.4 \times 10^6 \text{ m}^3$ oil in place and $238,713 \times 10^6 \text{ m}^3$ gas in place (Switzer *et al.* 1994). The study of reef facies and diagenesis was originally undertaken by Andrichuk (1958) in order to gain understanding of this huge play, and to use the knowledge obtained towards the interpretation of similar potential reservoirs elsewhere in the Alberta Basin. Previous studies concentrated on oil migration and entrapment (Gussow 1968, Stoakes and Creaney 1985, Allan and Creaney 1991, Marquez 1994), facies analysis (Andrichuk 1958, McNamara and Wardlaw 1991, Drivet 1993, Weissenberger 1994, Wendte 1994), reef inception (Andrichuk 1958, Wendte 1994), diagenesis (Illing 1959), and porosity and permeability development (Andrichuk 1958, Drivet 1993, Amthor *et al.* 1993, Amthor *et al.* 1994, Marquez 1994, Mountjoy and Amthor 1994).

The Rimbey-Meadowbrook Reef Trend developed on carbonate shoals of an underlying shallow water platform, the Cooking Lake Platform (Wendte 1994, Weissenberger 1994). The reef trend was probably formed as the result of a relative sea

Figure 4. Schematic cross section and stratigraphic sequence of the Woodbend Group and Lower Winterburn Group (Wtbn.) in the Alberta Basin. Location of cross section is shown on Figure 2.



level rise, which also allowed the development of deep basins surrounding the reefs (Moore 1989, Wendte 1994, Weissenberger 1994).

As the reefs began to grow, forming the lower Leduc Formation of the reef trend, argillaceous carbonates of the basinal Duvernay Formation were deposited on portions of the underlying Cooking Lake Platform not covered by reefs. During the growth of upper Leduc Formation reef facies, the calcareous shales of the Ireton Formation were deposited off reef, covering first the Duvernay Formation, and eventually the Leduc Formation reefs during a drowning due to relative sea level rise (Moore 1989, Wendte 1994, Weissenberger 1994). The reefs reached a thickness of about 275m (Switzer *et al.* 1994).

During the Upper Devonian, the Nisku Formation and Camrose Member of the Winterburn Group were deposited on top of the Ireton Formation marls and shales. This Group is Frasnian in age, and is comprised of carbonate platform deposits and marly-shale slope deposits, with coeval silty marls and mud outer shelf deposits. The sedimentary rocks of this Group indicate a relative sea level fall followed by a gradual relative sea level rise (Machel and Anderson 1989, Switzer *et al.* 1994). The Winterburn Group is, in turn, overlain by the Upper Devonian Wabamun Group of Famennian age, which is comprised of a series of stacked ramp and shelf fossiliferous carbonates and associated evaporites (Halbertsma 1994).

The pervasively dolomitized Rimbey-Meadowbrook Reef Trend directly overlies the partially dolomitized Cooking Lake Platform and carbonate shoals (Wente 1994). The western edge of the Cooking Lake Platform lies 2 to 10 km to the west of the reef trend (Figures 1 and 2) (Switzer *et al.* 1994). To the east of the reef trend the Cooking Lake Platform decreases in thickness and extends at least 150 km underlying the East Shale Basin. The dolomite content of the Cooking Lake Platform decreases significantly to the east and west of the reef trend, and is confined to the upper layers of the Cooking Lake Platform (Figure 4) (Andrichuk 1958, Machel and Mountjoy 1987, Switzer *et al.* 1994).

The Western Canada Sedimentary Basin developed as a foreland basin in two stages, Middle Jurassic to Early Cretaceous and Late Cretaceous to Eocene, when a wedge of imbricate thrust sheets formed on the supracrustal cover as a result of two oceanic collisions. These collisions created the Rocky Mountain foreland basin by isostatic

flexure and rapid deposition of clastic detritus from the thrust belt (Porter *et al.* 1982, Underschultz and Erdmer 1991, Allan and Creaney 1991, Wright *et al.* 1994). The reef trend was buried to depths of at least 3000 m as a result of the foreland basin development, possibly > 5000 m in the deepest areas (Figure 3) (Wright *et al.* 1994). There has been at least 500 m of isostatic basinal uplift since the Eocene (Allan and Creaney 1991, Wright *et al.* 1994).

DIAGENETIC REGIME AND PARAGENETIC SEQUENCE

The Rimbey-Meadowbrook Reef Trend has a complex diagenetic history. The main feature is the pervasiveness of matrix dolomitization. It was suggested that the reef trend, initially limestone, was replaced to dolomite by chemically modified Late Devonian seawater in an intermediate (approximately 300 to 1600 m) burial environment at estimated temperatures of about 45 to 75°C during the Late Devonian to Mississippian (Illing 1959, Machel and Mountjoy 1987, Amthor *et al.* 1993, Drivet 1993, Machel *et al.* 1993, Amthor *et al.* 1994, Mountjoy and Amthor 1994, and Marquez 1994). These authors proposed the burial environment for dolomitization as a result of the extensive investigation of the petrographic textures, spatial relationships to facies and structure, paragenetic relationships to limestone diagenesis and stylolitization, trace elements, stable isotopes, $^{87}\text{Sr}/^{86}\text{Sr}$ -ratios, associated sulfates, recrystallization, and fluid inclusions of the grey matrix dolomites that comprise the reef trend. They also proposed that chemically modified Late Devonian seawater, that was buried along with the reef trend in the surrounding shale basin and farther to the southwest, was the dolomitizing fluid. Illing (1959), Amthor *et al.* (1993), and Mountjoy and Amthor (1994) suggest that this modified seawater was expelled from compacting shales (Ireton and Duvernay) and strata downdip from the reef trend. Amthor *et al.* (1993) recognized that compaction fluids alone are not sufficient for this pervasive dolomitization event and additional fluid and magnesium sources are required. These additional sources, however, are still undetermined. For most of these and additional reasons, recrystallization was considered to be "insignificant" (as defined on p.7), and difficult to constrain (Amthor *et al.* 1993, Drivet 1993, Machel *et*

al. 1993, Marquez 1994).

The reef trend is pervasively dolomitized except for the Golden Spike, Redwater, Strachan D3B, and Phoenix reefs (Figures 1 and 2). The first three have minor amounts of dolomite, but are primarily limestone (Machel and Mountjoy 1987, Amthor *et al.* 1993, Drivet 1993, Amthor *et al.* 1994, Mountjoy and Amthor 1994, and Marquez 1994), whereas the Phoenix reef is mostly dolostone, with zones of partially dolomitized limestone. All four reefs are off the main reef trend which follows the western margin of the underlying Cooking Lake Platform, this may be the reason for their partial dolomitization (Amthor *et al.* 1993).

A generalized paragenetic sequence was well defined by several authors (*e.g.*, Amthor *et al.* 1993, Drivet 1993, Marquez 1994) and includes replacement dolomitization timing, early calcite cementation, wispy stylolitization, later dolomite and anhydrite cementation, bitumen emplacement, late stage calcite and quartz cementation, as well as sulphide and sulphur emplacement (Figure 5). This sequence does not include recrystallization. There are several slightly varied paragenetic sequences, specifically for the Strachan-Ricinus area (Figures 1 and 2) (Marquez 1994). The paragenetic sequence included here is a general one for the entire reef trend, irrespective of local variations.

MATRIX DOLOMITE TYPES AND LITHOFACIES

Four matrix dolomite types, R1 to R4, have been defined for the pervasively dolomitized Rimbey-Meadowbrook Reef Trend (Drivet 1993, Marquez 1994). These types are based on the petrographic criteria of size, texture, and precursor fabrics, as well as the genetic interpretation that these matrix dolomites were formed during replacement dolomitization and not subsequently altered (Amthor *et al.* 1993, Drivet 1993, Marquez 1994). Cathodoluminescence is described as blotchy and dull in all of these dolomite types.

Replacement dolomite type R1, is a fine-crystalline, planar-e dolomite ranging in size from 35 to 60 μm (Gregg and Sibley 1984, Sibley and Gregg 1987, Drivet 1993, Marquez 1994). This dolomite type is commonly found either as mosaics coated by dark

Figure 5. Generalized paragenetic sequence based on Amthor et al. (1993) and Drivet (1993). Replacement dolomitization is interpreted to have occurred during intermediate burial (see also Figure 3). Timing of recrystallization was not identified in any previous study.

Paragenetic sequence of reef trend dolostones

Diagenetic Event	Early	Late
Isopachous calcite cementation	—————	—————
Submarine cementation	—————	—————
Stylolitization	—————	—————
Replacement dolomitization	—————	—————
Dolomite cementation	—————	—————
Anhydrite cementation and replacement	—————	—————
Calcite cementation	—————	—————
Quartz cementation	—————	—————
Bitumen emplacement	—————	—————
Sulfur and sulphide emplacement	—————	—————

Sea Floor Shallow Burial (< 500 m) Intermediate Burial (500 - 2000 m) Deep Burial (> 2000 m)

organic material or discrete fine crystals within coarser matrix dolomites (Figure 6).

Replacement dolomite type R2, is a medium-crystalline, planar-s dolomite ranging in size from 60 to 250 μm (Figure 6) (Gregg and Sibley 1984, Sibley and Gregg 1987, Amthor *et al.* 1993, Drivet 1993, Marquez 1994, Mountjoy and Amthor 1994). R2 is the most common matrix dolomite type in this reef trend. In most samples this type is fabric destructive, but there are examples of biochem ghosts. This type generally has poor intercrystalline porosity, although it is associated with fenestral, vuggy and moldic pores.

Replacement dolomite type R3, is a coarse-crystalline, planar-e dolomite ranging in size from 250 to 700 μm (Figure 6) (Gregg and Sibley 1984, Sibley and Gregg 1987, Amthor *et al.* 1993, Drivet 1993, Marquez 1994, Mountjoy and Amthor 1994). This matrix dolomite type occurs as either dense planar-s cloudy crystals or porous planar-e crystals with cloudy cores and clear rims.

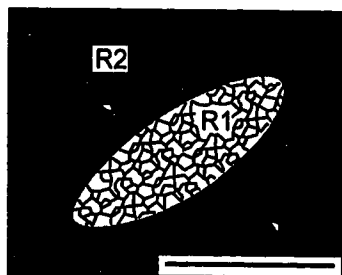
Replacement dolomite type 4, R4, is a coarse-crystalline, nonplanar anhedral dolomite characterized by both fibrous and equant crystals (Figure 6) (Amthor *et al.* 1993, Drivet 1993, Marquez 1994, Mountjoy and Amthor 1994). This type mimics the crystal habits of fibrous and isopachous calcite cements with sweeping extinction and sutured crystal contacts. The crystal boundaries are typically irregular and poorly defined. R4 commonly radiates from the boundaries of biochems and pore walls.

Biochems found within the R1, R2, and R3 matrix dolomite types include echinoderms, bryozoans, stromatoporoids, brachiopods, and coral fragments. There are six facies types defined by Drivet (1993), and all matrix dolomite types are found in most facies. R1 is the predominant matrix type in those facies dominated by mudstones. These facies types are defined primarily by fossil assemblages, pore shapes, and relict primary crystal textures (*e.g.*, McLean 1992, Shields and Geldsetzer 1992, McLean and Mountjoy 1993), and not water energy zones as defined by Machel and Hunter (1994) based on Dunham (1962), Embry and Klovan (1972), Wilson (1975), Flügel (1982), James (1983), Stearn (1984), and James and Bourque (1992), because the reef trend was dolomitized, which creates difficulty in primarily defining the locations of water energy zones.

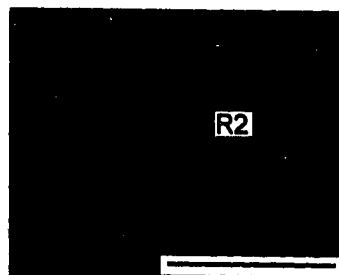
The **Stromatoporoid facies** consists of mudstones and rudstones with associated

Figure 6. Previous replacement dolomite textures of matrix types R1 to R4 in the Rimbey-Meadowbrook Reef Trend. Descriptions of matrix types found in the text. Grey pattern in matrix box R3 may be either inter-crystalline bitumen or anhydrite, or open pore space. Diagram modified from Amthor *et al.* (1993), and Drivet (1993). Scale bars = 0.05 mm.

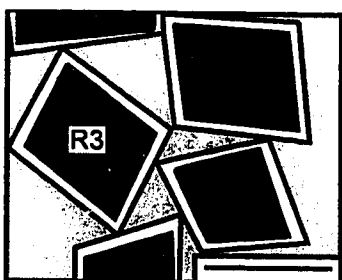
R1



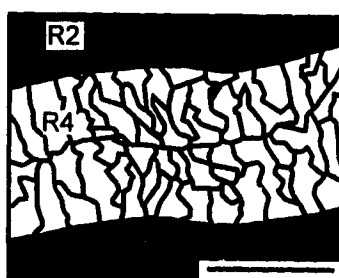
R2



R3



R4



relict biochems, stromatoporoids *Amphipora*, *Thamnopora*, *Alveolites*, *Stachyodes*, as well as brachiopods. This facies is most abundant along the buildup margins. The **Skeletal grainstone facies** consists of coarse grained and massive grainstones, with skeletal fragments making up most grains. This facies occurs as layers and is commonly in contact with dolomudstones in the buildup interior and occasionally the buildup margin. The **Amphipora facies** consists of wackestones, packstones, and grainstones with abundant *Amphipora* molds and grains. This facies is most abundant in the buildup interiors, but is also found along buildup margins. The **Stromatolitic facies** consists of finely laminated dolomudstones in the buildup interiors and associated with skeletal grainstones and the **dolomudstone facies**. The **dolomudstone facies** consists of fine R1 crystals with abundant inter-crystalline mud. The **Skeletal packstone facies** consists of stromatoporoid and coral fragments interbedded with mudstones and wackestones in the buildup flanks.

GENERAL HYDROGEOLOGIC REGIME

The Rimbey-Meadowbrook Reef Trend has long acted as an aquifer with the underlying Cooking Lake Platform in the WCSB. Throughout most of its extent (as shown in Figure 2), this aquifer presently channels formation fluids (groundwater) towards the northeast (Hitchon 1969a, Hitchon 1969b, Hitchon and Friedman 1969, Machel and Mountjoy 1987, Paul 1994, Bachu 1995).

Hitchon and Friedman (1969) and Hitchon (1969) proposed that, prior to the Laramide orogeny, fluid flow was southwestward through the reef trend and that topographic effects of the orogeny changed the flow pattern to a northeastward direction. Bachu (1995), in contrast with the earlier authors, suggests that the pre-Laramide flow system was northeastward as a result of an undefined pre-Cretaceous tectonic compression, prior to the development of the Rocky Mountain foreland basin.

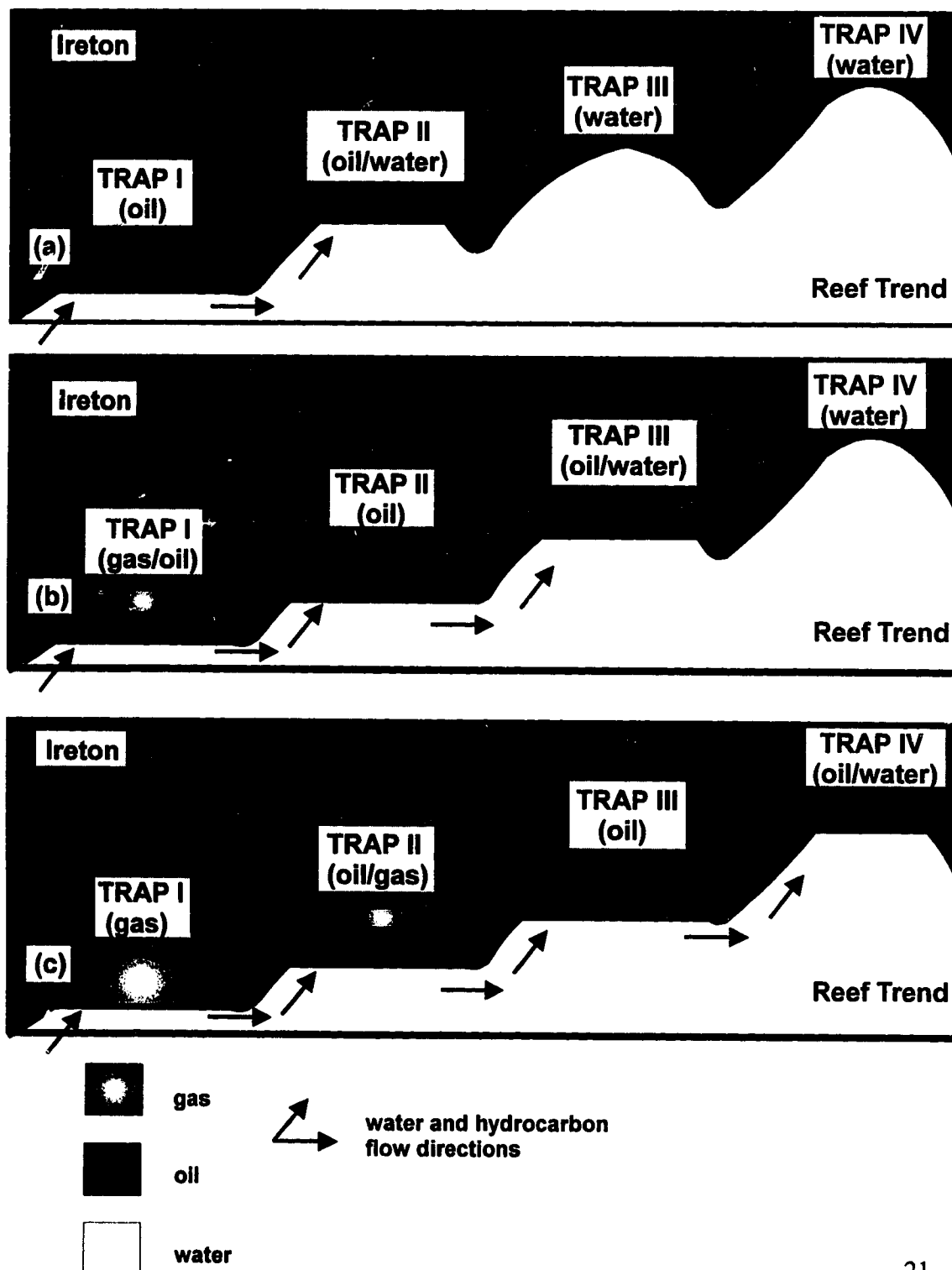
During post-Laramide time, meteoric waters entered the hydrogeologic system of the Rimbey-Meadowbrook Reef Trend from the northeast flowing counter to the topographically driven flow (Bachu 1995). Geochemical evidence indicates that the groundwater within the northeastern part of the Rimbey-Meadowbrook Reef Trend reflects partial mixing of two endmembers, seawater evaporated beyond halite saturation and post-

Laramide, pre-Pliocene meteoric water (Hitchon and Friedman 1969, Hitchon *et al.* 1971, Connolly *et al.* 1990, Bachu 1995).

Late Cretaceous oil migration into the reef trend is postulated to have originated downdip in the southwest, and to have followed the groundwater flow pathway (Gussow, 1968, Stoakes and Creaney 1985, Machel and Mountjoy 1987). Oil and gas hypothetically filled one reef to the "spill point" then "spilled" to the next reef along the migration pathway (Figure 7) (Gussow 1968, Stoakes and Creaney 1985). Rostron (1995), however, found that additional hydrogeologic features complicate this general pattern. Specifically, several reefs appear to have leached hydrocarbons through their top seals after initial oil emplacement.

Evidence from various studies indicates that present day subsurface fluids in the reef trend do not appear to affect the dolomite (neither dissolving nor precipitating) in their northeasterly flow (Hitchon 1969, Hitchon and Friedman 1969, Hitchon *et al.* 1971, Connolly *et al.* 1990, Bachu 1995). Paleofluid chemistries are unknown, but are assumed to have been derived from buried Late Devonian seawater (Machel and Mountjoy 1987, Connolly *et al.* 1990, Amthor *et al.* 1993, Drivet 1993, Marquez 1994, Mountjoy and Amthor 1994, Bachu 1995).

Figure 7. Schematic diagram of the process of differential oil and gas entrapment within the Rimbey-Meadowbrook Reef Trend. Modified from Rostron (1995).



CHAPTER THREE

DOLOMITE DIAGENESIS

REPLACEMENT DOLOMITIZATION

It is important to understand replacement dolomitization before discussing dolomite recrystallization because the conditions of replacement ultimately affect later recrystallization. The requirements for replacing CaCO_3 (calcite) with $\text{CaMg}(\text{CO}_3)_2$ (dolomite) are deceptively simple, high $\text{Mg}^{2+}/\text{Ca}^{2+}$ ratio, high $\text{CO}_3^{2-}/\text{Ca}^{2+}$ ratio (high supersaturation with respect to dolomite), and a sufficient fluid flow rate (for extensive Mg^{2+} supply) for massive, formation-wide dolomitization (Morrow 1982, Land 1985, Machel and Mountjoy 1986, 1987, Machel 1990, Amthor *et al.* 1993, Amthor *et al.* 1994). Whether a certain temperature, PCO_2 , or amount of sulphate is required is a matter of debate (Baker and Kastner 1981, Sibley 1982, Gregg and Sibley 1984, Land 1985, Machel and Mountjoy 1986, 1987, Sibley and Gregg 1987, Machel 1990). These are only some of the possible thermodynamic and kinetic factors inferred to be involved with dolomitization.

The chemistry and texture of replacement dolomite depend on the chemical composition and grain size of the precursors. The chemical composition of the precursor fabric determines the susceptibility to dolomitization, *e.g.*, high-magnesium calcite is more susceptible than low magnesium calcite (Sibley 1990). This compositional susceptibility guides certain aspects of the replacement dolomite chemistry, *e.g.*, $\delta^{13}\text{C}$ values and concentrations of trace elements such as strontium (Pingitore 1982). The grain size of the precursor fabric determines the distribution of nucleation sites, which in turn, determine dolomite crystal sizes and shapes (Sibley 1982). In a reef trend, *e.g.*, the Rimbey-Meadowbrook Reef Trend, the wide variations of these factors (chemistry and grain size of the precursor calcite reef network) complicate the interpretation of the timing and composition of replacement dolomitization fluids. This complexity makes it difficult to unquestionably define replacement dolomitization in a reef environment.

Gregg and Sibley (1984) and Sibley and Gregg (1987) have described dolomite textures that may indicate certain degrees of fluid supersaturation and/or temperature

during formation. These authors defined planar dolomite as a texture commonly formed from solutions with low supersaturation and/or at low temperatures (< 50°C), and nonplanar dolomite as a texture commonly formed from solutions with high supersaturation and/or at higher temperature (Sibley and Gregg 1987, Woody *et al.* 1996). The temperature of about 50°C is defined as the Critical Roughening Temperature, or CRT, above which dolomite crystals commonly form nonplanar textures (Gregg and Sibley 1984, Sibley and Gregg 1987, Woody *et al.* 1996). Planar and nonplanar textures may form by cementation, replacement dolomitization, or dolomite recrystallization (Gregg and Sibley 1984, Sibley and Gregg 1987).

Land (1982, 1985) and Friedman and O'Neil (1977) attempted to calculate replacement dolomitization temperatures from $\delta^{18}\text{O}$ values of dolomites, calcite and dolomitizing fluids using the following equations:

$$(1) \ 10^3 \ln \frac{(^{18}\text{O}/^{16}\text{O})_{\text{calcite}} + 1000}{(^{18}\text{O}/^{16}\text{O})_{\text{fluid}} + 1000} \approx 2.78 \times 10^6 (T)_{\text{fluid}}^{-2} (^{\circ}\text{K}) - 2.89 \text{ for calcite; (Friedman and O'Neil 1977)}$$

$$(2) \ T_{\text{fluid}} = [2.78 \times 10^6 / ((10^3 \ln \frac{^{18}\text{O}/^{16}\text{O}_{\text{dolomite}}}{^{18}\text{O}/^{16}\text{O}_{\text{fluid}}} + 1000) - 0.91)]^{1/2} \quad (\text{Land 1985})$$

where $^{18}\text{O}/^{16}\text{O}_{\text{fluid}}$ in eq. (1) represents the $\delta^{18}\text{O}$ value of the fluid forming the precursor calcite; $^{18}\text{O}/^{16}\text{O}_{\text{calcite}}$ in eq. (1) represents the $\delta^{18}\text{O}$ value of the precursor calcite; T_{fluid} in eq. (1) represents the temperature of the fluid precipitating the precursor calcite; and T_{fluid} in eq. (2) represents the replacement dolomitization fluid temperature. Many variables in these two equations cannot be obtained from most ancient successions, making these equations only partially useful for the determination of replacement dolomitization temperatures. Values that cannot be directly obtained from most ancient successions are: original temperature of the fluids forming the precursor calcite (T_{fluid} in eq. (1)) the original $\delta^{18}\text{O}$ values of the precursor calcite (eq.(1)), the original $\delta^{18}\text{O}$ values of the fluids forming the precursor calcite (eq. (1)), and the $\delta^{18}\text{O}$ values of the replacement dolomitization fluid (eq. (2)). Using reasonable estimates for these unknown values, however, it is possible to determine a temperature range for dolomitization. This has been done for the Rimbey-Meadowbrook Reef Trend through the use of presumably unaltered calcite biochems from the Golden Spike reef and equations (1) and (2) to derive

replacement dolomitization temperatures of about 45 to 75°C (Carpenter *et al.* 1991, Amthor *et al.* 1993, Drivet 1993).

With "significant recrystallization" (p.6-7) it is possible that the replacement dolomitization environment indicators may be obscured through the recrystallization event (Land 1980, Land 1985, Gregg and Shelton 1990, Gao and Land 1991, Montanez and Read 1992 Malone *et al.* 1994, Machel *et al.* in press). Therefore, dolomitization temperatures determined from $\delta^{18}\text{O}$ values or from the differentiation of planar and nonplanar crystal textures (the CRT) may not, in fact, be representative of either the replacement dolomitization fluid temperatures or the dolomite recrystallization fluid temperatures.

Echinoderm fragments

Replacement dolomitization of echinoderm fragments has been reported in the literature (Lohmann and Meyers 1977, Blake *et al.* 1982, Richter 1985, Bruckschen *et al.* 1990). What has not been determined is whether or not these biochems are susceptible to dolomite recrystallization. When echinoderm fragments are replaced by dolomite, as opposed to matrix replacement dolomitization, the process commonly begins with the partial replacement of the original high-magnesium calcite (HMC) echinoderm stereom by scattered microdolomite crystals that are optically continuous with the remaining HMC fragment (Lohmann and Meyers 1977). Commonly, Mg^{2+} , derived from the HMC stereom during early stages of diagenesis, is responsible for this microdolomite formation, through dissolution-reprecipitation before or while the stereom is transformed to LMC, and while the matrix surrounding the fragment continues to be limestone (Lohmann and Meyers 1977, Blake *et al.* 1982, Richter 1985, Bruckschen *et al.* 1990). With further burial and time, these scattered microdolomite crystals in the LMC stereom may recrystallize into more stoichiometric and better ordered crystals (Blake *et al.* 1982, Fagerstrom 1983, Sibley 1982, Bruckschen 1990, Brand 1990).

The entire echinoderm stereom may be dolomitized during the replacement dolomitization of the matrix surrounding the fragment. As a result of the size of the

original scattered microdolomites, and the optically continuous nature of the original HMC stereom, a stereom commonly dolomitizes into optically continuous, unimodal crystals (Blake *et al.* 1982, Gregg and Sibley 1984, Sibley and Gregg 1987). It has been further suggested by Fagerstrom (1983) and Brand (1990) that echinoderm fragments become impermeable after being completely replaced with dolomite, so that no other diagenetic alteration will affect the stereom after replacement dolomitization. It is possible that if echinoderm fragments are susceptible to dolomite recrystallization, they may then in turn represent the fluid chemistry during dolomite recrystallization.

RECRYSTALLIZATION

Dolomite recrystallization is a much debated subject between carbonate sedimentologists. In brief, recrystallization of dolomite is the transition of dolomite to dolomite through a change in one or a combination of three variables; structure, trace element and isotopic composition, and crystal texture by means of a dissolution-reprecipitation process (see p.6). There is a debate whether or not all ancient dolomite formations have been diagenetically recrystallized. Several authors (Land 1980, 1985, Coniglio *et al.* 1988, Banner *et al.* 1988, Sibley 1990, Gao 1990a, Gregg and Shelton 1990, Gao and Land 1991, Gregg *et al.* 1992, Montanez and Read 1992, Smith and Dorobek 1993, Kupecz and Land 1994, Malone *et al.* 1994, Banner 1995) proposed that typical replacive dolostones are originally formed as a disordered, non-stoichiometric phase, *i.e.*, 'protodolomite,' and undergo recrystallization. The major driving forces for this type of recrystallization are thought to be fluid chemistry changes, increased temperature, and increased pressure. Recrystallization of a metastable dolomite to a more stable form may be a continuous process, or it may occur stepwise with multiple dissolution and reprecipitation events (Sperber *et al.* 1984, Smith and Dorobek 1993), through either thin-film (removal of ions from recrystallization reaction site without replacing them) or bulk solution (ion exchange between bulk aquifer solution and recrystallization reaction site) (Banner 1995). The resulting changes may include crystal coarsening, with development of sweeping extinction, the destruction of

cathodoluminescence zoning, decrease of trace element concentrations, decrease of $\delta^{13}\text{C}$ and $\delta^{18}\text{O}$, decrease or increase of radiogenic isotope ratios (e.g., $^{87}\text{Sr}/^{86}\text{Sr}$), increase in cation ordering, increase in Mg^{2+} concentration, and an increase in stoichiometry (Montanez and Read 1992, Gao *et al.* 1992, Smith and Dorobek 1993, Malone *et al.* 1994). Other authors (Tan and Hudson 1971, Machel 1990, Machel *et al.* 1996) proposed that once dolomite is formed, specifically in the burial environment, it is resistant to changes in isotopic or trace element concentrations unless there is a *major* change in temperature, pressure, or pore fluid composition.

Both burial replacement dolomitization of limestone and recrystallization of earlier formed dolomites can generate dolomite with low $\delta^{18}\text{O}$ values, high $^{87}\text{Sr}/^{86}\text{Sr}$ -ratios, fluid inclusions with hot temperatures and high saline contents, and coarse crystals (Mattes and Mountjoy 1980, Banner *et al.* 1988, Cander *et al.* 1988, Gao *et al.* 1992, Montanez and Read 1992, Smith and Dorobek 1993, Banner 1995). The overlap of burial replacement dolomite characteristics with recrystallization characteristics makes the determination of recrystallization in a burial environment difficult. Tan and Hudson (1971), Mattes and Mountjoy (1980), Machel (1990), and Machel *et al.* (1996) suggested that no matter where in the burial environment it formed, burial dolomite is more stable than marine and evaporitic dolomite, and is therefore less likely to be recrystallized.

CHAPTER FOUR

METHODS

SAMPLING SELECTION AND PREPARATION

Sample selection was guided by two major constraints, (a) to obtain a sample set as representative of the matrix dolomites as possible, and (b) to collect a number of samples that can be analyzed within the available time frame and budget. Fortunately, previous studies showed that the matrix dolomites of the Rimbey-Meadowbrook Reef Trend are remarkably homogeneous, although minor differences have been noted. Previous and ongoing studies of the Rimbey-Meadowbrook Reef Trend have focused on reefs in that trend (McNamara and Wardlaw 1991, Amthor *et al.* 1993, Machel *et al.* 1993, Drivet 1993, Marquez 1994, Q. Ning Ph.D. thesis in progress, University of Alberta). McNamara and Wardlaw (1991), who examined 1044 m of core from 8 wells in the Westrose reef, observed little facies differentiation between the reef margin and interior, with slightly more differentiation between the lower and upper reef. This indicates minor differences in facies characteristics throughout this dolomitized reef. Amthor *et al.* (1993), in a study based on the cored intervals of 21 wells from 11 reefs, noted that the matrix dolomite, stable isotopes, and major and trace elements are similar throughout the reef trend between Morinville and Caroline, with no apparent covariant, regional, or stratigraphic trends (Figure 8). Furthermore, there appears to be homogeneity even on a very small scale, as microprobe traverses across matrix dolomite rhombs did not show any Ca, Mg, Fe, or Mn zonations (Amthor *et al.* 1993). Mountjoy and Amthor (1994) also noted that matrix dolomites in the Rimbey-Meadowbrook Reef Trend have similar textural characteristics and tightly clustered isotopic and geochemical data. These observations indicate only slight horizontal and vertical differentiation of textural characteristics and geochemical trends in the reef trend dolostones. These data, therefore, indicate that the dolostones are vertically and horizontally homogeneous.

Sample selection was limited to the Leduc Formation with usually three samples per well, forming a 30 m band (Table 1), about 75 meters above the Cooking Lake Platform, on the assumption that this would restrict variations in dolomite formation

Figure 8. Stable isotope and radiogenic strontium data of matrix dolomite from the Rimbey-Meadowbrook Reef Trend compiled from several wells in the Bonnie C and Westrose reefs (Amthor *et al.* 1993), the Medicine River and Sylvan Lake reefs (Drivet 1993), and the Strachan and Ricinus reefs (Marquez 1994). All data points, taken from stratigraphically different 30 meter intervals in the respective reefs as the result of the available data, are representative of the isotope ranges found throughout the reef trend and show very little vertical (or horizontal) variation. This indicates that the reef trend matrix dolomite samples have relatively homogeneous chemical characteristics.

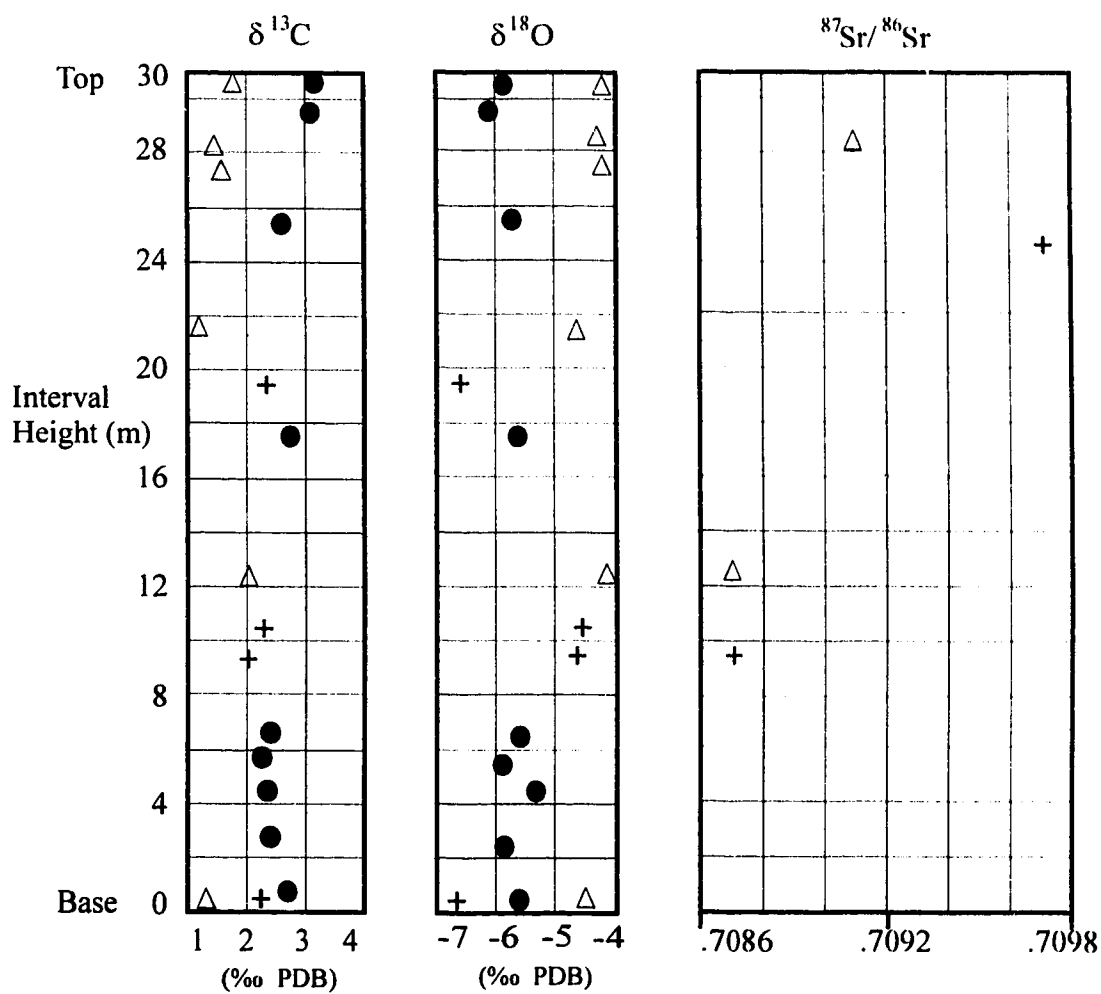


Table 1. List of wells studied, ordered by field from NE to SW.
All material is from the Leduc Formation.

Well I.D.	Number of samples per well	Field	Interval (m)
Thin sections and slabs:			
3-21-57-24W4	three	Morinville	1229-1242
9-30-56-24W4	one	Morinville	1278.3
7-15-55-25W4	three	Morinville	1358-1366
2-16-55-25W4	three	Morinville	1487-1624
6-22-55-26W4	three	Morinville	1562-1654
2-14-53-26W4	three	Acheson	1525-1545
2-35-52-26W4	two	Acheson	1539-1547
15-23-52-26W4	one	Acheson	1563.9
6-11-51-26W4	two	Leduc	1745-1759
8-17-50-26W4	three	Leduc	1590-1936
3-22-48-27W4	two	Wizard Lake	1977-2020
3-20-47-27W4	three	Bonnie Glen	1871-2034
8-4-46-28W4	three	Westerose	2207-2241
16-30-45-28W4	one	Westerose	2121
1-36-45-1W5	one	Westerose	2245
11-7-43-1W5	one	Homeglen Rimbey	2375
3-29-43-1W5	one	Homeglen Rimbey	2390
7-22-42-2W5	one	Homeglen Rimbey	2402
11-25-42-2W5	one	Homeglen Rimbey	2429
11-3-42-2W5	one	Homeglen Rimbey	2390
14-5-41-2W5	three	Homeglen Rimbey	2514-2533
10-7-40-2W5	three	Homeglen Rimbey	2615-2629
14-28-39-3W5	three	Homeglen Rimbey	2823-2845
8-30-38-4W5	one	Medicine River	3134.6
16-11-38-4W5	one	Medicine River	3071
6-20-38-4W5	one	Medicine River	3134.3
16-32-37-4W5	two	Sylvan Lake	2982-2989
10-17-37-3W5	one	Sylvan Lake	2863
8-27-36-6W5	two	Garrington	3583-3593
16-25-36-6W5	one	Garrington	3470
11-10-35-5W5	three	Caroline	3355-3365
13-9-33-4W5	three	Harmattan	3425-3467
15-23-36-10W5	three	Ricinus West	4495-4592
10-33-36-10W5	four	Ricinus West	4522-4661
11-27-36-10W5	two	Ricinus West	4476-4489
7-26-36-10W5	one	Ricinus West	4397.9
6-24-34-8W5	two	Ricinus	4379-4385
6-14-34-8W5	two	Ricinus	4285-4286
10-29-37-7W5	one	Chedderville	3656
6-30-37-7W5	one	Chedderville	3532
11-28-37-8W5	one	Crimson	3699.7
10-31-37-9W5	three	Strachan	4300-4325
7-32-37-9W5	two	Strachan	4085-4112
5-13-37-12W5	two	Ram River	5047-5067
7-9-39-12W5	two	Phoenix	4739-4737

fluids, burial conditions, timing of replacement dolomitization, and later dolomite recrystallization. In some wells, however, this 30 m wide band varies up to 160 meters above the selected 75 m horizon (wells homogeneous as described in previous paragraph and Figure 8) because of poor core coverage.

A total of seventy samples were collected at the Energy Resources Conservation Board (ERCB) Core Laboratory, eighteen were used from Q. Ning's thesis study (Ph.D. thesis in progress, University of Alberta). These samples were selected based on their location in core descriptions provided by McNamara and Wardlaw (1991), Amthor *et al.* (1993), Drivet (1993), and Marquez (1994), from Resistivity logs, and Q. Ning (Ph.D. thesis in progress, University of Alberta). Samples were also selected for their potential to provide evidence for or against dolomite recrystallization (*i.e.*, the presence of fine grain sizes, or $^{87}\text{Sr}/^{86}\text{Sr}$ -ratios close to theoretical Late Devonian marine values). During sample collection at the ERCB, when samples could not be obtained from predetermined core intervals, samples were taken with dolomite textures similar to those described in previous studies. These samples were then located on core descriptions after collection (core descriptions located in McNamara and Wardlaw 1991, Amthor *et al.* 1993, Drivet 1993, Marquez 1994).

Seventy polished and unstained thin sections were made. Following initial thin section study, dolomite matrix types and biochems were selected for microdrilling. Powder samples were drilled from 65 hand samples with a Healthco dental drill with a steel bit. At least 200 mg of powder were drilled from each sample to produce a single homogeneous sample to be aliquoted for analysis of cation ordering and lattice parameters by XRD, major elements by ion chromatography, trace elements by ICP-MS, and carbon, oxygen, and strontium isotopic compositions by mass spectrometry.

PETROGRAPHY

Thin sections were studied with a petrographic microscope, epifluorescent microscope (blue-light 450 nm), and a cathodoluminescence (CL) microscope. The CL microscope is an Olympus BH-2 with a luminoscope vacuum attachment to the stage and an EG&G detector interface to an IBM compatible computer. The luminoscope is an

ELM-3R. The CL running conditions were <50 torr, 10-15kV and 0.5mA.

Epifluorescence was performed to determine if textures that were present prior to dolomitization were visible (Dravis and Yurewicz 1985). This analysis was also performed to distinguish dolomite matrix types.

SEM analysis was performed to determine crystal sizes and shapes for both calcite and dolomite echinoderm fragments. Two samples, one calcite, 7-9-39-12W5 at 4739.9 m in the Phoenix reef, and one dolomite, 10-7-40-2W5 at 2615.2 m in the Homeglen-Rimbey reef, were chosen for SEM (JEOL Scanning Microscope 6301FXV running at an acceleration voltage of 2.5 kV) study because these were the only two that had echinoderm fragments visible to the naked eye. The samples were broken to 1cm³ pieces, and etched with a 3:1 distilled water: acetic acid mix. A second piece of the dolomite sample 10-7-40-2W5 at 2615.2 m was etched for 25 seconds to enhance crystal boundaries. All samples were mounted onto a sample stub with silver glue and then gold coated.

X-RAY DIFFRACTION

Sixty-five samples were analyzed by X-ray Diffraction (XRD) in order to measure two separate aspects of matrix dolomite types along the reef trend, *i.e.*, lattice parameters and cation ordering. Ten mg of powder was mixed with an internal quartz standard (quartz = 30% of dolomite sample weight), then fixed as an ethanol slurry to a quartz plate transparent to X-rays. Samples were run on a Co-radiation Rigaku X-ray Diffractometer, measured from 10° to 90° 2 theta in a single scan, with an amplification such that the dolomite {104} peak (Intensity=100) was on scale. Peak locations (d_{hkl} = spacings) and intensities were obtained from the Rigaku Peaks Program.

The a_0 and c_0 of the unit cell parameters were determined by entering the d-spacings (Å) of all peaks into a least squares program (Benoit 1988) after being corrected relative to the internal quartz standard. Mole % CaCO₃ was calculated for each sample by the equation (Lumsden 1979):

$$\text{CaCO}_3 \text{ mol \%} = (333.33)d_{(104)} - 911.99$$

where $d_{(104)}$ is the d-spacing (Å) of the 104 plane of the sample dolomite, after it was

corrected relative to the internal quartz standard.

In order to calculate the errors associated with the determination of unit cell parameters and mole% CaCO_3 , the variations of the measured d-spacing of the quartz peaks {101} and {110} from the respective JCPDS (1986) d-spacings were averaged to be ± 0.0037 in this study. When this variation (± 0.0037) is entered into the least squares program (Benoit 1988), the errors for the unit cell parameters a_0 and c_0 are ± 0.01 and ± 0.03 , respectively. To determine the error for mole % CaCO_3 , the JCPDS (1986) d-spacing of the {104} dolomite peak at 2.888 \AA and the respective value corrected for the average error ($2.888 - 0.0037$) were each plugged into the equation by Lumsden (1979). The resulting two values were subtracted ($50.667 - 49.433$) leaving an average error of about 1 mole %, or ± 0.6 mole % applicable only to mole % CaCO_3 values. A similar error was calculated by comparison of XRD derived mole % CaCO_3 and mole % MgCO_3 with microprobe data of the same compounds in one sample set (Huebscher, pers. comm.).

Cation ordering was estimated by dividing the intensity of the dolomite {015} peak by the {110} peak (Goldsmith and Graf 1958). The {015} (ordering) peak has an intensity of about 3% relative to that of d_{104} ($I_{\text{max}} = 100$), and the {110} (diffraction) peak has a relative intensity of about 7% relative to d_{104} . To determine the reproducibility of the intensity measurements of these two small peaks (machine error), and to assess possible effects of preferred orientation (sample preparation error), four endmember samples were analyzed by the procedure outlined above. Two of these samples are presumed to be well ordered and stoichiometric (Cathedral Formation, Radium Hot Springs, BC, and Devonian Pine Point saddle dolomite), and two are relatively poorly ordered and non-stoichiometric (Permian San Andres dolomudstone, and Upper Devonian Grosmont Platform dolomite).

Five replicate runs performed on a single mount, without being removed from the XRD chamber, of the well ordered sample from the Cathedral Formation gave ordering and diffraction peak ({015} and {110}, respectively) intensities and ratios of:

{015}	{110}	{015/110}
18.4	25.2	0.730
21.3	27.4	0.777

18.9	30.5	0.619
22.2	27.7	0.801
18.9	26.3	0.719.

Accordingly, the in-run calculated ratio (015/110) variation is 0.619 to 0.801. if there is a correlation between the variation in intensities of the ordering {015} peak with the variation in intensities of the diffraction {110} peak. If no correlation is assumed, the minimum and maximum error of the ratios can be calculated. The minimum {015/110} variation is $18.4/30.5 = 0.600$, and the maximum variation is $22.2/25.2 = 0.880$. These intensity variations are a good representation of the in-run variations caused by machine error (this error does not apply to d-spacings *i.e.*, unit cell parameters or mole % CaCO_3).

To determine the possible effect of preferred orientation on intensity measurements and the reproducibility of sample preparation (in contrast to the above error calculation), three duplicate mounts were made from one powder mixture (with 30% quartz) of each of the four endmember samples and run separately using the preparation technique described above. The three Cathedral Formation samples gave:

{015}	{110}	{015/110}
1.9	2.9	0.655
0.8	2.1	0.381
20.2	9.2	2.196

with an {015/110} ratio variation from 0.381 to 2.196. The calculated minimum and maximum {015/110} ratios results in a range of 0.800 to 9.600. An average variation of ± 0.643 is estimated to be the 2θ error of each ordering value that is determined using this preparation technique. This error was determined by averaging the variations in the ordering ratios of the four endmember samples, but is statistically invalid because of the paucity of data. Therefore, the sample preparation procedure used above should not be used if cation ordering ratios are desired, presumably because of the high incidence of preferred orientation of the grains. This conclusion is consistent with observations made by Reeder (pers. comm., 1991). This finding is echoed by the great extent to which Mumme *et al.* (1996) went in order to avoid preferred orientation effects in determining intensity measurements from clays and micas with XRD analysis. Goldsmith and Graf

(1958) avoided this problem of preferred orientation by using a single crystal for analysis. The fine crystal size of dolomite matrix used in this study precluded the use of single crystals for XRD analysis. Because of the very large error calculated here, the ordering parameters cannot and have not been used in the interpretations regarding dolomite recrystallization that follow.

MAJOR AND TRACE ELEMENT ANALYSIS

For each of the sixty-one powder samples analyzed, fifty-five major and trace element concentrations were measured using ion chromatography and ICP-MS, respectively, at the Institute for Sedimentary and Petroleum Geology (ISPG) in Calgary. Complete results are listed in Appendix A, Table 3.

Using a microwave sample preparation system (MDS-2100) with Teflon lined bombs (Appendix B) 20 mg of powder was dissolved in 800 μ l of HNO_3 :HCl, 3:1. This strong acid mixture was used in this procedure in accordance with requirements for the subsequent dilution process and sample analysis. After cooling for one half hour, the solution was diluted to a measured volume of 10 ml (500x dilution) in weighed 10 ml Simport culture tubes.

For determination of Mg^{2+} and Ca^{2+} , a 1 ml aliquot of the sample solution was further diluted 20 x for ion liquid chromatography, on a Dionex 500 liquid chromatograph system (ILS) (details in Appendix C). Fifty-three trace element concentrations were determined on a Fisons inductively coupled plasma mass spectrometer (ICP-MS). One aliquot of the sample solution was run unspiked. A second aliquot was spiked with an internal standard solution containing 25 trace elements. Each sample solution was run in triplicate to ensure reproducibility of element concentrations. One blank was included for every eleven dolomite samples. Two separate multi-element standard solutions, a blank, and a flush solution, were each run three times between samples. External and internal standard (STDA, STDB, spike-C) and flush solution compositions are listed in Appendix A along with error calculations and details of the method.

STABLE ISOTOPE ANALYSIS

Stable isotope ratios $\delta^{13}\text{C}$ and $\delta^{18}\text{O}$ were analyzed on 29 powder samples. Ten to twenty mg aliquots of sample powder were used for analyses, which were conducted according to the techniques of Degens and Epstein (1964). Stable isotope values were collected with a Finnigan-Mat 252 mass spectrometer at the University of Alberta. All values are reported as ‰ in the δ notation, relative to the PeeDee Belemnite (PDB) standard. Analytical error is estimated to be less than 0.2‰ for $\delta^{13}\text{C}$, and less than 0.3‰ for $\delta^{18}\text{O}$. The $\delta^{18}\text{O}$ values were corrected by -0.82 for phosphoric acid fractionation (Sharma and Clayton 1965, Land 1980, 1985).

RADIOGENIC STRONTIUM ANALYSIS

Twenty-seven samples were analyzed for $^{87}\text{Sr}/^{86}\text{Sr}$ -ratios. Samples were chosen for analysis following petrographic and trace element analysis to ensure a range of matrix types that also had > 50 ppm Sr. Sample selection focused on matrix types R1 and R2 because of their varying crystal sizes and textures. Selected samples of each matrix type are distributed along the reef trend.

One hundred to one hundred-sixty mg of powder (dependent on amount of Sr determined by ICP-MS) were weighed into centrifuge tubes and dissolved in 2.25 ml of 1N HCl, at room temperature, for at least 18 hours. Millipore water (0.75 ml) was added to dilute the solution to 0.75N HCl. Samples were centrifuged and Sr was separated from the supernatant solution using standard cation exchange techniques, as described in Appendix D. The purified Sr was loaded as a chloride onto the side filament of a double rhenium assembly. Isotope ratios were determined on a VG 354 mass spectrometer. Repeated measurements ($n = 6$) of Sr isotopic standard NBS 987 during this study gave a value of 0.71026 ± 3 . Total reproducibility is estimated at ± 3 in the fifth decimal place.

CHAPTER FIVE

PETROGRAPHIC OBSERVATIONS

Throughout the following text, several hand specimen and thin section samples will be singled out with respect to both petrographic observations and geochemical characteristics. These samples will be identified and given a short label the first time they are mentioned. Their labels contain the name or abbreviation of the reef the particular sample is from, and the depth in meters. The locations of all labelled samples are shown on the map in Figure 9.

MATRIX

The terminology of the matrix types R1 to R4 that have been described in Chapter Two is used in this section. The R is an abbreviation for "replacement dolomite," as in the original definition by Amthor *et al.* (1993). Dolomites discussed here are originally replacement dolomites. If recrystallization has affected the reef trend dolostones, to any "significant" (p.6-7) extent, those samples affected may no longer resemble the original replacement matrix dolomite chemically, physically, or both. Definition of the matrix as replacement (R) would then be misleading. Therefore, the terms R1 to R4 will be used for continuity with previous studies, referring to descriptions of size and texture of originally replacement dolomites in this observation section. Any interpretation regarding recrystallization will not be made here.

Matrix R1

Matrix dolomite type R1 is a fine-crystalline, planar-s, uncommonly planar-c, crystal mosaic (Plate 1A, 1B). Crystals range in size from 20 to 75 μm in diameter (Figure 10). This type occurs throughout much of the reef trend as matrix and as discrete zones and stringers in other matrix types. It is absent in the deep part of the reef trend, *i.e.*, Ricinus, Chedderville, Ram River and Crimson areas, and it is rare in the Strachan and Phoenix reefs (Figure 2).

Zones of R1 are associated with small vugs, small fractures or minor amounts of

Figure 9. Township and range map of study area, indicating the locations of the samples that are singled out in the text with respect to petrographic observations and geochemical data. These samples are identified here by their simplified labels which are defined in the text. A complete list of sample locations and depths is given in Table 1.

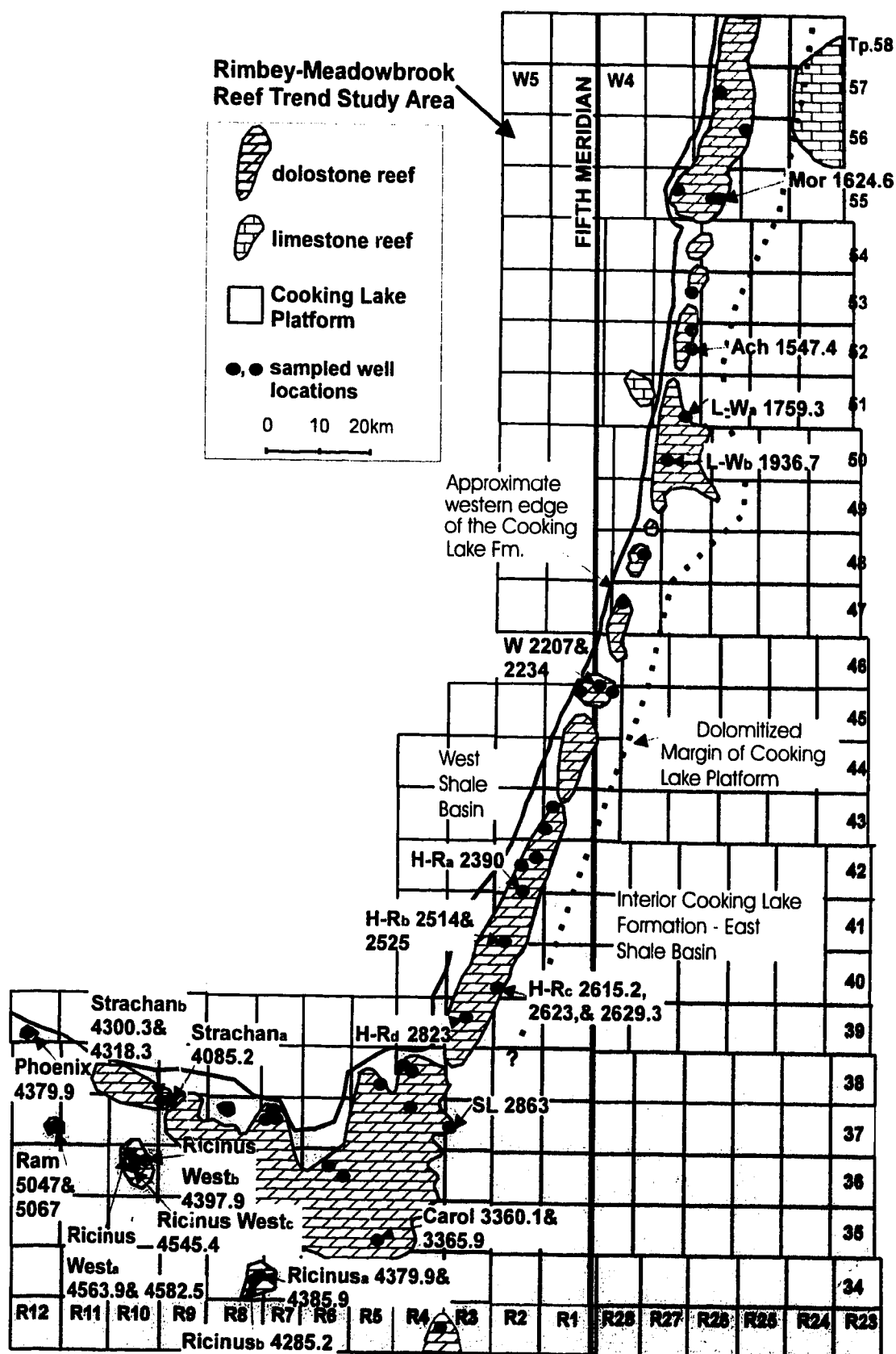


Plate 1. PHOTOMICROGRAPH ILLUSTRATIONS OF MATRIX TYPE R1.

A) Matrix R1 (R1) (75 μm in diameter) sample with bitumen (o) and no biochems. Matrix is comprised of planar-s crystals. Sample well 11-10-35-5W5 3360.1 m, Caroline reef (Carol 3360.5a). Transmitted light, crossed polars. Scale bar is 200 μm .

B) Matrix type R1 (75 μm in diameter) with interstitial clay (c). Matrix is comprised of planar-e crystals. Sample well 8-4-46-28W4 2234 m, Westeros reef. Transmitted light, crossed polars. Scale bar is 200 μm .

C) Zone of matrix R1 (75 μm in diameter) in matrix type R3 (R3) (200 μm in diameter). Both matrix types are comprised of planar-s crystals. Sample well 11-28-37-8W5 3699.7 m, Crimson reef. Transmitted light, crossed polars. Scale bar is 200 μm .

D) Stringer of matrix R1 (50 μm in diameter) in matrix type R2 (R2) (100 μm in diameter). The R1 stringer is adjacent to a stylolite (l). Both matrix types form nonplanar anhedral crystal mosaics. Sample well 3-20-47-27W4 1998.9 m, Bonnie Glen reef. Transmitted light, crossed polars. Scale bar is 200 μm .

E) Matrix R1 (25 μm in diameter) containing bitumen (o) and biochems. Biochems in this photomicrograph are quartz filled brachiopod (br) and dolomite echinoderm (e) fragments. Sample well 10-7-40-2W5 2615.2 m, Homeglen-Rimbey reef (H-R_c 2615.2). Transmitted light, crossed polars. Scale bar is 200 μm .

F) Cathodoluminescence photomicrograph of bright echinoderm fragment (e) surrounded by matrix R1 (R1) of sample shown in E. The echinoderm with bright CL is representative of the CL of most biochems. Sample well 10-7-40-2W5 2615.2 m, Homeglen-Rimbey reef (HR_c 2615.2). Scale bar is 100 μm .

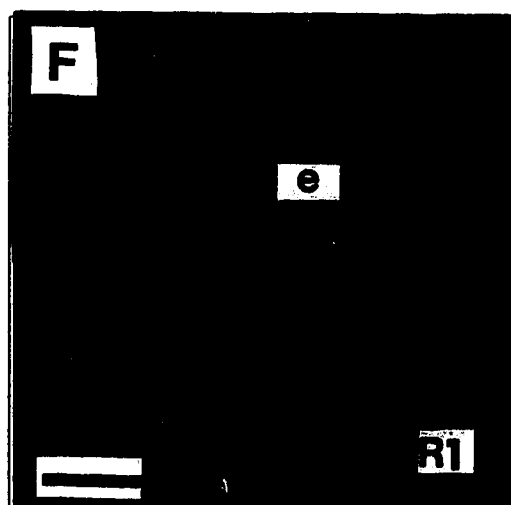
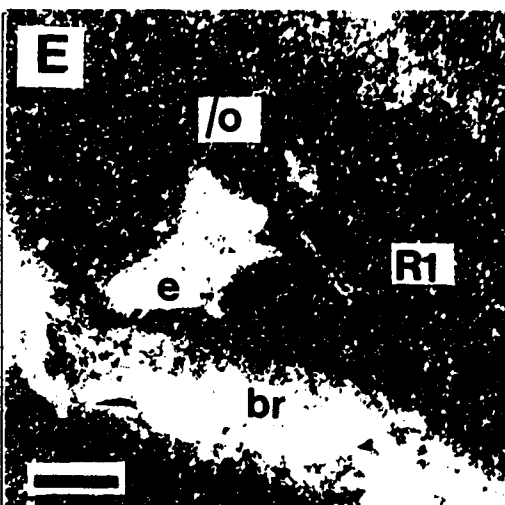
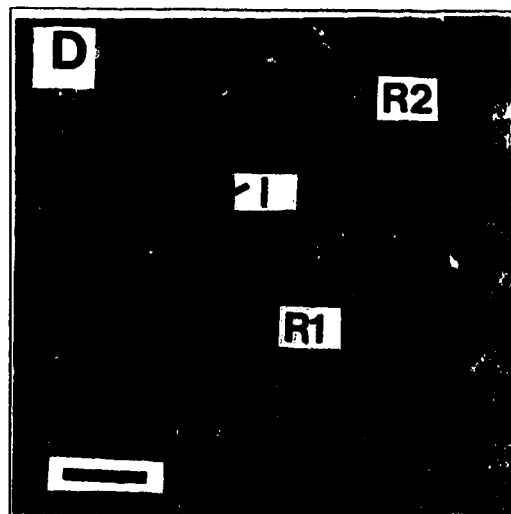
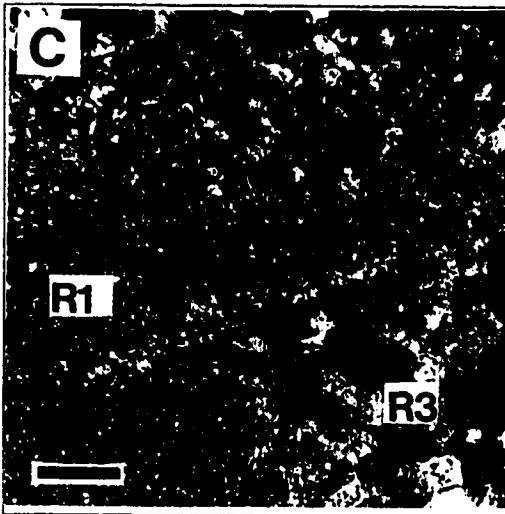
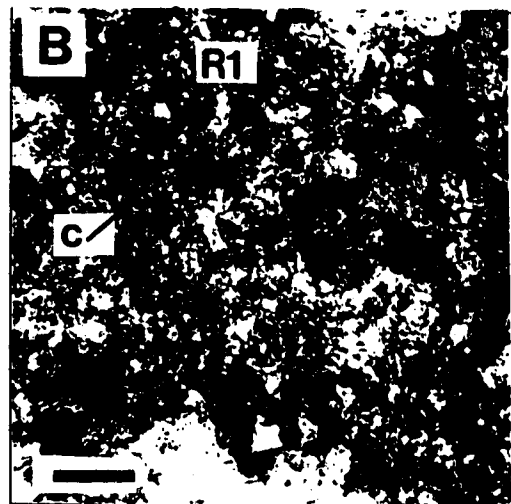
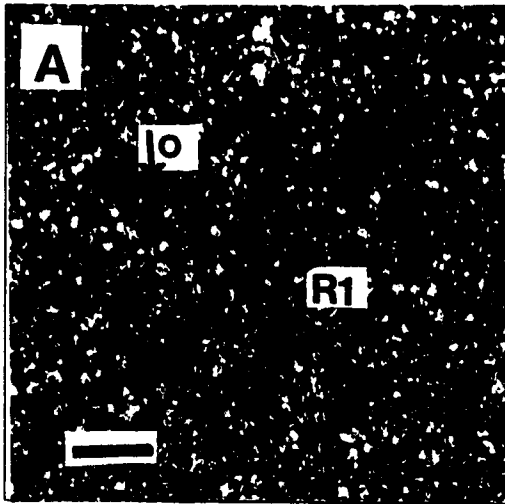
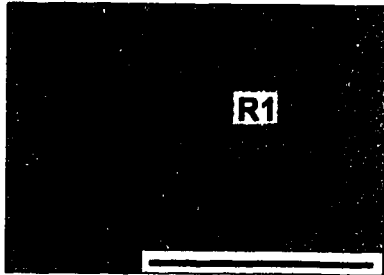
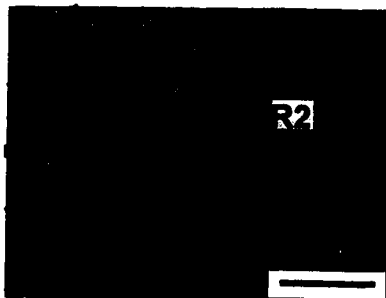


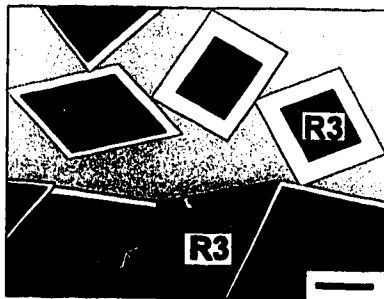
Figure 10. Dolomite Textures for Rimbey-Meadowbrook Reef Trend.
Adapted from previous studies to incorporate new observations, see text
for details.



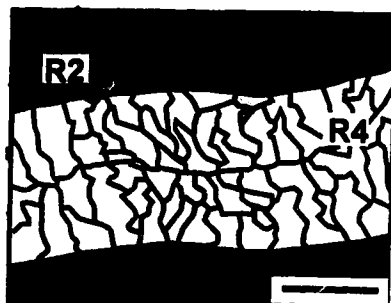
Matrix Type R1 also found as zones and stringers in matrix types R2 and R3.
Scale bar = 0.025 mm.



Matrix Type R2 occurs as either planar or nonplanar crystal mosaics.
Scale bar = 0.025 mm.



Matrix Type R3 occurs as either porous crystal masses (as in the upper portion of figure) or dense mosaics. Grey pattern may be either inter-crystalline bitumen or anhydrite, or open pore space.
Scale bar = 0.025 mm.



Matrix Type R4 normally found adjacent to biochems or relict biochems.
Scale bar = 0.025 mm.

cement, and are distinguishable from other matrix types by crystal size only (plate 1C). In some cases stringers of R1 are adjacent to stylolites (Plate 1D). Matrix R1 commonly contains well preserved biochems in the reef trend, some filled with quartz (Plate 1E), bitumen, and clay, although not all R1 samples contain biochems (Plate 1A, 1B).

R1 commonly has dull red CL (Plate 1F), at times blotchy with slightly lighter, orange-red patches surrounded by dull red dolomite. It is not always possible to distinguish R1 with CL when it occurs as zones or patches within other matrix types. R1 encloses crystals of matrix type R2 size and texture in some locations (Plate 2A, 2B). R1 has a fluorescent core with a nonfluorescent rim when analyzed under blue-light epifluorescence, no observable precursor textures (Dravis and Yurewicz 1985) (Plate 2B).

Matrix R2

Matrix dolomite type R2 forms medium-crystalline, planar-s crystal mosaics (Plate 2C, 2D). Crystals range in size from 100 to 400 μm in diameter (Figure 10). Matrix type R2 is the most abundant matrix type throughout the reef trend and is associated with both matrix R1 and R3 crystals in some locations. Biochems are sparse and poorly-preserved in R2 matrix mosaics. These mosaics commonly contain abundant fluid inclusions which create cloudy crystals in transmitted light, but are generally too small for analysis. R2 dolomites occasionally contain intercrystalline bitumen (Plate 2C). They show dull, irregularly blotchy red CL, sometimes with light orange-red cores surrounded by dull red dolomite (Plate 2E). R2 has a fluorescent core with a nonfluorescent rim when analyzed under blue-light epifluorescence (Plate 2B).

Samples from the depths of 2514 m and 2525 m from well 14-5-41-2W5 in the Homeglen-Rimbey reef (H-R_b 2514 and H-R_b 2525, respectively) (Figure 9) contain matrix R2 dolomite, unzoned in transmitted light, similar to all other matrix R2 samples in the reef trend. Both samples, however, exhibit matrix dolomite mottled CL with bright orange-red patches in darker red crystals, which is different from all other matrix R2 samples in the reef trend (Plate 2F). This mottled texture may be created from a previously zoned CL texture obscured by patches lighter than the matrix background cutting across the zonations.

Plate 2. PHOTOMICROGRAPH ILLUSTRATIONS OF MATRIX TYPE R2.

A) Matrix type R1 (20 μm in diameter) with scattered nonplanar crystals matrix R2 sized (250 μm in diameter). Sample well 11-3-42-2W5 2390 m, Homeglen-Rimbey reef (H-R_a 2390). Transmitted light, crossed polars. Scale bar is 200 μm .

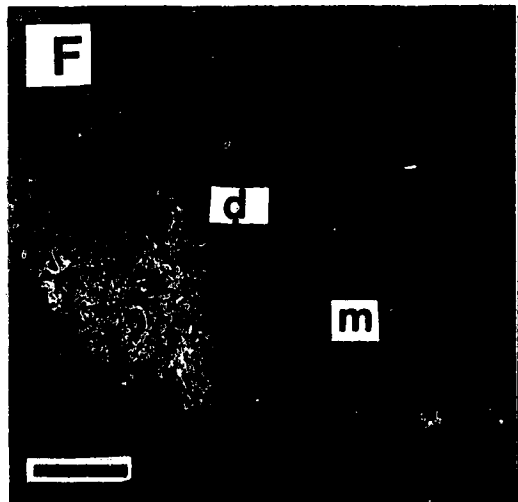
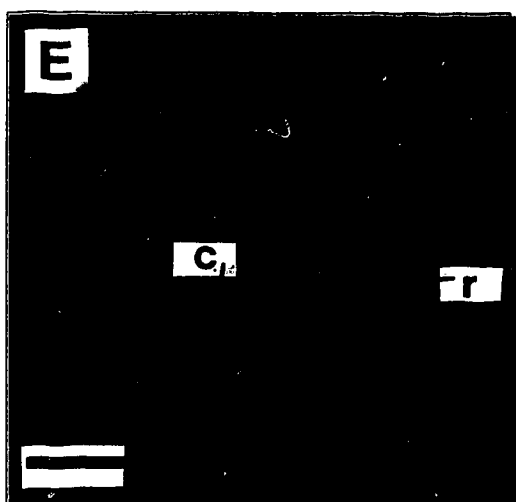
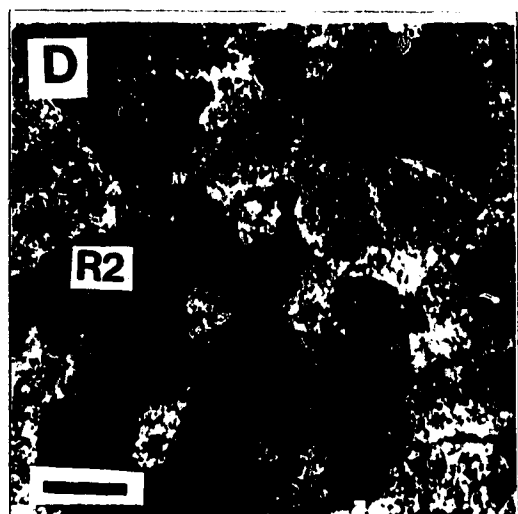
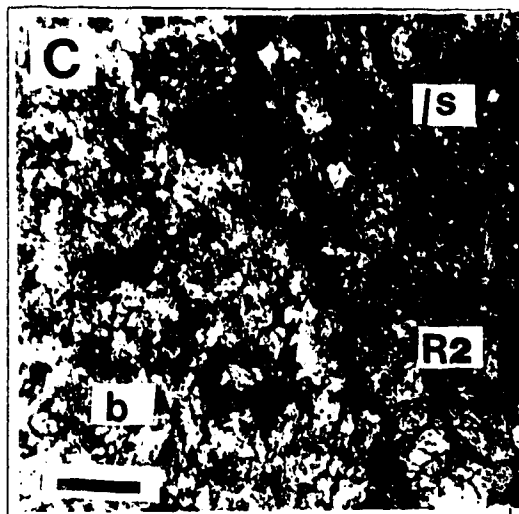
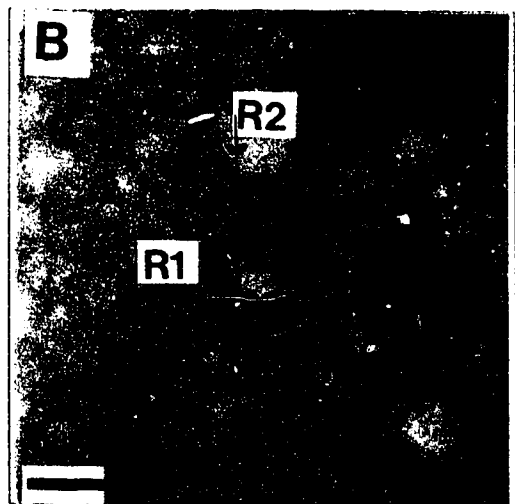
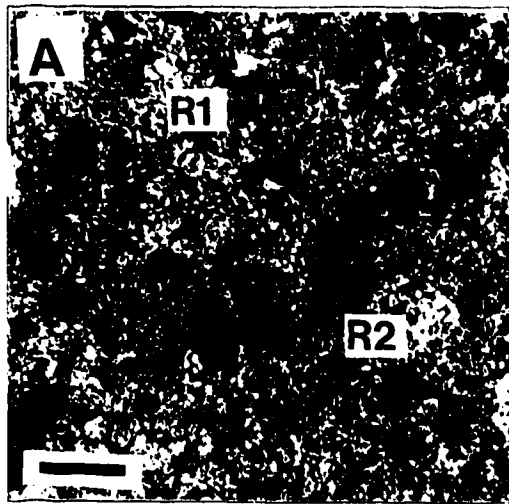
B) Photomicrograph of A taken under blue-light epifluorescence. The fluorescent, planar-s crystals (light color) are scattered R2 (R2). The darker mass represents matrix R1 (R1). Precursor textures are not visible. Sample well 11-3-42-2W5 2390 m, Homeglen-Rimbey reef (HR_a 2390). Scale bar is 100 μm .

C) Matrix R2 (200 μm in diameter) sample with stylolites (s) and biochems (b), matrix stained brown by bitumen. R2 is comprised of planar-s crystals. Sample well 6-24-34-8W5 4385.9 m, Ricinus reef (Ricin_a 4385.9). Transmitted light, crossed polars. Scale bar is 200 μm .

D) Nonplanar anhedral crystal mosaic of matrix type R2 (300 μm in diameter). Fabric-destructive matrix type. Sample well 2-16-55-25W4 1487.4 m, Morinville reef. Transmitted light. Crossed polars. Scale bar is 200 μm .

E) Cathodoluminescence photomicrograph of matrix R2 of sample shown in D. The dolomite exhibits blotchy CL with brighter cores (c) surrounded by dark rims (r). Sample well 2-16-55-25W4 1487.4 m, Morinville reef. Scale bar is 100 μm .

F) Cathodoluminescence photomicrograph of matrix type R2. Uncommon mottled signature evident by randomly oriented light patches (m) within the dark red matrix (d). Sample well 14-5-41-2W5 2525 m, Homeglen-Rimbey reef (H-R_b 2525). Scale bar is 100 μm .



Matrix R3

Matrix dolomite type R3 forms coarse-crystalline, porous, planar-e crystals (Plate 3A), frequently interlocking or dense (Plate 3B, 3C). R3 dolomites commonly have cloudy cores, usually surrounded by clear rims when viewed in transmitted light (Plate 3B). Crystals range in size from 150 to 850 μm in diameter (Figure 10). This matrix type is abundant in the shallow Morinville reef, and in the deepest part the reef trend in the Strachan, Ricinus, Chedderville, and Crimson areas. Biochems are rare in this matrix type. R3 dolomites commonly contain abundant fluid inclusions in the cloudy cores and sparse to no inclusions in the clear rims. R3 has fluorescent and nonfluorescent zonations when analyzed under blue-light epifluorescence (Plate 3C). R3 has blotchy and sparsely zoned CL with either light orange-red cores and dark red to bright red (cement) rims or dull cores with blood red rims (Plate 3D).

Matrix R4

Matrix dolomite type R4 forms elongated bladed to small and blocky crystals with undulose extinction and sutured edges (Plate 4A, 4B). The blades range in length from 500 μm to >1 mm and the blocks range in diameter from 20 to 200 μm (Figure 10). This type of dolomite typically lines the outer edges of relict biochems (Plate 4C) and is commonly associated with dolomitized biochems. This is the least abundant matrix type in the reef trend, present in the central portion in the Acheson, Leduc-Woodbend, Bonnie Glen, Westeros, and Homeglen-Rimbey reefs, and absent from extreme north and south ends of the reef trend. R4 dolomite has dull to non-luminescent cathodoluminescence, rarely discernable only by the outline of adjacent and brighter luminescent biochems (Plate 4D). R4 is not discernable under blue-light epifluorescence.

Cathodoluminescence Properties

Matrix R1 Zoning

Apart from infrequent occurrences of dully CL zoned matrix types R2 and R3 in the reef trend, there is only one sample of brightly CL zoned dolomite. This sample is from well 7-9-39-12W5 sample 4739.9 m (Phoenix 4739.9) (Figure 9). Phoenix 4739.9

Plate 3. PHOTOMICROGRAPH ILLUSTRATIONS OF MATRIX TYPE R3.

A) Porous matrix type R3 (pR3) (200 - 400 μm in diameter) with bitumen (o) filled pore space. R3 crystals are typically zoned with a cloudy interior and clear rim. Sample well 8-4-46-28W4 2207 m, Westrose reef. Transmitted light, crossed polars. Scale bar is 200 μm .

B) Dense mosaic of matrix type R3 (dR3) (300 μm in diameter) with scattered, open, bitumen lined pores (p). R3 crystals are typically zoned with a cloudy interior and white rim. Sample well 7-15-55-25W4 1360.6 m, Morinville reef. Transmitted light, crossed polars. Scale bar is 200 μm .

C) Photomicrograph of B taken under blue-light epifluorescence. Crystals have fluorescent (light) and nonfluorescent (dark) zones. Precursor textures are not visible. Sample well 7-15-55-25W4 1358.8 m, Morinville reef. Scale bar is 100 μm .

D) Cathodoluminescence photomicrograph of matrix R3. Crystals have zoned CL with orange-red cores (c) surrounded by bright red rims (r). Sample well 7-15-55-25W4 1358.8 m, Morinville reef. Scale bar is 100 μm .

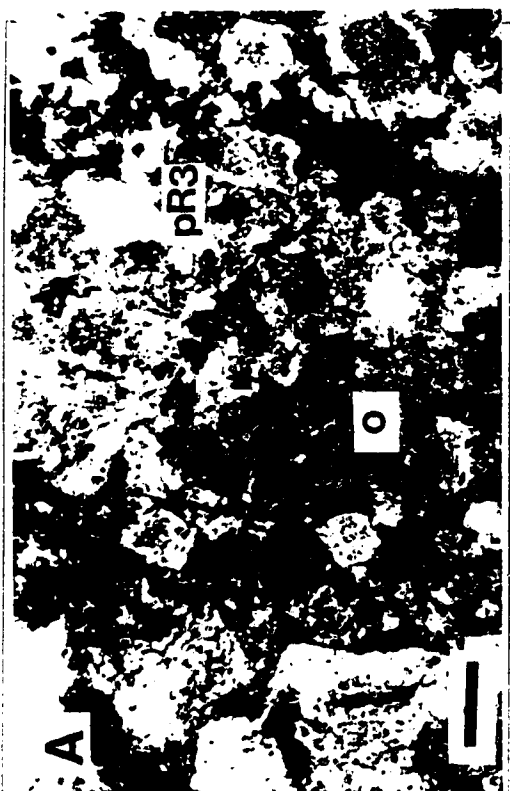
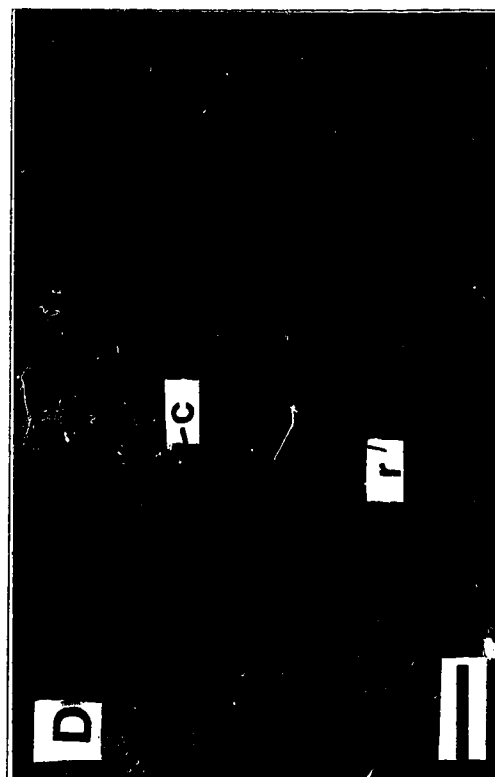


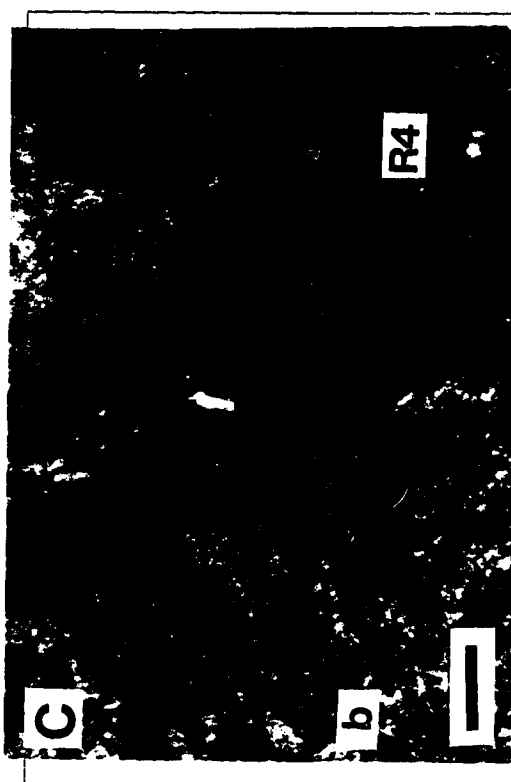
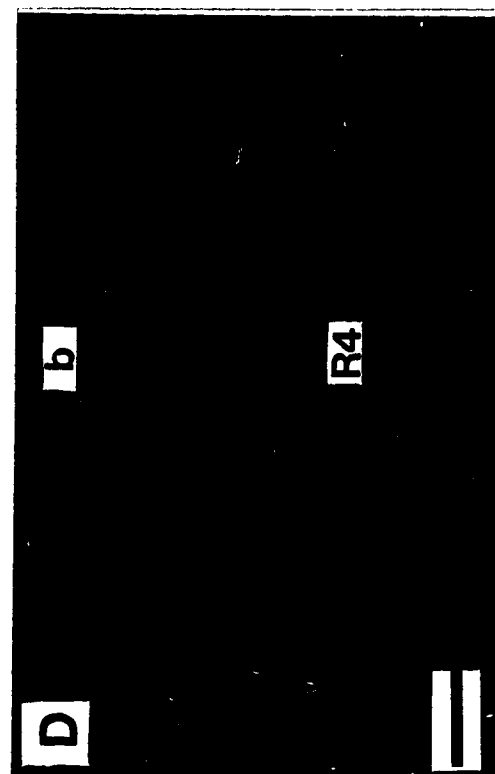
Plate 4. PHOTOMICROGRAPH ILLUSTRATIONS OF MATRIX TYPE R4.

A) Elongated bladed crystals of matrix type R4 in matrix type R1 with sutured crystal contacts. Sample well 14-28-39-3W5 2845 m, Homeglen-Rimbey reef. Transmitted light, crossed polars. Scale bar is 200 μm .

B) Bladed and blocky matrix type R4 with undulose extinction in matrix type R2. Sample well 2-14-53-26W4 1525.8 m, Acheson reef. Transmitted light, crossed polars. Scale bar is 200 μm .

C) Elongated bladed crystals of matrix type R4 adjacent to dolomitized biochem (b) filled by R1 dolomite. Sample well 8-34-50-1W4 1590.9 m, Leduc-Woodbend reef. Transmitted light, crossed polars. Scale bar is 200 μm .

D) Cathodoluminescence photomicrograph of matrix R4 of sample shown in A. Matrix R4 (R4) has slightly lighter CL than the adjacent biochem (b). Sample well 14-28-39-3W5 2845 m, Homeglen-Rimbey reef. Scale bar is 100 μm .



is primarily limestone with R1 sized dolomite crystals partially replacing the calcite micrite matrix (Plate 5A, 5B). This dolomite has brightly zoned CL (Plate 5B) and a planar-e texture. Smaller 10 μ m sized dolomite crystals partially replacing a large echinoderm fragment are only visible with CL (Plate 5C, 5D). There is no dolomite cement or dolomite replacing calcite cement.

Partial Dolomite Replacement of Calcite Cement

Sample 4300.3 m from well 10-31-37-9W5 from the Strachan reef (Strachan_a, 4300.3) (Figure 9) is also primarily limestone, calcite micrite matrix with calcite biochems and cements (Plate 5E). Dolomite in this sample has replaced calcite cements and has unzoned CL (Plate 5F). There is no dolomite either in the matrix or the biochems.

BIOCHEMS

General Observations

Most matrix samples have very dull CL. Most biochems have brighter orange-red CL than does the surrounding matrix. Matrix R1 contains the best preserved biochems, these include stromatoporoids, *renalcis*, echinoderm fragments, coral fragments, ostracods, and brachiopods. Sparse and less recognizable stromatoporoids and echinoderm fragments are also found in matrix type R2.

In 25 hand samples from the deepest part of the reef trend (Strachan, Ricinus, Chedderville, Ram River, and Crimson areas) transmitted light and/or CL showed biochems in only 4 samples. These were the partially dolomitized sample Strachan_a, 4300.3, noted in the previous section, and three other samples from Ricinus, well 15-23-36-10W5, 4592.5 m (Ricinus West_a, 4582.5), well 6-24-34-8W5, 4385.9 m and 4379.9 m (Ricinus_a, 4385.9 and Ricinus_a, 4379.9, respectively) (Figure 9). The samples without biochems in this area are primarily coarse grained R3 matrix with calcite, anhydrite and dolomite cements. Some of these samples contain sulfur, some bitumen. All of these samples have similar blotchy orange-red CL.

Plate 5. PHOTOMICROGRAPH ILLUSTRATIONS OF PARTIALLY DOLOMITIZED LIMESTONES.

A) Biochem (b) rich calcite micrite matrix (m) with 50 μm sized dolomite crystals (d) interspersed in the micrite. Dolomite crystals are planar-e. Sample well 7-9-39-12W5 4739.9 m, Phoenix reef (Phoenix 4739.9). Transmitted light. Scale bar is 200 μm .

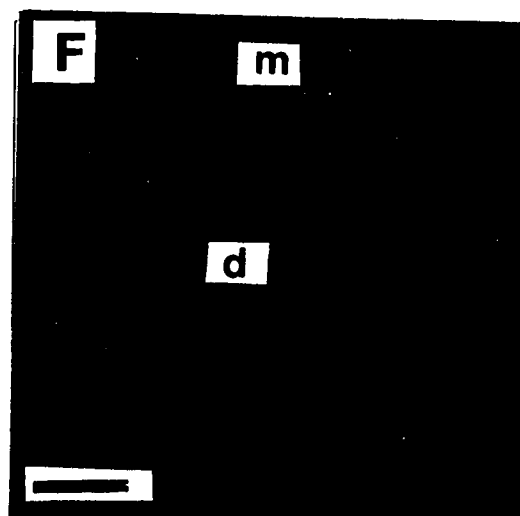
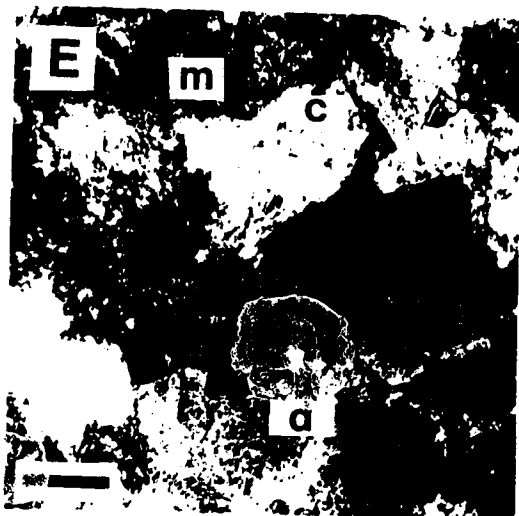
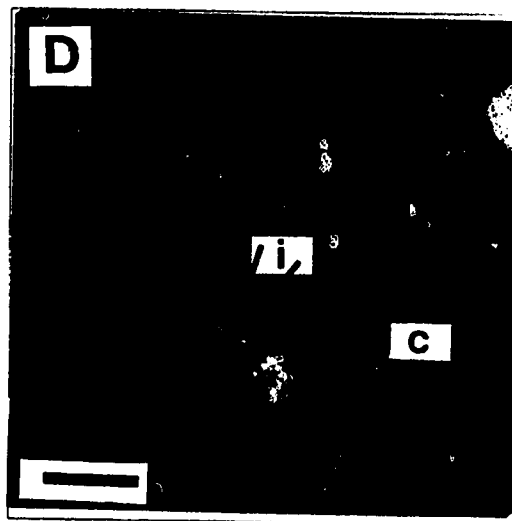
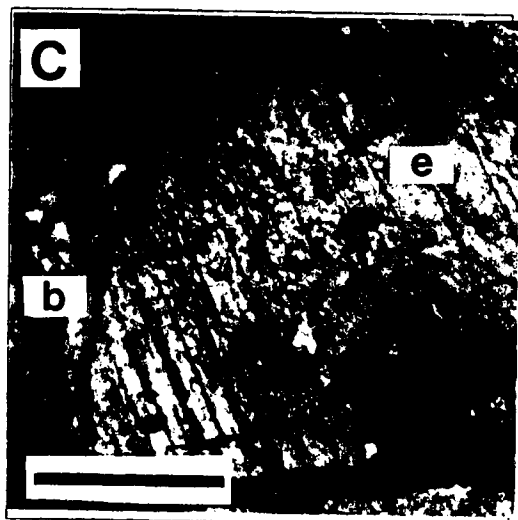
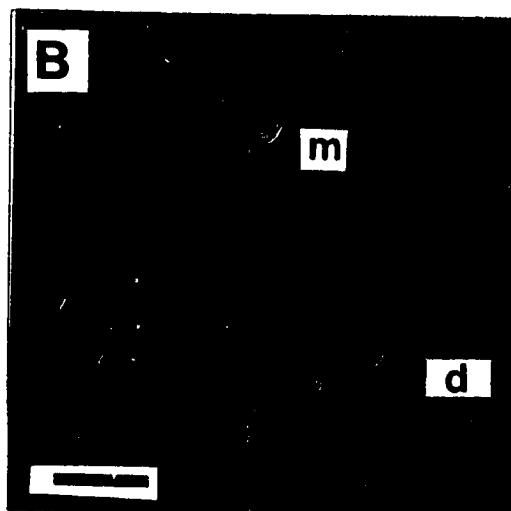
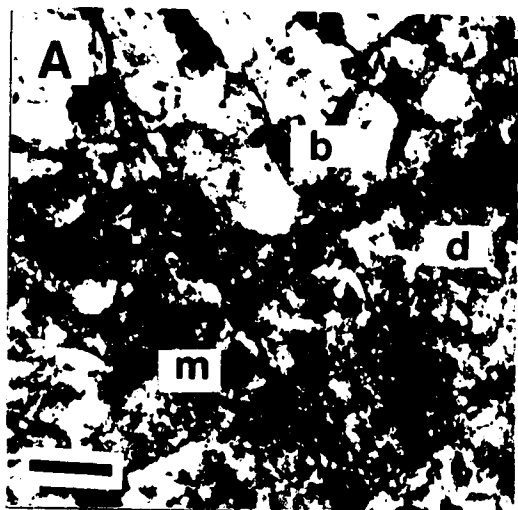
B) Cathodoluminescence photomicrograph of micrite matrix (m) and dolomite crystals (d) of sample shown in A. The dolomite crystals are planar-e and have zoned CL. Sample well 7-9-39-12W5 4739.9 m, Phoenix reef (Phoenix 4739.9). Scale bar is 100 μm .

C) Calcite echinoderm crinoid fragment (e) surrounded by other biochems (b) and micrite matrix. Replacement dolomite crystals not visible in transmitted light. The fracture was created during thin section preparation. Sample well 7-9-39-12W5 4739.9 m, Phoenix reef (Phoenix 4739.9). Transmitted light, crossed polars. Scale bar is 400 μm .

D) Cathodoluminescence photomicrograph of echinoderm fragment of sample shown in C, showing microdolomite inclusions (i) within the calcite (c) fragment. Sample well 7-9-39-12W5 4739.9 m, Phoenix reef (Phoenix 4739.9). Scale bar is 100 μm .

E) Calcite micrite matrix (m) with large blocky calcite (c) and dolomite (d) vein filling cements. There is no dolomite replacing the micrite matrix. Sample well 10-31-37-9W5 4300.3 m, Strachan reef (Strachan_b, 4300.3). Transmitted light. Scale bar is 200 μm .

F) Cathodoluminescence photomicrograph of dolomite cement (d) in micrite sample (m) shown in E. Dolomite cement has unzoned under CL. Sample well 10-31-37-9W5 4300.3 m, Strachan reef (Strachan_b, 4300.3). Scale bar is 100 μm .



Echinoderm Fragments

Echinoderm stem fragments are sporadically present throughout the reef trend in matrix R1 and matrix R2 (Plates 6 and 7). In some areas the fragments are visible in hand sample and in others, CL is required for recognition. Some fragments not visible in transmitted light are set apart from the matrix by having brighter red CL (Plate 1F). The CL signature of the fragments blends in with the blotchiness of the matrix when the average size of the echinoderm fragment is similar to that of the matrix, *e.g.*, when in matrix R2 (Plate 6).

In well 10-7-40-2W5, 3 samples show several interesting petrographic textures. The shallowest sample, H-R_c 2615.2 has R1 matrix and contains abundant bioherms (echinoderm, bryozoan, brachiopod, and ostracod fragments). The echinoderm fragments exhibit brighter orange-red luminescence than the matrix (Plate 1F). Two crystal sizes are distinguishable in the fragments by a combination of transmitted light and SEM analysis. The fragments are composed of vuggy 50 μm sized crystals which are optically continuous in transmitted light and therefore indistinguishable as distinct crystals, but they reveal crystal boundaries and hence their small crystal sizes when etched and examined by SEM (Plate 8). This unimodal dolomite encloses areas of larger crystals, up to 100 μm , which are not optically continuous in transmitted light, and therefore observable in thin section without the use of SEM (Plate 7A). These fragments are hence called bimodal crystal echinoderm fragments, to illustrate that they contain two crystal sizes within the dolomitized stereoms.

The two deeper samples in this well, H-R_c 2623 and H-R_c 2629.3, are similar to H-R_c 2615.2, but contain finer R1 matrix crystals and bitumen filling both pores and axial canals of echinoderm fragments. In these two samples, the echinoderm fragments are bimodal crystal echinoderm fragments, but are much smaller and most contain bitumen (Plate 7B). One bimodal crystal fragment retains part of the original skeletal structure, although it is entirely dolomitized (Plate 9A).

In H-R_c 2629.3, a grainstone, one bifold crystal echinoderm fragment exhibits a "flame"-like region in the stereom (Plate 7C, a. and b.). This "flame" has a different color distinct from the rest of the fragment. It originates from one edge of the fragment and

Plate 6. PHOTOMICROGRAPH ILLUSTRATIONS OF ECHINODERM FRAGMENTS.

A) Bimodal crystal echinoderm fragment (e) in matrix type R2. The fragment is replaced entirely by optically discontinuous crystals. Sample well 3-20-47-27W4 1871.5 m, Bonnie Glen reef. Transmitted light, crossed polars. Scale bar is 200 μm .

B) Bimodal crystal echinoderm fragment in nonplanar matrix R2. Striations are due to thin section preparation. Optically continuous crystals (c) are shown at extinction and comprise the majority of the fragment. Because these crystals are optically continuous, discrete crystals are indistinguishable under transmitted light. The larger, optically discontinuous crystals (d) are scattered throughout the fragment. Sample well 14-28-39-3W5 2834 m, Homeglen-Rimbey reef. Transmitted light, crossed polars. Scale bar is 200 μm .

C) Cathodoluminescence photomicrograph of echinoderm fragment (e) in matrix R2 (R2) of sample shown in B. There is no distinction between the fragment and the matrix. Sample well 14-28-39-3W5 2834 m, Homeglen-Rimbey reef. Scale bar is 100 μm .

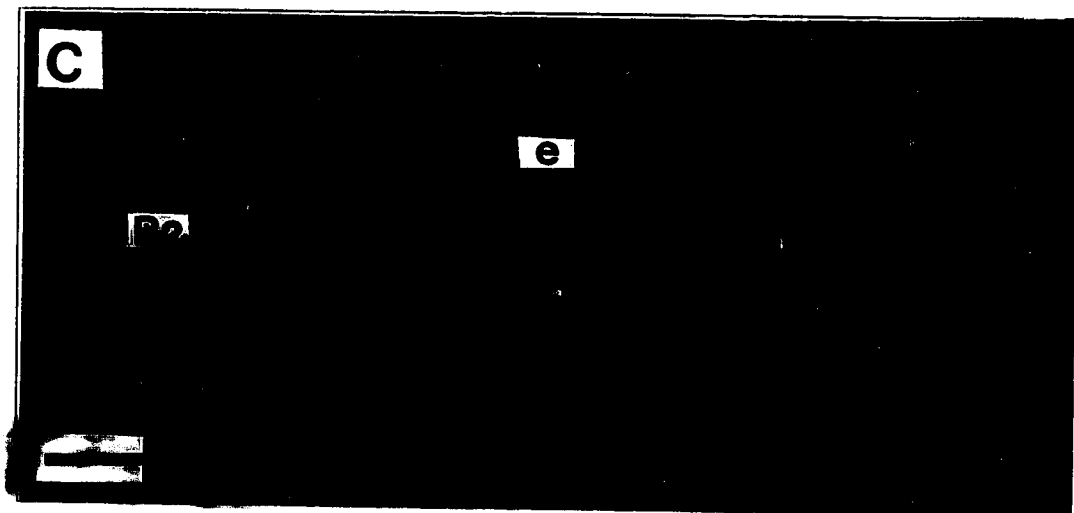
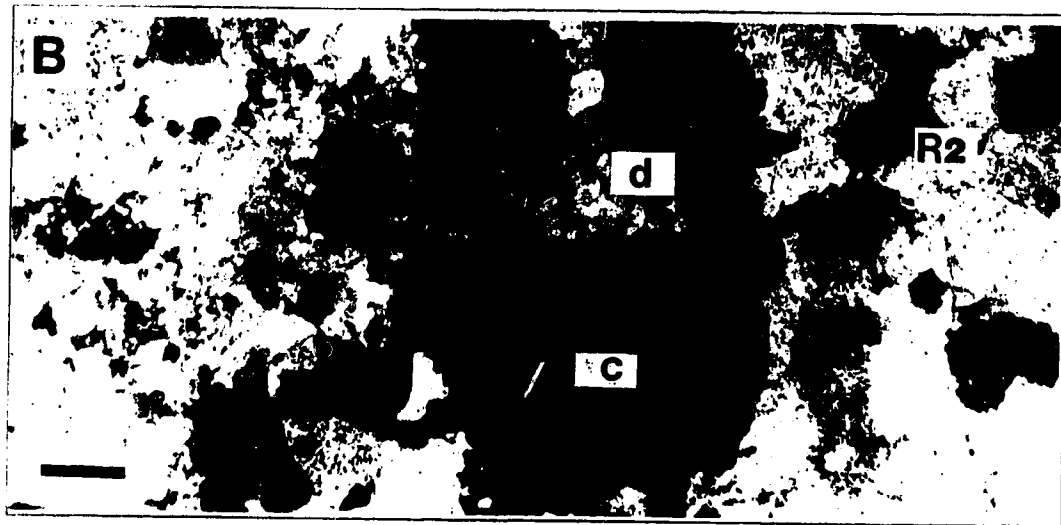
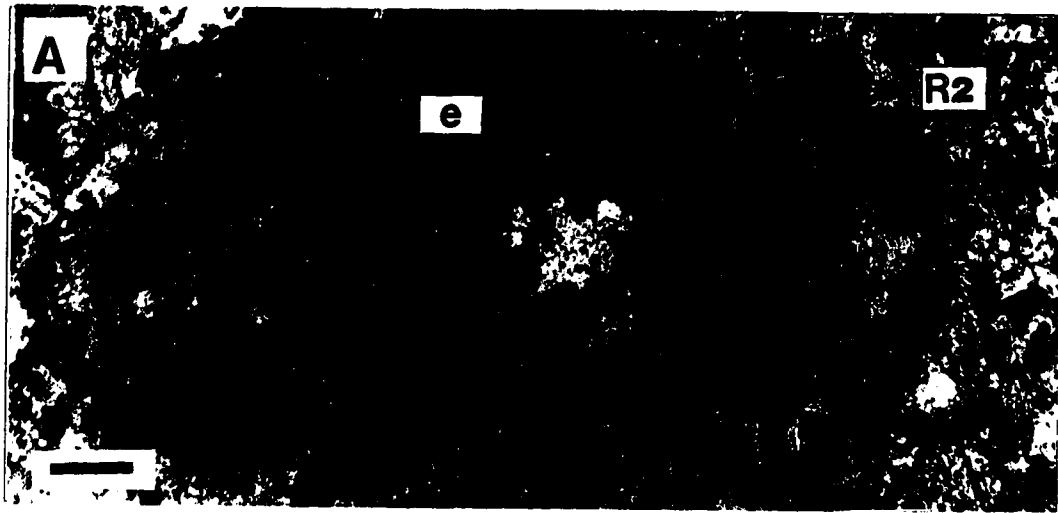


Plate 7. PHOTOMICROGRAPH ILLUSTRATIONS OF ECHINODERM FRAGMENTS

A) Bimodal crystal echinoderm crinoid fragment in matrix R1. 50 μm crystals in length in optical continuity (c) are shown at extinction and therefore discrete crystals are indistinguishable in transmitted light. 100 μm crystals in length in optical discontinuity (d) are not at extinction and are both abundant in the center of the fragment and surround the fragment. Sample well 10-7-40-2W5 2615.2 m, Homeglen-Rimbey reef (H-R_c 2615.2). Transmitted light crossed polars. Scale bar is 200 μm .

B) Bimodal crystal echinoderm fragment which contains bitumen (o) in the axial canal and is surrounded by matrix R1. Optically continuous crystals are shown at extinction (c). The optically discontinuous crystals (d) are not at extinction and are abundant throughout the fragment. Sample well 10-7-40-2W5 2623 m, Homeglen-Rimbey reef (H-R_c 2623). Transmitted light crossed polars. Scale bar is 100 μm .

C) a. Bimodal crystal echinoderm fragment within matrix R1 grainstone sample. Optically continuous crystals are shown at extinction (c). Optically discontinuous crystals are not at extinction (d). Note "flame"-like structure (f) surrounding optically discontinuous crystals. Sample 10-7-40-2W5 2629.8 m, Homeglen-Rimbey (H-R_c 2629.8). Transmitted light. Scale bar is 200 μm . b. Trace of echinoderm and the discolored "flame"-like structure (f) which surrounds several optically discontinuous crystals (d).

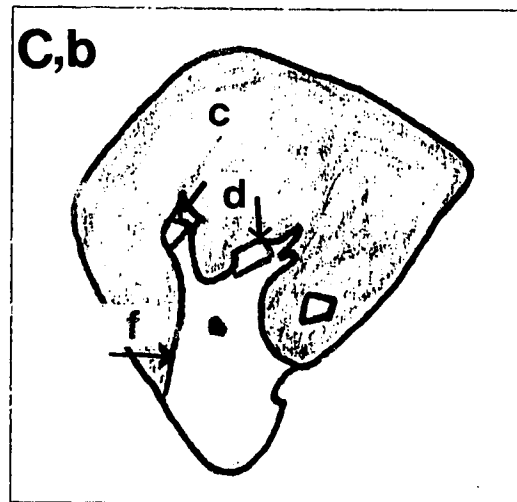
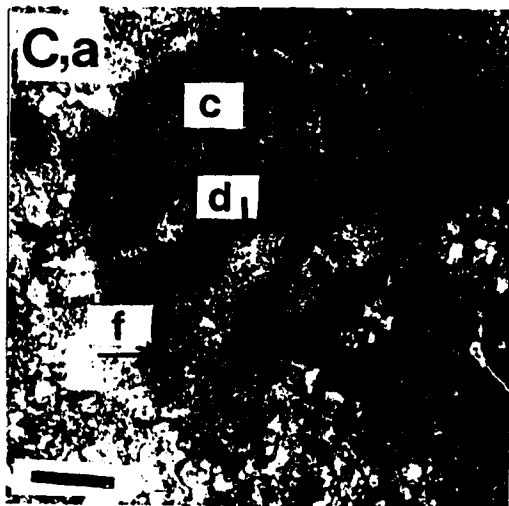
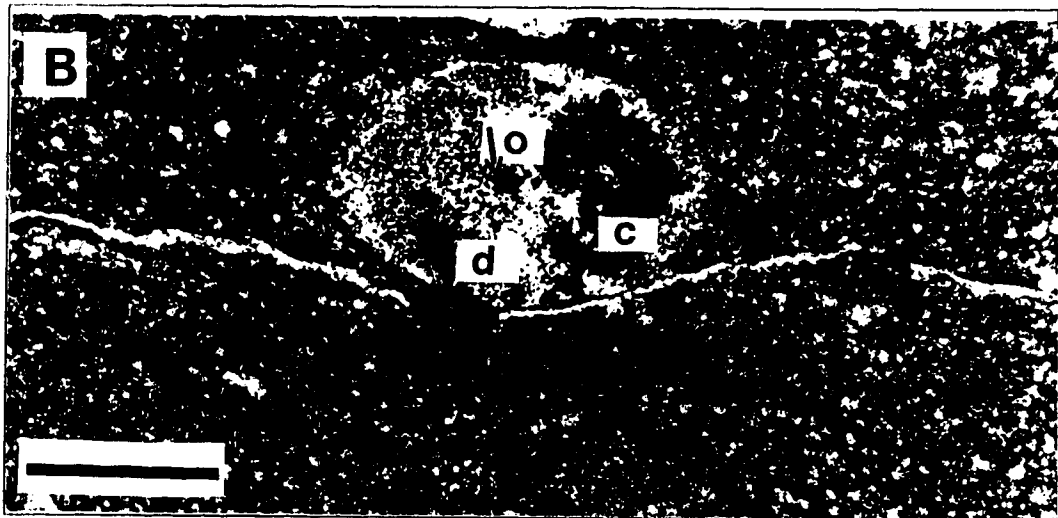
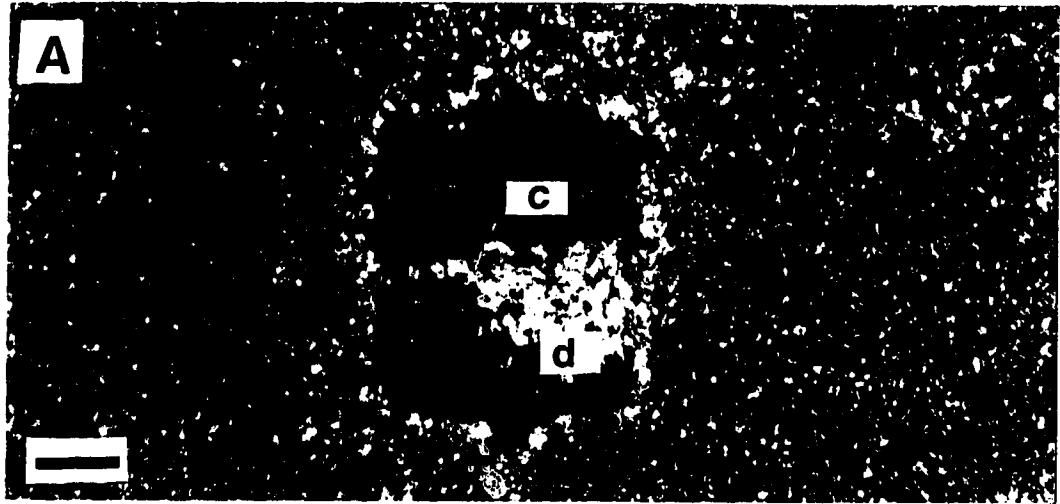


Plate 8. SEM PHOTOMICROGRAPH OF ECHINODERM FRAGMENT

A) SEM photomicrograph entirely of an echinoderm with unimodal crystals (c) which are defined as optically continuous in transmitted light as shown in the previous photomicrographs. Notice the abundant vugs (v). Crystal boundaries are marked by undulating contours (u), one of which is highlighted in black. Echinoderm used here is surrounded by matrix R1 in hand sample. Sample well 10-7-40-2W5 2615.2 m, Homeglen-Rimbey (H-R_c 2615.2). Scale bar is 10 μm .



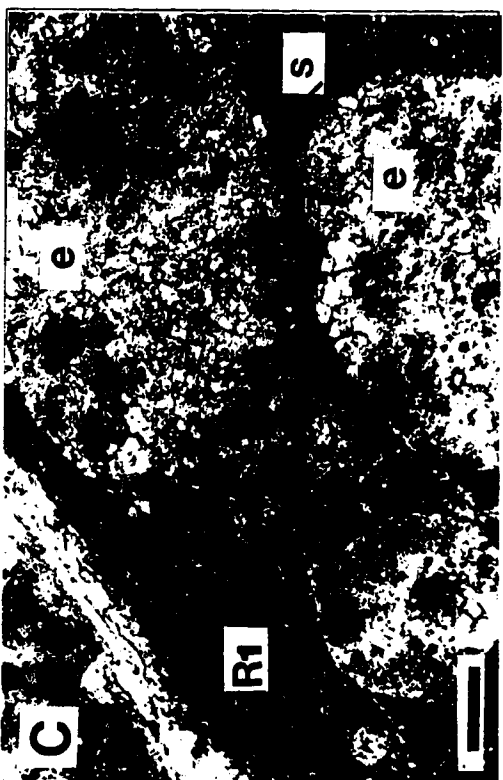
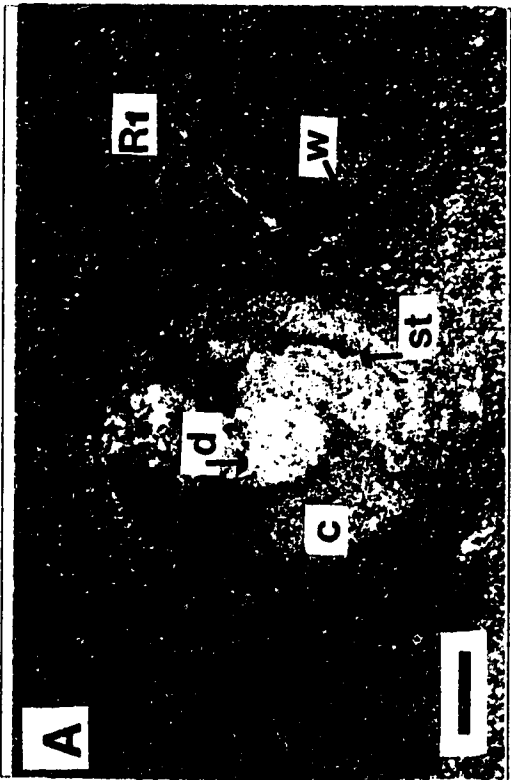
Plate 9. PHOTOMICROGRAPH ILLUSTRATIONS OF STYLOLITES ADJACENT TO ECHINODERM FRAGMENTS.

A) Dolomitized bimodal echinoderm fragment in matrix type R1. Wispy stylolites (w) are abundant within the matrix. Although fragment is entirely dolomitized, there is a section retaining a part of the original stereom structure (st) with a crenulated interior. Optically continuous crystals indicated by (c). Optically discontinuous crystals in the center of the fragment indicated by (d). Sample well 10-7-40-2W5 2623 m, Homeglen-Rimbey reef (H-R_c 2623). Transmitted light. Scale bar is 200 μm .

B) Intraclast comprised of H-R_c 2623 matrix R1 (R1), and surrounded by stylolite (s), in a grainstone sample H-R_c 2629.8. Sample well 10-7-40-2W5 2629.8 Homeglen-Rimbey reef (H-R_c 2629.8). Transmitted light. Scale bar is 400 μm .

C) Several bimodal, bitumen rich echinoderm fragments (e) and quartz filled brachiopod fragments in matrix R1. A stylolite (s) is running between three echinoderm fragments. The optically discontinuous crystals are abundant. Sample well 10-7-40-2W5 2615.2 m, Homeglen-Rimbey reef (H-R_c 2615.2). Transmitted light. Scale bar is 200 μm .

D) Partial bimodal echinoderm fragment (e) in matrix type R2. The stylolite seams (s) are evidence that the fragment underwent pressure solution. Optically continuous crystals indicated by (c). Optically discontinuous crystals indicated by (d). Sample 6-24-34-8W5 4379.9 m, Ricinus (Ricinus_a 4379.9). Transmitted light crossed polars. Scale bar is 200 μm .



includes several optically discontinuous crystals that are larger than the optically continuous crystals. Also in this sample, H-R_c 2629.3, are bitumen rimmed intraclasts of dolomite with the same texture and appearance as sample H-R_c 2623, showing pressure solution contacts with biochems of the deepest grainstone sample (Plate 9B). This is not the only example of pressure solution contacts in echinoderm bearing samples. There are wispy stylolites adjacent to several bimodal crystal echinoderm fragments in both matrix types R1 and R2 (Plate 9A, 9C, and 9D).

CHAPTER SIX

CHEMISTRY RESULTS AND DISCUSSION

No samples of R4 were analyzed because of the paucity of this matrix type, and it was difficult to distinguish from other matrix types in hand sample. Matrix R3 samples were not analyzed for $\delta^{13}\text{C}$, $\delta^{18}\text{O}$ or $^{87}\text{Sr}/^{86}\text{Sr}$ -ratios because of the paucity of sample powder.

X-RAY DIFFRACTION DATA

Unit Cell Parameters

Unit cell parameters indicate how closely the structures of the studied dolomites approach that of ideal dolomite (Table 2) (Land 1980, Malone *et al.* 1994). The $a_0 \pm 0.01$ and $c_0 \pm 0.03$ unit cell parameters (derived from *d-spacings*) of the reef trend matrix samples all lie in a close range near "ideal" dolomite unit cell parameters, 4.8092 Å for a_0 and 16.020 Å for c_0 , with matrix type R1 and one biochem sample trending towards a more calcian composition and less ideal structure (Table 2, Figure 11) (Land 1980).

The range of mole % CaCO_3 determined by measurement of d_{104} for all samples is $51.17 - 47.17 \pm 0.6$ mole %. It is possible to determine mole % MgCO_3 using the a_0 and c_0 unit cell parameters in reference to ideal CaCO_3 and MgCO_3 unit cell parameters (Goldsmith and Graf 1958). This determination is inaccurate in the presence of significant concentrations of iron and manganese which substitute for Mg^{2+} in the dolomite lattice. The high iron content in most Rimbey-Meadowbrook Reef Trend samples precludes its use here (Goldsmith and Graf 1958).

Cation Ordering

Cation ordering can be useful in studies of dolomite recrystallization to separate well ordered recrystallized dolomite from poorly ordered replacement dolomite (Land 1980, McKenzie 1981, Land 1985, Carballo *et al.* 1987, Gregg *et al.* 1992, and Malone *et al.* 1994). High degrees of ordering are interpreted as evidence for recrystallized samples, as well as slow growth, usually in the burial environment. Whereas low degrees

Table #2a. Matrix type R2 dolomite lattice parameters derived from X-ray Diffraction data.

Sample Location	depth (m)	~label	*015/110	mol%CaCO ₃	a	c
3-21-57-24W4	1229.6a	Ach 1547.4	0.72	49.80	4.81	16.01
7-15-55-25W4	1358.8a		0.54	48.90	4.81	16.02
6-22-55-26W4	1562.25		0.60	49.87	4.81	16.01
6-22-55-26W4	1654.2		0.74	50.37	4.81	16.02
2-14-53-26W4	1545.1		0.61	49.87	4.81	16.01
15-23-52-26W4	1547.4		0.68	49.10	4.81	16.01
8-17-50-26W4	1704.4a		0.59	48.37	4.81	16.01
8-17-50-26W4	1704.4b		0.54	50.53	4.81	16.03
8-17-50-26W4	1704.4c		0.58	49.10	4.81	16.01
3-22-48-27W4	1994.37		0.56	50.97	4.81	16.01
3-22-48-27W4	2020.5a	W 2207a	0.48	49.40	4.81	16.02
8-4-46-28W4	2207a		0.61	49.10	4.81	16.02
16-33-45-28W4	2121	H-R ^a 2390	0.53	48.37	4.81	16.00
11-7-43-1W5	2390		0.75	49.10	4.81	16.02
7-22-42-2W5	2402.5a		0.50	49.03	4.81	16.02
7-22-42-2W5	2402.5b	H-R ^b 2514	0.77	50.57	4.81	16.00
14-5-41-2W5	2514		0.61	49.76	4.81	16.01
14-5-41-2W5	2525a		0.87	50.00	4.81	16.01
14-5-41-2W5	2525b	H-R ^b 2525b	0.77	49.86	4.81	16.01
14-28-39-3W5	2823a	H-R ^d 2823a	0.64	49.10	4.81	16.00
14-28-39-3W5	2823b	H-R ^d 2823b	0.67	49.63	4.81	16.00
10-17-37-3W5	2863	SL 2863	0.57	49.40	4.81	16.02
16-32-37-3W5	2982	Strac ^b 4318.3	0.57	49.86	4.81	16.01
13-9-33-4W5	3467		0.66	48.60	4.81	16.01
10-31-37-9W5	4318.3		0.54	49.10	4.81	16.02
7-32-37-9W5	4085.2a		0.50	49.63	4.81	16.01
10-33-36-10W5	4563.9a		0.59	48.37	4.81	16.00
10-33-36-10W5	4661	Ric ^b 4285.2	0.79	49.17	4.81	16.00
11-27-36-10W5	4489.9		0.65	49.83	4.81	16.00
6-14-34-8W5	4285.2		0.81	48.36	4.81	16.01
6-14-34-8W5	4286.9	Ram 5047a	0.65	47.66	4.81	16.02
5-13-37-7W5	5047a		0.53	49.67	4.81	16.01
5-13-37-7W5	5067		0.60	49.17	4.81	16.02
Averages			0.63	49.38	4.81	16.01

*015/110 = cation ordering ratio.

~Labels represent samples discussed in text.

Table #2b. Matrix type R1 dolomite lattice parameters derived from X-ray Diffraction data.

Sample Location	depth (m)	label	015/110	mol%CaCO ₃	a	c
3-21-57-24W4	1229.6b	L-W ^b 1936.7	0.60	49.87	4.81	16.01
8-17-50-26W4	1936.7		0.51	51.17	4.81	16.05
8-4-46-28W4	2207b		0.72	49.60	4.81	16.01
8-4-46-28W4	2234	W 2234	0.56	48.90	4.81	16.02
10-7-40-2W5	2615.2	H-R ^c 2615.2	0.66	50.43	4.81	16.02
10-7-40-2W5	2623	H-R ^c 2623	0.44	49.40	4.81	16.04
16-11-38-5W5	3071	Carol 3360.1a	0.55	49.86	4.81	16.02
11-10-35-5W5	3360.1a		0.63	50.13	4.81	16.02
11-10-35-5W5	3365.9		0.54	50.80	4.81	16.02
7-32-37-9W5	4085.2b	Strac ^a 4085.2b	0.58	49.10	4.81	16.01
Averages			0.58	49.93	4.81	16.02

Table #2c. Matrix type R3 dolomite lattice parameters derived from X-ray Diffraction data.

Sample Location	depth (m)	label	015/110	mol%CaCO ₃	a	c
7-15-55-25W4	1358.8b	RW ^c 4545.4	0.52	50.33	4.81	16.01
15-23-36-10W5	4545.4		0.78	50.37	4.81	16.02
10-33-36-10W5	4563.9b		0.65	48.90	4.81	16.01
10-33-36-10W5	4577.4	RW ^b 4397.9	0.73	49.40	4.81	16.02
7-26-36-10W5	4397.9		0.68	50.00	4.81	16.01
5-13-37-12W5	5047b			49.93	4.81	16.03
Averages			0.67	49.82	4.81	16.02

Table #2d. Dolomitized biochem dolomite lattice parameters derived from X-ray Diffraction data.

Sample Location	depth (m)	label	015/110	mol%CaCO ₃	a	c
15-23-52-26W4	1547.4		0.63	49.57	4.81	16.01
3-22-48-27W4	2020.5b		0.75	50.87	4.81	16.03
8-4-46-28W4	2207c		0.89	50.13	4.81	16.02
11-10-35-5W5	3360.1b		0.66	50.00	4.81	16.02
15-23-36-10W5	4592.5		0.64	47.17	4.81	16.01
6-24-34-8W5	4379.9		0.75	48.90	4.81	16.02
Averages			0.72	49.44	4.81	16.02

Figure 11. Plot of a_0 and c_0 unit cell parameters in angstroms. Symbols represent matrix types and dolomitized biochems. All samples are grouped around the ideal unit cell parameters of $a_0 = 4.8092 \text{ \AA}$ and $c_0 = 16.020 \text{ \AA}$, which represents near ideal dolomite unit cell parameters.

Figure 12. Plot of major elements Ca^{2+} and Mg^{2+} in weight percent. Ideal dolomite contains 13 weight % Mg^{2+} and 21 weight % Ca^{2+} . All non-ideal dolomites with different Mg^{2+} and Ca^{2+} weight percents should fall on the modelled line with negative slope between 28 wt% Mg^{2+} and 40 wt % Ca^{2+} . Data points for the reef trend samples lie on a positive line due to variable contaminants. A correction for the Ca^{2+} and Mg^{2+} concentrations would produce a cluster of samples around 13 wt % Mg^{2+} and 21 wt % Ca^{2+} except for the one R1 sample LW_b 1936.7 set off from the majority.

FIGURE 11

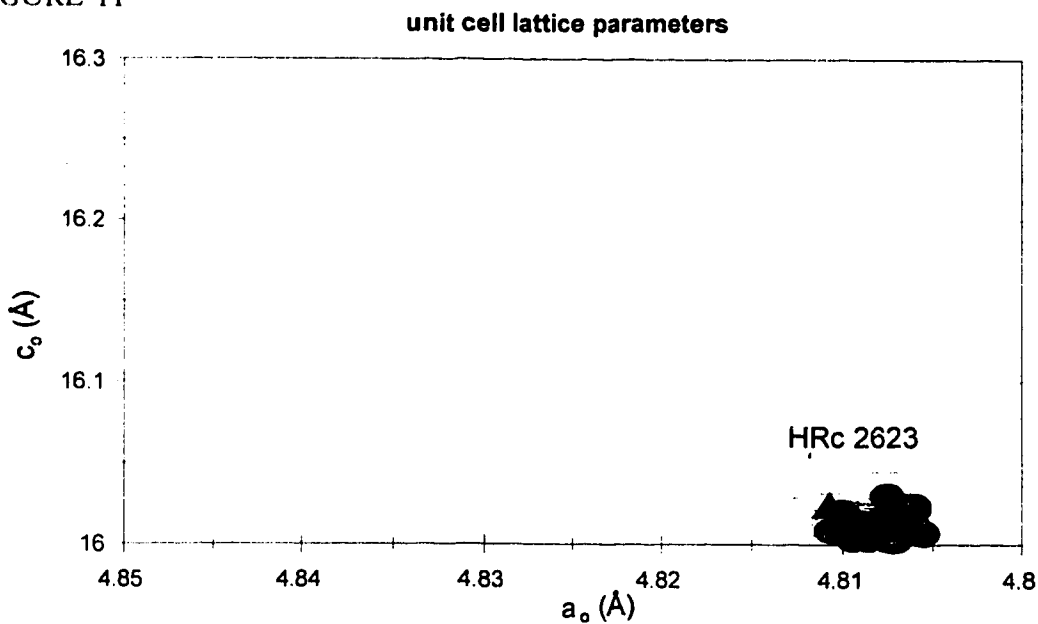
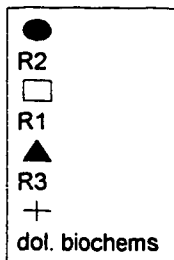
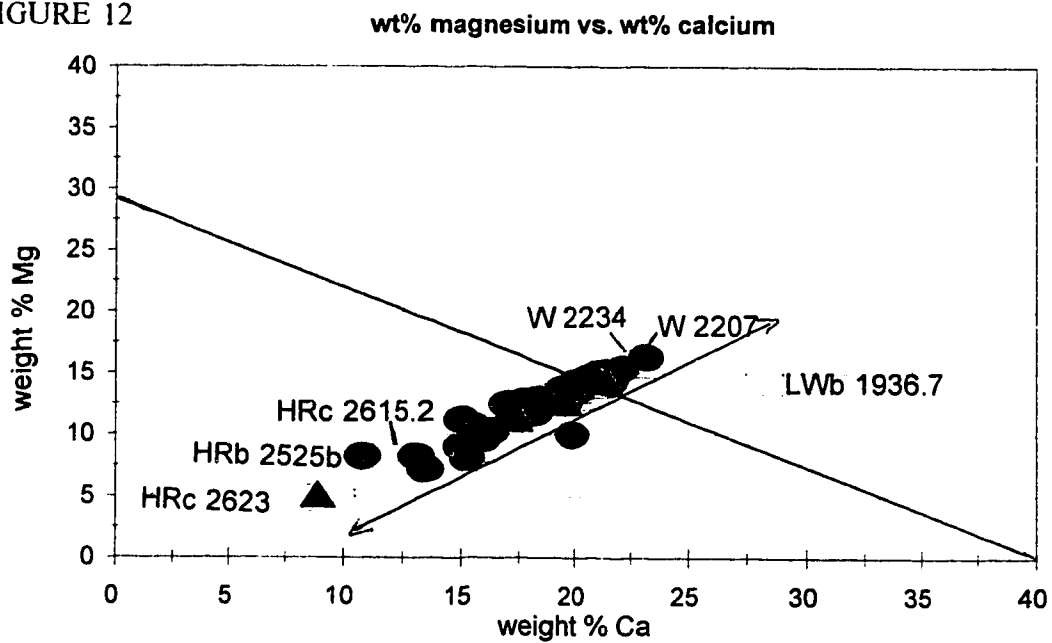


FIGURE 12



of ordering are commonly interpreted as evidence of replacement dolomite, or fast crystal growth (Land 1980, McKenzie 1981, Gregg and Sibley 1984, Land 1985, Carballo et al. 1987, Sibley and Gregg 1987, Gregg et al. 1992, and Malone *et al.* 1994). Cation ordering ratios were determined by peak intensity ratios (Table 2), but they are imprecise for reasons discussed in Chapter 4. The presence of the ordering peak {015} in the XRD analyses suggests that all matrix types and dolomitized biochems examined in this study are well ordered. Cation ordering averages are used to indicate the close range of the ordering ratios for each matrix type, but must not be used for any kind of interpretation;

	range	average
matrix R1	0.44 to 0.72	0.579,
matrix R2	0.48 to 0.81	0.639,
matrix R3	0.52 to 0.78	0.673,
biochems	0.64 to 0.89	0.721.

The determination of cation ordering ({015/110} peak intensity ratio) (Goldsmith and Graf 1958) was hindered by the sample preparation procedure used. Preferred orientation is a common problem for carbonates and may have been enhanced by the "alcohol slurry" procedure used here. XRD technique requires that for the determination of cation ordering ratios, the samples are randomly oriented so all possible grain orientations are represented, and so all the intensities of all possible diffraction peaks are measured accurately. Preferred orientation of the dolomite samples apparently impeded this requirement and resulted in widely varying intensities for the small peaks used for determination of ordering (015, ordering peak and 110, diffraction peak). Therefore, this sample preparation technique should not be used if ordering ratios are desired.

MAJOR ELEMENTS

Magnesium and Calcium

Well ordered and stoichiometric ('ideal') dolomite contains about 13 weight % Mg and 21 weight % Ca. On a plot of wt.% Ca vs wt.% Mg (Figure 12), nonideal dolomite (containing only Ca, Mg, and CO₃) should produce a negative trend through 'ideal dolomite' composition, as modelled on Figure 12. The data from the reef trend form a

positive slope instead of the expected negative slope (Table 3, Figure 12). With the exception of one R1 sample, 8-17-50-26W4 1936.7 m (L-W_b 1936.7), the data lie close to the composition of well ordered and stoichiometric dolomite, around 13 wt. % Mg and 21 wt. % Ca, if the data for all samples are corrected (Appendix C) to fit the model dolomite line. The strong acid used in the standard ion chromatography and ICP-MS sample preparation (p. 34) probably dissolved minerals other than the desired carbonate, resulting in samples enriched and depleted in Ca and Mg. The samples under the theoretical line with negative slope on Figure 12 appear to have been contaminated by a substance with low concentrations of Ca and Mg (such as silica-rich detritus) creating the depleted wt. percents of Ca and Mg. The samples above the theoretical line with negative slope were probably contaminated by a substance rich in Ca and Mg (such as anhydrite and illite, respectively) creating the elevated weight percents of Ca and Mg. These non-carbonate substances have been observed adjacent to the dolomite matrix through petrographic analysis during this study (Plate 1E & 9C, 1B, respectively).

For the pure dolomite, concentrations of Ca can be calculated using mole % CaCO₃ from the XRD analysis. The Mg concentrations, however, cannot be calculated from the XRD analysis for reasons discussed above.

TRACE ELEMENTS

Aluminum and Silica

Aluminum and silica can be used to determine the extent of clay leaching into the trace element sample solutions. The highest concentrations of Al and Si are found in samples of matrix type R1 (Table 3, Figure 13) with lower concentrations in matrix R2 and matrix R3. There is a general positive trend in Figure 13 except for two outliers, matrix R1 sample H-R_c 2615.2, and matrix R2 sample H-R_d 2823b (well 14-28-39-3W5). The finer grained matrix R1 probably originally replaced a finer grained, and muddier, precursor than the coarser grained matrix R2 and R3 dolomites, which, in turn, probably resulted in the lower degree of contamination observed for matrix R2 and R3 samples. Figure 13 shows an apparently higher Al:Si ratio in leachate from matrix R1 dolomites compared to those of R2 and R3. This may indicate a difference in the type of impurity

Table #3a. Matrix type R2 major and selected trace element concentrations (ppm).

Sample Location	depth (m)	label	wt%Mg	wt%Ca	Al ppm	Si ppm
3-21-57-24W4	1229.6a	Ach 1547.4	15.42	22.06	113.76	14.73
7-15-55-25W4	1358.8a		12.69	19.61	17.71	18.00
6-22-55-26W4	1562.25		14.50	21.14	124.26	75.45
6-22-55-26W4	1654.2		8.12	15.23	1.64	7.54
2-14-53-26W4	1545.1		11.25	15.00	75.91	98.60
15-23-52-26W4	1547.4		11.80	18.23	9.76	16.18
8-17-50-26W4	1704.4a		10.33	16.30	85.91	106.01
8-17-50-26W4	1704.4b		12.48	16.93	82.41	90.66
8-17-50-26W4	1704.4c		9.02	14.97	174.40	55.04
3-22-48-27W4	1994.37		14.17	21.55	74.34	78.29
3-22-48-27W4	2020.5a	W 2207a	14.63	21.66	191.62	127.59
8-4-46-28W4	2207a		16.33	23.14	379.77	151.46
16-33-45-28W4	2121	H-R ^a 2390	14.71	20.67	< D.L.	13.57
11-7-43-1W5	2390		8.27	13.08	68.52	51.53
7-22-42-2W5	2402.5a	H-R ^b 2514	14.39	20.33	< D.L.	32.54
7-22-42-2W5	2402.5b		12.90	18.36	47.38	79.90
14-5-41-2W5	2514	H-R ^c 2525a	12.74	17.76	50.92	50.12
14-5-41-2W5	2525a	H-R ^d 2525b	14.27	20.00	37.84	55.04
14-5-41-2W5	2525b	H-R ^e 2823a	8.26	10.78	111.41	60.80
14-28-39-3W5	2823a	H-R ^f 2823b	10.74	15.46	1239.22	211.44
14-28-39-3W5	2823b	SL 2863	12.42	17.82	109.40	655.77
10-17-37-3W5	2863	Strac ^b 4318.3	7.23	13.46	1.95	5.52
16-32-37-3W5	2982		9.66	15.90	22.90	7.42
13-9-33-4W5	3467		15.11	21.34	< D.L.	71.95
10-31-37-9W5	4318.3		13.67	19.38	9.06	40.35
7-32-37-9W5	4085.2a		13.63	20.16	< D.L.	57.03
10-33-36-10W5	4563.9a	Ric ^b 4285.2	12.03	18.21	60.31	56.23
10-33-36-10W5	4661		11.24	17.49	28.27	32.10
11-27-36-10W5	4489.9		14.96	21.02	176.92	164.01
6-14-34-8W5	4285.2		10.03	19.87	7.32	49.87
6-14-34-8W5	4286.9		11.49	17.23	< D.L.	34.43
5-13-37-7W5	5047a	Ram 5047a	14.58	21.54	200.93	103.10
5-13-37-7W5	5067	Ram 5067	14.51	21.13	66.68	102.90
averages					108.20	84.09
LOD ppm (avg.)					1.088	0.9375

Table #3a. cont. Matrix type R2 major and selected trace element concentrations (ppm).

Sample Location	depth (m)	label	Fe ppm	Mn ppm	Rb ppm	Sr ppm
3-21-57-24W4	1229.6a	Ach 1547.4	537.17	93.10	0.35	65.01
7-15-55-25W4	1358.8a		590.21	73.58	0.07	50.07
6-22-55-26W4	1562.25		1311.63	90.13	0.59	81.19
6-22-55-26W4	1654.2		545.01	56.31	0.03	39.89
2-14-53-26W4	1545.1		680.48	67.93	0.28	37.02
15-23-52-26W4	1547.4		1613.72	158.84	0.06	33.85
8-17-50-26W4	1704.4a		948.61	61.76	0.31	45.44
8-17-50-26W4	1704.4b		647.26	73.30	0.30	42.95
8-17-50-26W4	1704.4c		2019.80	95.21	0.46	53.46
3-22-48-27W4	1994.37		1242.92	88.52	0.25	52.12
3-22-48-27W4	2020.5a	W 2207a	1360.37	89.39	0.55	81.16
8-4-46-28W4	2207a		3028.21	91.29	1.26	51.10
16-33-45-28W4	2121	H-R ^a 2390	468.45	69.15	< D.L.	35.25
11-7-43-1W5	2390		1287.50	57.24	0.18	22.27
7-22-42-2W5	2402.5a	H-R ^b 2514	1698.44	82.16	0.01	40.43
7-22-42-2W5	2402.5b		1438.41	88.00	0.16	56.63
14-5-41-2W5	2514	H-R ^b 2514	1637.98	88.17	0.26	45.11
14-5-41-2W5	2525a	H-R ^b 2525a	1384.03	80.85	0.40	53.80
14-5-41-2W5	2525b	H-R ^b 2525b	1067.19	55.77	0.25	43.75
14-28-39-3W5	2823a	H-R ^c 2823a	2409.45	69.15	2.87	47.12
14-28-39-3W5	2823b	H-R ^c 2823b	7699.39	232.67	0.64	58.92
10-17-37-3W5	2863	SL 2863	88.08	4.17	0.01	9.83
16-32-37-3W5	2982	Strac ^b 4318.3	50.78	66.76	0.06	50.05
13-9-33-4W5	3467		917.67	93.20	0.15	41.85
10-31-37-9W5	4318.3		1721.03	162.15	0.11	31.51
7-32-37-9W5	4085.2a		770.55	80.74	0.04	33.60
10-33-36-10W5	4563.9a		1433.04	102.26	0.47	54.36
10-33-36-10W5	4661	Ric ^b 4285.2	510.57	97.46	0.17	49.92
11-27-36-10W5	4489.9		1139.97	95.45	0.95	28.88
6-14-34-8W5	4285.2		1019.15	72.14	0.09	236.03
6-14-34-8W5	4286.9		1046.80	71.12	0.07	28.48
5-13-37-7W5	5047a	Ram 5047a	2892.96	347.17	0.33	63.54
5-13-37-7W5	5067	Ram 5067	2474.80	284.82	0.16	33.24
averages			1444.90	101.21	0.36	51.45
LOD ppm (avg.)			1.283	0.0105	0.0034	0.00545

Table #3b. Matrix type R1 major and selected trace element concentrations (ppm).

Sample Location	depth (m)	label	wt % Mg	wt % Ca	Al ppm	Si ppm
3-21-57-24W4	1229.6b		13.13	20.05	256.88	96.70
8-17-50-26W4	1936.7	L-W ^b 1936.7	14.43	28.21	175.55	125.79
8-4-46-28W4	2207b		13.67	19.95	506.06	134.84
8-4-46-28W4	2234	W 2234	15.79	22.92	188.46	175.00
10-7-40-2W5	2615.1	H-R ^c 2615.2	8.13	11.48	7166.85	227.00
10-7-40-2W5	2623	H-R ^c 2623	4.83	7.88	1558.59	326.42
16-11-38-5W5	3071		12.52	17.65	32.28	254.31
11-10-35-5W5	3360.1a	Carol 3360.1a	11.38	17.38	1280.54	236.99
11-10-35-5W5	3365.9	Carol 3365.9	14.10	20.68	1509.45	206.78
7-32-37-9W5	4085.2b	Strac ^a 4085.2b	13.07	19.23	31.36	95.50
averages			12.11	18.54	1270.60	187.93
LOD ppm (avg.)					1.088	0.9375

Table #3c. Matrix type R3 major and selected trace element concentrations (ppm).

Sample Location	depth (m)	label	wt % Mg	wt % Ca	Al ppm	Si ppm
7-15-55-25W4	1358.8b		11.40	17.41	12.58	27.59
15-23-36-10W5	4545.4	RW ^c 4545.4	14.60	20.88	98.46	227.00
10-33-36-10W5	4563.9 b	RW ^a 4563.9b	10.69	18.76	53.95	42.50
10-33-36-10W5	4577.4		8.98	8.92	12.25	75.14
7-26-36-10W5	4397.9	RW ^b 4397.9	14.78	20.89	< D.L.	81.29
5-13-37-12W5	5047b	Ram 5047b	14.41	21.35	42.27	52.17
averages			12.18	18.04	36.58	84.28
LOD ppm (avg.)					1.088	0.9375

Table #3d. Dolomitized biochem major and selected trace element concentrations (ppm).

Sample Location	depth (m)	label	wt % Mg	wt % Ca	Al ppm	Si ppm
15-23-52-26W4	1547.4		4.47	9.31	21.96	117.96
3-22-48-27W4	2020.5b		7.73	15.67	22.62	46.97
8-4-46-28W4	2207c		12.46	18.09	28.44	79.31
11-10-35-5W5	3360.1b		11.44	17.61	1194.24	156.68
15-23-36-10W5	4592.5		5.52	10.48	< D.L.	29.76
6-24-34-8W5	4379.9		13.91	20.55	7.20	18.31
averages			9.26	15.29	212.41	74.83
LOD ppm (avg.)					1.088	0.9375

Table #3b. cont. Matrix type R1 major and selected trace element concentrations (ppm).

Sample Location	depth (m)	label	Fe ppm	Mn ppm	Rb ppm	Sr ppm
3-21-57-24W4	1229.6b		926.49	77.23	0.87	54.98
8-17-50-26W4	1936.7	L-W ^b 1936.7	8191.53	217.15	0.61	47.63
8-4-46-28W4	2207b		1816.30	73.17	1.71	32.85
8-4-46-28W4	2234	W 2234	2159.61	87.33	0.47	66.45
10-7-40-2W5	2615.1	H-R ^c 2615.2	14189.14	315.53	13.22	45.65
10-7-40-2W5	2623	H-R ^c 2623	5567.19	174.48	6.22	34.41
16-11-38-5W5	3071		828.53	58.73	0.24	29.42
11-10-35-5W5	3360.1a	Carol 3360.1a	3727.98	77.08	5.34	55.39
11-10-35-5W5	3365.9	Carol 3365.9	1979.69	72.53	4.16	58.97
7-32-37-9W5	4085.2b	Strac ^a 4085.2b	1696.56	152.05	0.22	24.41
averages			4108.30	130.53	3.31	45.02
LOD ppm(ave)			1.283	0.0105	0.0034	0.0055

Table #3c. cont. Matrix type R3 major and selected trace element concentrations (ppm).

Sample Location	depth (m)	label	Fe ppm	Mn ppm	Rb ppm	Sr ppm
7-15-55-25W4	1358.8b		606.76	67.88	0.03	40.43
15-23-36-10W5	4545.4	RW ^c 4545.4	817.00	125.86	0.32	86.05
10-33-36-10W5	4563.9 b	RW ^a 4563.9b	919.55	155.58	0.21	32.70
10-33-36-10W5	4577.4		663.37	44.43	0.08	15.30
7-26-36-10W5	4397.9	RW ^b 4397.9	1350.30	125.53	0.07	30.93
5-13-37-12W5	5047b	Ram 5047b	2099.99	287.94	0.25	82.02
averages			1076.16	134.54	0.16	47.90
LOD ppm(ave)			1.283	0.0105	0.0034	0.0055

Table #3d. cont. Dolomitized biochem major and selected trace element concentrations (ppm).

Sample Location	depth (m)	label	Fe ppm	Mn ppm	Rb ppm	Sr ppm
15-23-52-26W4	1547.4		427.47	56.50	0.02	10.00
3-22-48-27W4	2020.5b		368.91	44.33	0.06	47.16
8-4-46-28W4	2207c		714.05	59.96	0.14	33.49
11-10-35-5W5	3360.1b		4203.08	79.75	5.25	58.39
15-23-36-10W5	4592.5		470.85	66.76	< D.L.	43.25
6-24-34-8W5	4379.9		< D.L.	66.42	0.18	63.06
averages			1030.73	62.28	0.94	42.56
LOD ppm(ave)			1.283	0.0105	0.0034	0.0055

Figure 13. Plot of trace elements aluminum and silica. Al and Si are indicators for clay content in the sample solutions analyzed.

Figure 14 A. Plot of iron vs. aluminum. Two trends are visible, one of increasing Fe and Al; the second of increasing Fe at relatively constant, low Al. Matrix R1 samples appear to follow the first trend while R2 and R3 appear to follow the second one.

FIGURE 13

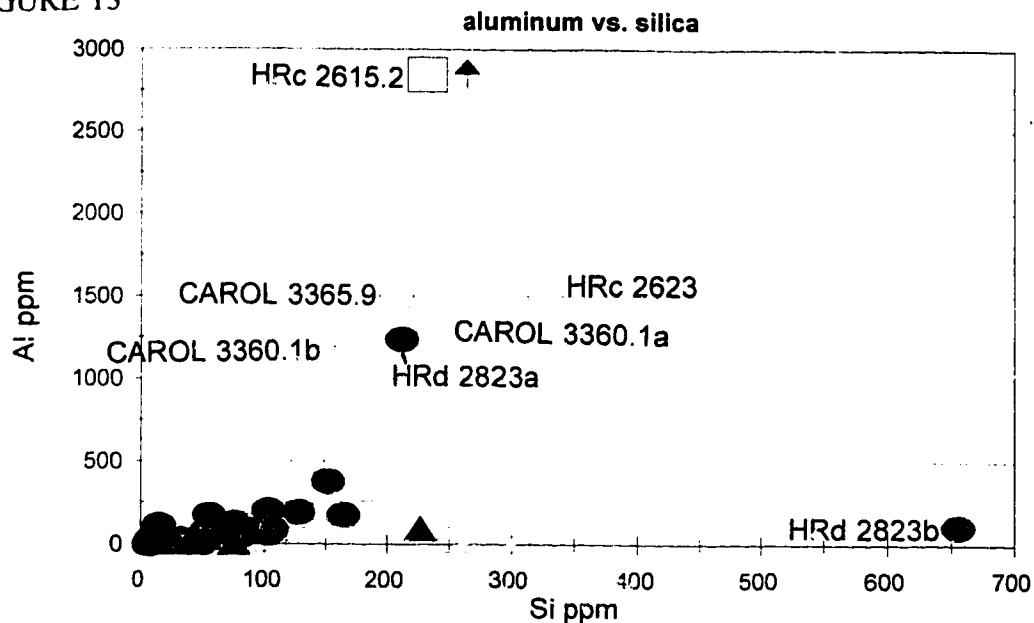
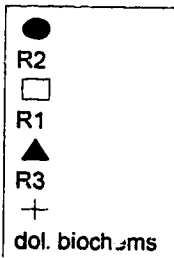
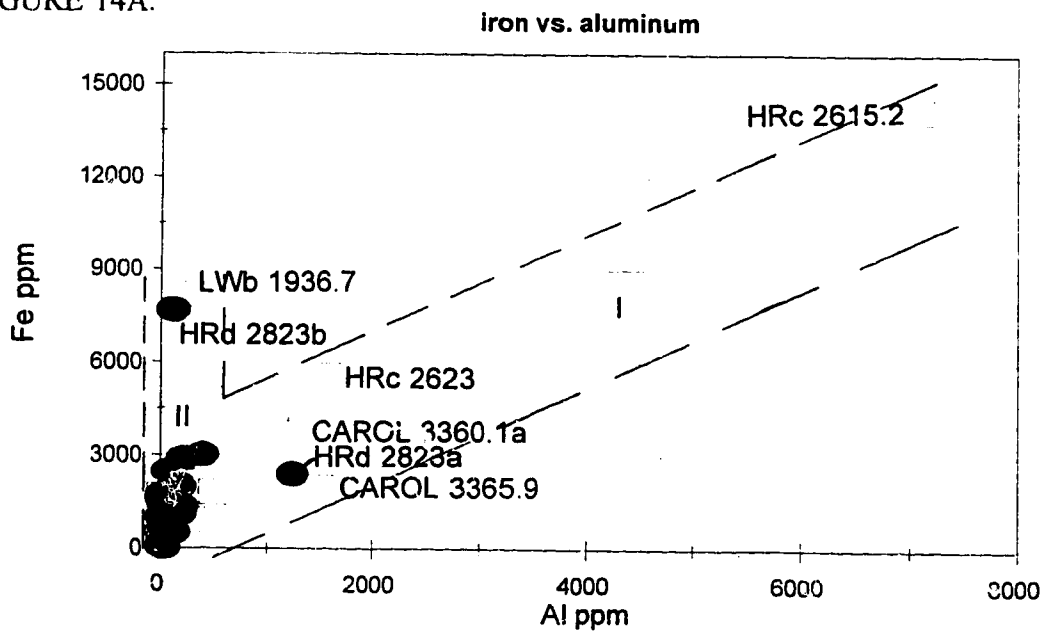


FIGURE 14A.



being leached in each case, *i.e.*, a difference in detrital grains or clay minerals. This varied impurity leaching occurs not only between matrix types, but within matrix R2 types as well, as listed in Table 3a, *e.g.*, samples H-R 2525a and b (previously mentioned with respect to CL mottling textures), where b contains higher Al and Si concentrations. Also H-R 2823a and b where a contains more Al, but b contains more Si, although both sets of samples have similar lattice parameters. This intra-matrix type variation, then, is probably the result of different impurities included in the samples, and is not proportional to the major element contamination discussed above.

Iron

Iron may be present in the carbonate structure or in detrital or authigenic impurities such as clays, pyrite, *etc.*, present as intercrystalline detritus with the carbonate. Matrix type R1 shows an Fe enrichment trend with corresponding Al and Si enrichment (Table 3, Figure 14). Matrix types R2, R3, and dolomitized biochems have lower Fe concentrations than the matrix type R1. All matrix R2 and R3 samples, except for one R2 sample, HR_d 2823b, have < 3000 ppm Fe in conjunction with low Al and Si concentrations as shown in Figure 13. Iron concentrations for all three matrix types are only poorly correlated with Al and Si (Figures 14A, 14B), except for R1, and may therefore be the result of a factor other than leaching of impurities discussed above (Figures 13, 14A and 14B). Matrix R2 samples H-R 2823a and b as listed in Table 3a contain varied Fe concentrations, as well as varied Al and Si concentrations as discussed above, which probably result from varied impurities leached into the sample solutions.

Manganese

Both Mn and Fe can enter the carbonate lattice in significant quantities only in their reduced valence states as Mn²⁺ and Fe²⁺. The presence of Fe and/or Mn in dolomite can give an indication of oxidation-reduction conditions of the fluids present during replacement dolomitization or dolomite recrystallization. On a plot of Fe vs Mn (Figure 15), two separate trends are visible. The samples that form trend I (matrix types R1 and R2) also have elevated concentrations of Al and Si, and the sample solutions are

Figure 14 B. Plot of iron vs. silica. There is a more dispersed pattern of increasing Fe and Si in contrast to the cluster in Figure 14 A.

Figure 15. Plot of trace elements manganese and iron. There are two visible trends, one with increasing Fe and Mn, and one with increasing Mn with a minor increase in Fe. The trend I, with both elevated Fe and Mn concentrations with five matrix R1 and two matrix R2 samples, is further evidence of contamination with clays in the sample solutions. The trend II, with elevated Mn with one matrix R1, four matrix R2, and four matrix R3 samples probably represents more reducing fluid conditions in the deep, southwestern area of the reef trend, during either replacement dolomitization or dolomite recrystallization.

FIGURE 14B.

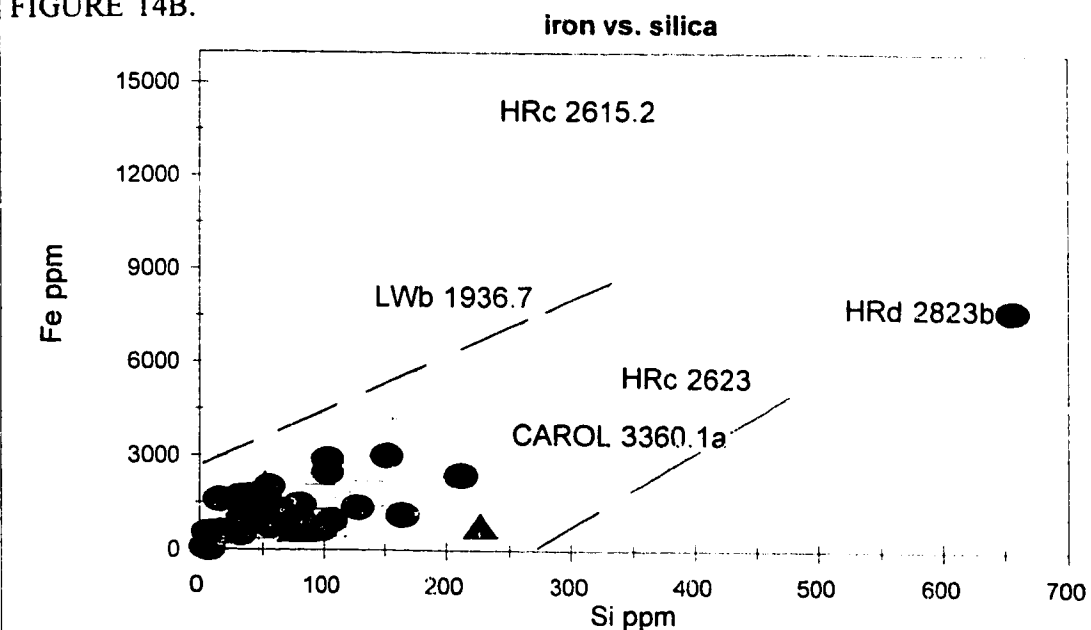
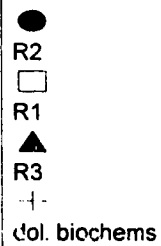
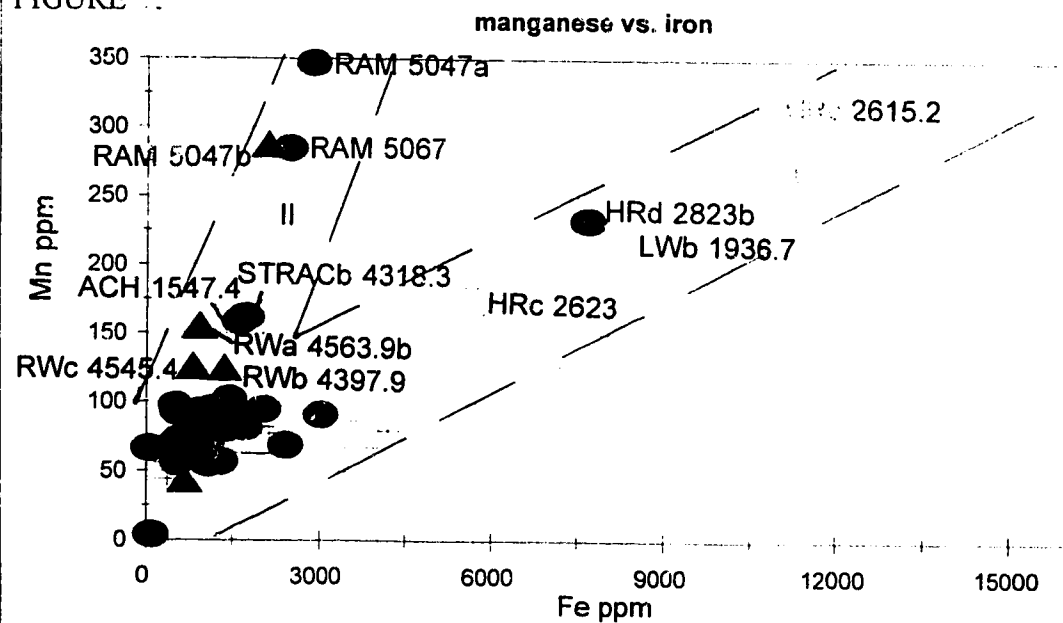


FIGURE 14C.



interpreted to have been contaminated by impurities (Figure 13).

The samples that form trend II, on the other hand, have low Al and Si concentrations, suggesting that this Fe vs Mn trend is probably intrinsic to the carbonates. The samples in trend II are matrix R2 samples Strachan_b 4318.3, Ram River 5047a (5-13-37-7W5 Ram River reef), and Ram River 5067, matrix R3 samples Ricinus West_a 4563.9b, Ricinus West_b 4397.9 (7-26-37-10W5 Ricinus West reef), Ricinus West_c 4545.4 (15-23-36-10W5), and Ram River 5047b, and matrix R1 sample Strachan_a 4085.2b (7-32-37-9W5) from the deepest areas of the reef trend. The concurrence of the Mn enrichment in these deep locations of the reef trend strongly indicates the presence of reducing fluids in this area affecting all three matrix types. In the presence of these reduced fluids (reduction induced by burial depths), the available Mn oxides are reduced, and Mn²⁺ is available to be incorporated into the dolomite, during either replacement dolomitization or dolomite recrystallization (Burns *et al.* 1988). Either (1) the dolomites in this southwestern end of the reef trend have recrystallized under more reducing conditions, (2) the different concentrations of Mn were present in different fluids at different depths (deep matrix R1, R2 and R3 samples vs shallow matrix R1, R2, and R3 samples) during replacement dolomitization of the tilted reef trend, granted that all samples at the same stratigraphic level were under the same temperature and pressure conditions, or (3) the reducing dolomitizing fluid originated in this deep, southwestern part of the reef trend and lost Mn concentrations as it flowed and dolomitized towards the northeast, with decreasing Mn concentrations along the flow path.

There is one shallow matrix R2 sample, the only analyzed sample from the shallower areas of the reef trend, Ach 1547.4 (15-23-52-26W4 Acheson reef), that also has an Mn enrichment with depleted Ca and Mg concentrations (Figure 12). This sample may be evidence that the dolomitizing fluid did flow northeastward, decreasing in Mn content.

Rubidium and Strontium

Rubidium

Rubidium concentrations are usually insignificant as trace elements in the lattice

sites of carbonates where there is no place for such a large ion in the structure, but Rb is more enriched in clays where it commonly enters the K' site. Rb concentrations are assessed in this study because of the influence of clays on analyzed powder samples recognized from the presence of elevated Al and Si concentrations in Figure 13, and inferred from Ca, Mg, Fe, and Mn data where the effects of clay leaching mingle with the dolomite contribution (Figures 12, 14, 15). The elevated concentrations of trace elements, as measured in this study, cannot be part of the carbonate structure. In contrast, most samples contain very low concentrations of Rb (< 1 ppm) (Table 3, Figure 16A). Those samples with ppm Rb > 1 (trend I) are also enriched in Al, Si, Fe, and Mn, and are more likely to have clay impurities contributing to the analyzed solution (e.g., Figure 16B). There is a possibility that an enrichment of Rb, at least 1 ppm in inter-crystalline clays per 50 ppm Sr in the dolomite, can cause an anomalously high radiogenic $^{87}\text{Sr}/^{86}\text{Sr}$ -ratio (Banner 1995) through in-situ decay of the clays. Several samples analyzed in this study show this elevated Rb/Sr ratio. The error associated with this ratio is estimated to be no greater than 0.0003 in the measured $^{87}\text{Sr}/^{86}\text{Sr}$ (Banner 1995). Although this error is low, the measured $^{87}\text{Sr}/^{86}\text{Sr}$ values will not be the original values of these carbonates.

Strontium

Strontium concentrations may reflect paleoenvironments of dolomitization, although most Paleozoic dolostones contain < 200 ppm Sr (Land 1980, Banner 1995). This generalization holds true for the Upper Devonian Rimbey-Meadowbrook Reef Trend where most samples contain less than 100 ppm Sr (Table 3, Figure 16). One R2 sample, Ricinus₆ 4285.2 (6-14-34-8W5), has > 200 ppm Sr, and this anomalously high value may represent the original replacement dolomite phase. There appears to be a second trend, II, in Figure 16A (trend I discussed above), with varying concentrations of Sr in all matrix types. Since all samples, except the one previously mentioned, are within the range of most ancient dolomites, this apparent trend may represent the variability of clay contamination affecting the trace element analysis.

Figure 16. A. Plot of trace elements rubidium and strontium. The majority of reef trend samples have < 100 ppm Sr and < 1 ppm Rb. There is one trend, I, with five matrix R1 and three matrix R2 samples that have elevated Rb concentrations with low Sr concentrations. Rb is usually insignificant in dolomite and is suggested to be concentrated in these samples through clay contamination during sample preparation. There appears to be a second trend, II, with varying concentrations of Sr in all matrix types. Considering that all samples, except one, are within the range of most ancient dolomites, this apparent trend may represent the variability of the amount and type of clay contamination during sample preparation. B. Plot of rubidium and silica. This plot shows the enrichment of silica in samples with > 1 ppm Rb, indicating that clays may be the source for the measured elevated Rb concentrations (> 1 ppm).

FIGURE 16A.

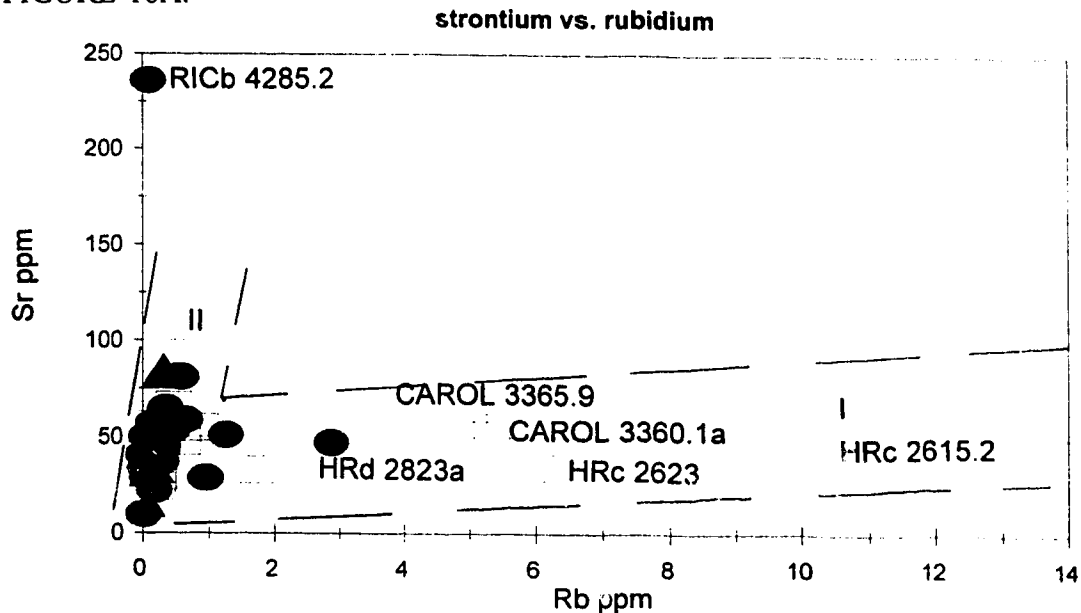
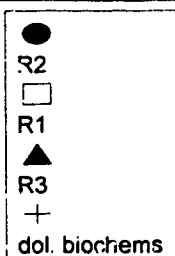
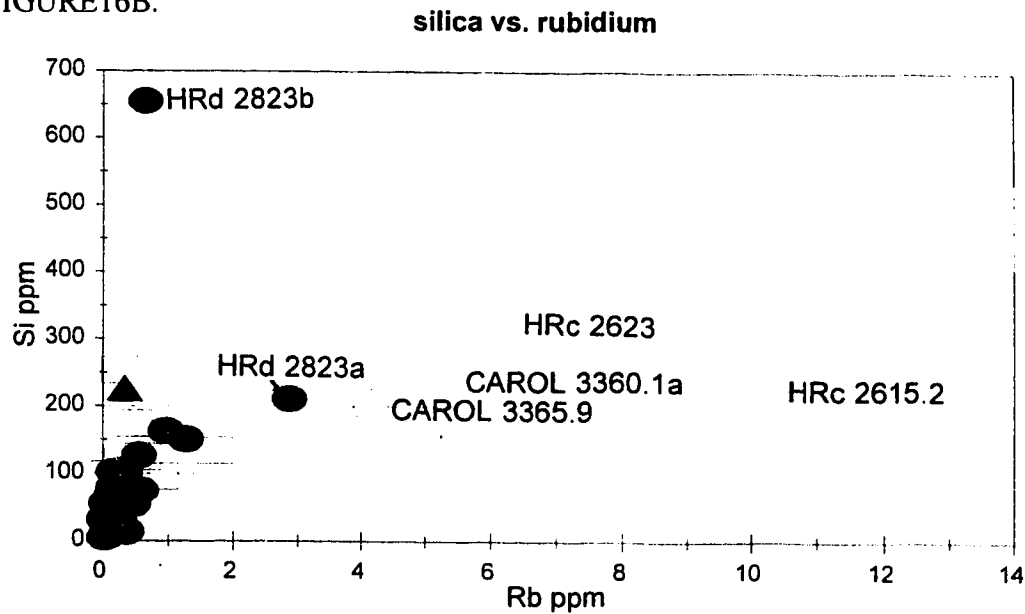


FIGURE 16B.



STABLE ISOTOPES

$\delta^{13}\text{C}$

The carbon isotope composition of replacement dolomite is usually representative of the precursor carbonate material because the original limestone is the major carbon reservoir, and because there is little fractionation of carbon during replacement, even at elevated temperatures. Any variation of $\delta^{13}\text{C}$ from what it may be expected to be after replacement dolomitization in a specific environment, *i.e.*, near seawater values after dolomitization in marine derived fluids, may be the result of the breakdown of organic material in the burial replacement environment, or the recrystallization environment (Curtis *et al.* 1972, Irwin *et al.* 1977, Malone *et al.* 1994).

Most $\delta^{13}\text{C}$ ratios of the 27 samples analyzed in this study lie within the theoretical Late Devonian marine range of +1.5 to +3.5 ‰ PDB for the precursor reef trend limestone (Table 4, Figure 17) (theoretical values derived in Amthor *et al.* 1993 and Drivet 1993). Three matrix R1 samples and two matrix R2 samples lie outside this range. Three of the five outliers, two matrix R1, Mor 1624.6 (Morinville reef 2-16-55-25W4) and L-W_b, 1936.7, and one matrix R2, Strachan_b, 4318.3, are slightly more positive than the hypothetical range, between +4.0 and +5.0 ‰ PDB. Mor 1624.6 has not been mentioned previously, but L-W_b, 1936.7 was previously discussed with respect to Mg and Ca major element concentrations, and Strachan_b, 4318.3 has elevated Mn concentrations. These three samples may have slightly elevated $\delta^{13}\text{C}$ values from bacterial methanogenesis (carbon dioxide reduction or fermentation) during replacement dolomitization (Figure 18) (Irwin *et al.* 1977, Malone *et al.* 1994). The other two outliers, both matrix R1, H-R_c, 2623, discussed with respect to bimodal crystal echinoderm fragments, and Carol 3365.9 (Caroline reef 11-10-35-5W5), not previously mentioned, are more negative than the hypothetical range, lying near 0 ‰ PDB (Figure 17). For these two negative outliers, the depleted values may represent replacement dolomitization in either the zone of bacterial methanogenesis or thermocatalytic decarboxylation of organic matter (Figure 18) (Claypool and Kaplan 1974, Malone *et al.* 1994).

Table #4a. Matrix type R2 carbon, oxygen, and strontium isotope compositions.

Sample Location	depth (m)	label	$\delta^{13}\text{C}^*$	$\delta^{18}\text{O}^*$	$^{87}\text{Sr}/^{86}\text{Sr}^*$
3-21-57-24W4	1229.6a	Ach 1547.4	1.30	-5.58	0.70825 \pm 2
6-22-55-26W4	1562.25		1.99	-5.65	
6-22-55-26W4	1654.2		1.57	-5.37	0.70851 \pm 3
2-14-53-26W4	1545.1		2.75	-6.65	0.70852 \pm 3
15-23-52-26W4	1547.4		2.10	-5.92	0.70849 \pm 3
8-17-50-26W4	1704.4a		2.05	-6.07	0.70842 \pm 2
8-17-50-26W4	1704.4b		2.20	-5.92	0.70831 \pm 2
3-22-48-27W4	2020.5a		1.97	-6.36	0.70825 \pm 3
16-33-45-28W4	2121		2.87	-5.67	0.70827 \pm 2
7-22-42-2W5	2402.5b		2.44	-6.54	0.70843 \pm 3
14-5-41-2W5	2525a	H-R ^b 2525a	1.73	-5.81	0.70873 \pm 3
14-5-41-2W5	2525b	H-R ^b 2525b	1.48	-6.51	0.70870 \pm 2
14-28-39-3W5	2823a	H-R ^d 2823a	2.41	-6.39	0.70850 \pm 4
10-17-37-3W5	2863	SL 2863	2.22	-6.17	0.70822 \pm 3
16-32-37-3W5	2982	Strac ^b 4318.3	1.83	-5.3	0.70833 \pm 3
13-9-33-4W5	3467		2.92	-5.7	0.70833 \pm 3
10-31-37-9W5	4318.3		5.03	-3.04	0.70878 \pm 2
10-33-36-10W5	4661	Ram 5047a	1.85	-6.55	
5-13-37-7W5	5047a		1.65	-9.87	0.70888 \pm 2
averages			2.23	-6.06	0.70846

Table #4b. Matrix type R1 carbon, oxygen, and strontium isotopic compositions.

Sample Location	depth (m)	label	$\delta^{13}\text{C}$	$\delta^{18}\text{O}$	$^{87}\text{Sr}/^{86}\text{Sr}$
2-16-55-25W4	1624.6	Mor 1624.6	4.12	-3.73	0.70841 \pm 2
6-11-51-26W4	1759.3	L-W ^a 1759.3	2.82	-6.44	0.70902 \pm 2
8-17-50-26W4	1936.7	L-W ^b 1936.7	3.91	-6.07	0.70861 \pm 3
8-4-46-28W4	2234	W 2234	3.39	-6.00	0.70942 \pm 3
11-3-42-2W5	2390	H-R ^a 2390	1.78	-5.79	0.70836 \pm 3
10-7-40-2W5	2623	H-R ^c 2623	-0.20	-7.21	0.71023 \pm 3
16-11-38-5W5	3071	Carol 3365.9	2.63	-6.24	0.70843 \pm 3
11-10-35-5W5	3365.9		0.30	-4.81	0.70891 \pm 4
averages			2.34	-5.78	0.70892

* $\delta^{13}\text{C}$ and $\delta^{18}\text{O}$ are quoted in permil relative to the Pee Dee Belemnite (PDB) standard. 2 theta errors are estimated at 0.2 permil and 0.3 permil, respectively. $^{87}\text{Sr}/^{86}\text{Sr}$ errors quoted are individual in-run precision, 2 theta.

Figure 17. Plot of stable isotopes $\delta^{13}\text{C}$ and $\delta^{18}\text{O}$ in ‰ PDB. Data points for the majority of reef trend samples plot within the field of hypothetical marine values for $\delta^{13}\text{C}$ and within a four ‰ spread of $\delta^{18}\text{O}$ (theoretical values calculated by Amthor et al. 1993, Drivet 1993, and Marquez 1995), with five outliers. The two matrix R1 samples with heavy $\delta^{13}\text{C}$ values, Mor 1624.6 and LW_b 1936.7, are interpreted to represent either precursor diagenesis or replacement dolomitization of these two samples during methanogenesis (bacterial sulfate reduction) resulting in elevated $\delta^{13}\text{C}$ (Malone *et. al.* 1995). The two matrix R1 samples with light $\delta^{13}\text{C}$ values (near 0 ‰) may have crystallized during either bacterial methanogenesis or thermocatalytic decarboxylation. The R2 sample Ram 5047a has depleted $\delta^{18}\text{O}$ possibly indicating recrystallization in a hot fluid. The matrix R2 and R1 samples, Strac_b 4318.3 and Mor 1624.6 & Carol 3365.9, respectively, may have crystallized in the zone of bacterial methanogenesis.

Figure 18. Carbon isotopic variation during organic matter diagenesis. Depth increases from 0 meters (surface) and varies to about 500 to greater than 1000 meters depth (Hennesy and Knauth 1986). Adapted from Claypool and Kaplan (1974).

FIGURE 17

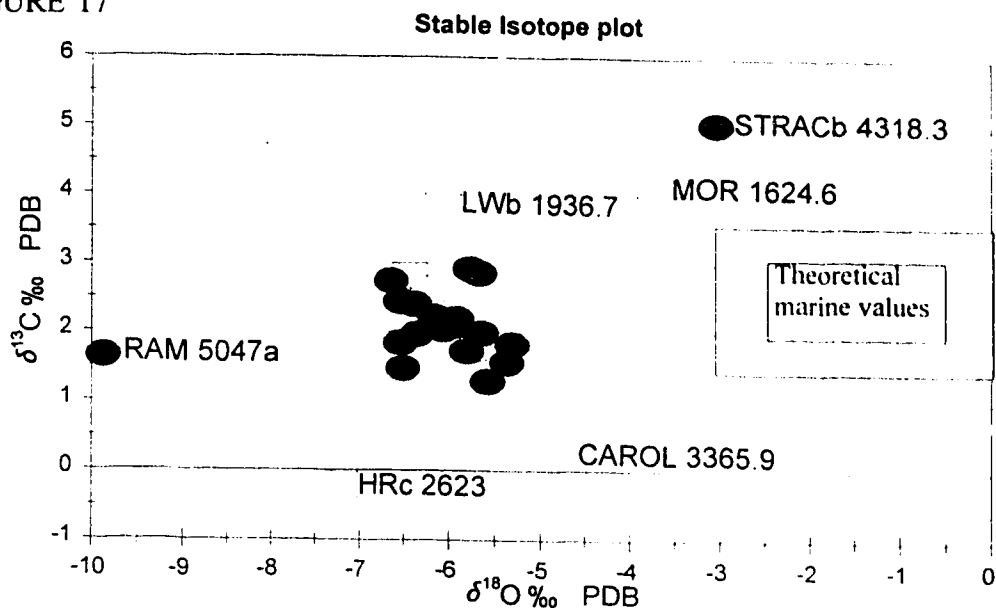
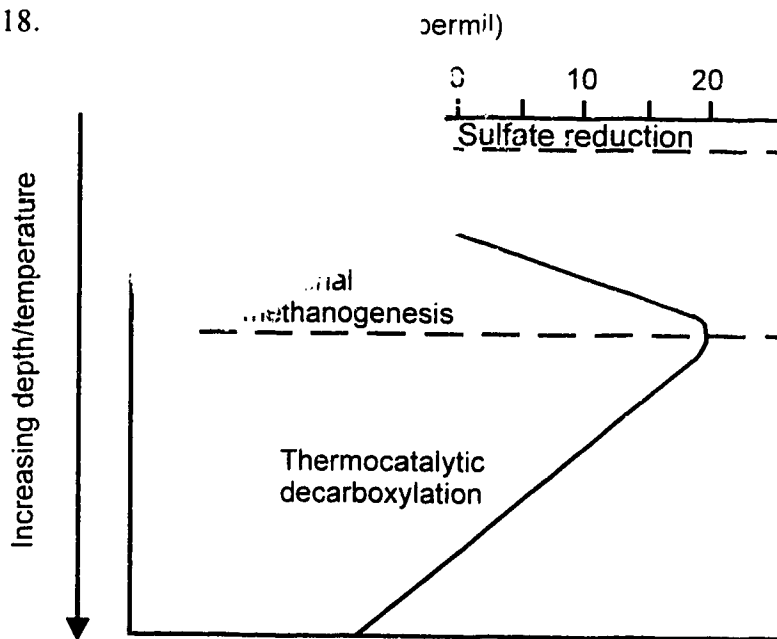


FIGURE 18.



$\delta^{18}\text{O}$

The oxygen isotope composition usually represents both the $\delta^{18}\text{O}$ content of the fluid present during either replacement dolomitization or dolomite recrystallization, and the temperature of dolomite precipitation, either during replacement dolomitization or dolomite recrystallization (the higher the temperature the more negative the ratio, see eq. 2 p.23). Most $\delta^{18}\text{O}$ ratios of the samples analyzed lie within a tight range between -5.3 and -6.7 ‰ PDB (Table 4, Figure 17). This range is 3 to 4 ‰ from the theoretical marine values. This spread indicates that either replacement dolomitization occurred during burial or dolomite recrystallization occurred during burial, both indicating that fluids hotter (between about 45 and 75°C, eq. 2's p.23), and/or more depleted in ^{18}O than Late Devonian sea water created these depleted values.

Of the five outliers, four are also $\delta^{13}\text{C}$ outliers discussed above. Three $\delta^{18}\text{O}$ outliers are more positive than the majority of the samples, two matrix R1, Mor 1624.6, and Carol 3365.9, and one matrix R2, Strachan_b, 4318.3, and lie between -3.0 and -5.0 ‰ PDB (Figure 17). For the Mor 1624.6 sample, also enriched in $\delta^{13}\text{C}$, the ^{13}C and ^{18}O enrichment is suggested to be in agreement with dolomitization in the zone of bacterial methanogenesis as previously suggested. The Carol 3365.9 sample is both enriched in ^{18}O and depleted in ^{13}C , which suggests it was dolomitized at shallow depths and lower temperatures of bacterial methanogenesis (Figure 18). The one enriched $\delta^{18}\text{O}$ value of matrix R2 sample Strachan_b, 4318.3, which has elevated Mn concentrations, (-3.0 ‰ PDB), lies close to the hypothetical marine value for oxygen. This sample also has elevated $\delta^{13}\text{C}$ (+5.0‰ PDB) and was probably affected by bacterial methanogenesis during replacement dolomitization at relatively shallower burial depths and at lower temperature than that at which the majority of sampled matrix dolomites were formed.

The other two $\delta^{18}\text{O}$ outliers, one matrix R1, H-R_c 2623, and one matrix R2, Ram River 5047a, are more depleted than the majority of analyzed samples, and lie between -7.2 and -9.9 ‰ PDB (Figure 17). Sample H-R_c 2623 was mentioned previously with respect to echinoderm fragments and has a depleted $\delta^{13}\text{C}$, may indicate that this sample was in the zone of thermocatalytic decarboxylation during replacement dolomitization (Figure 18). Sample Ram River 5047a was mentioned previously with respect to elevated

Mn concentrations, and the depleted $\delta^{18}\text{O}$ value of this sample may indicate either contamination by calcite or replacement dolomitization, or dolomite recrystallization in a hotter fluid than those that affected the majority of reef trend samples (about 98°C , p.23). The latter scenario is more likely because calcite was not detected in this sample.

RADIOGENIC STRONTIUM ISOTOPES

The strontium isotope composition ($^{87}\text{Sr}/^{86}\text{Sr}$ -ratio) of dolomites is unaffected by the temperature and pressure of crystallization, unlike the compositions of carbon and oxygen ($\delta^{13}\text{C}$ and $\delta^{18}\text{O}$). The $^{87}\text{Sr}/^{86}\text{Sr}$ -ratios reflect the contributions from (1) the host rock (limestone, dolomite, and impurities), (2) any fluids from external sources, and hence (3) the degree of fluid-rock interaction. Prior studies of the Rimbey-Meadowbrook Reef Trend (Amthor *et al.* 1993, Drivet 1993, Mountjoy and Amthor 1994, and Marquez 1994) concluded that replacement dolomites precipitated from fluids chemically evolved from Late Devonian seawater (with $^{87}\text{Sr}/^{86}\text{Sr}$ ranging between 0.7080 and 0.7083) and at slightly elevated (burial) temperatures (about 45° to 75°C).

On a plot of $\delta^{18}\text{O}$ vs $^{87}\text{Sr}/^{86}\text{Sr}$ (Figure 19) the grey rectangle represents theoretical marine values for dolomite precipitation at 25°C in equilibrium with Late Devonian seawater. This field is included in order to place the matrix dolomite samples analyzed in this study in a time frame relative to theoretical Late Devonian seawater at a hypothetical temperature of 25°C . Matrix dolomite types R1 and R2 from the reef trend plot slightly above and to the left of the marine dolomite field, clearly indicating that both matrix types precipitated in the presence of fluids carrying strontium that was more radiogenic than that of seawater, and that these dolomites probably formed at temperatures well above 25°C . These general observations are in accord with prior studies.

The data for R1 and R2 dolomites differ. Radiogenic strontium isotope data for the R2 samples ($n=19$) cluster tightly in both $\delta^{18}\text{O}$ and $^{87}\text{Sr}/^{86}\text{Sr}$ (0.7082-0.7087). There are two outliers (in $\delta^{18}\text{O}$) in the R2 group, Strachan₆ 4318.3 and Ram River 5047a, as discussed in the previous section, but the $\delta^{18}\text{O}$ values for this group appear to be independent of the $^{87}\text{Sr}/^{86}\text{Sr}$ values.

R1 samples, on the other hand ($n=8$) generally have values of $^{87}\text{Sr}/^{86}\text{Sr}$ that are

Figure 19. Plot of $\delta^{18}\text{O}$ vs $^{87}\text{Sr}/^{86}\text{Sr}$. The cross-hatched box represents values calculated for dolomites formed in equilibrium with theoretical Late Devonian seawater at 25°C (Amthor *et al.* 1993, Drivet 1993, Mountjoy and Amthor 1994, Marquez 1994). Data points for the majority of the reef trend samples lie close to or slightly higher than the calculated Late Devonian seawater $^{87}\text{Sr}/^{86}\text{Sr}$ -ratios (Burke *et al.* 1982, Smalley *et al.* 1994). The $\delta^{18}\text{O}$ values of the majority of reef trend samples are lower than the calculated marine value (Amthor *et al.* 1993, Drivet 1993). The highest radiogenic matrix R1 $^{87}\text{Sr}/^{86}\text{Sr}$ -ratio coincides with the highest matrix R1 Rb concentration in Figure 16, and with the lowest R1 $\delta^{13}\text{C}$ and $\delta^{18}\text{O}$ values in Figure 17. This matrix R1 sample may therefore have been affected by a relatively hot fluid which may have incorporated in situ decayed organic matter and inter-crystalline clays rich in ^{87}Sr resulting in the observed ratio.

Figure 20. Plot of trace element rubidium and radiogenic strontium isotopes. The majority of reef trend samples do not show any correlation between Rb and radiogenic strontium ratios. There is a trend, however, with two matrix R1 samples and one matrix R2 sample that show an increase in $^{87}\text{Sr}/^{86}\text{Sr}$ -ratios with an increase in Rb concentrations. The matrix R1 sample with the highest radiogenic $^{87}\text{Sr}/^{86}\text{Sr}$ -ratio (0.7102) and Rb concentrations (6 ppm) may be the only sample in the reef trend to have its radiogenic $^{87}\text{Sr}/^{86}\text{Sr}$ -ratios influenced by clays. The $^{87}\text{Sr}/^{86}\text{Sr}$ -ratios of the two other samples in this trend were probably not influenced by Rb concentrations. See text for specific details for these and samples in trend II.

FIGURE 19

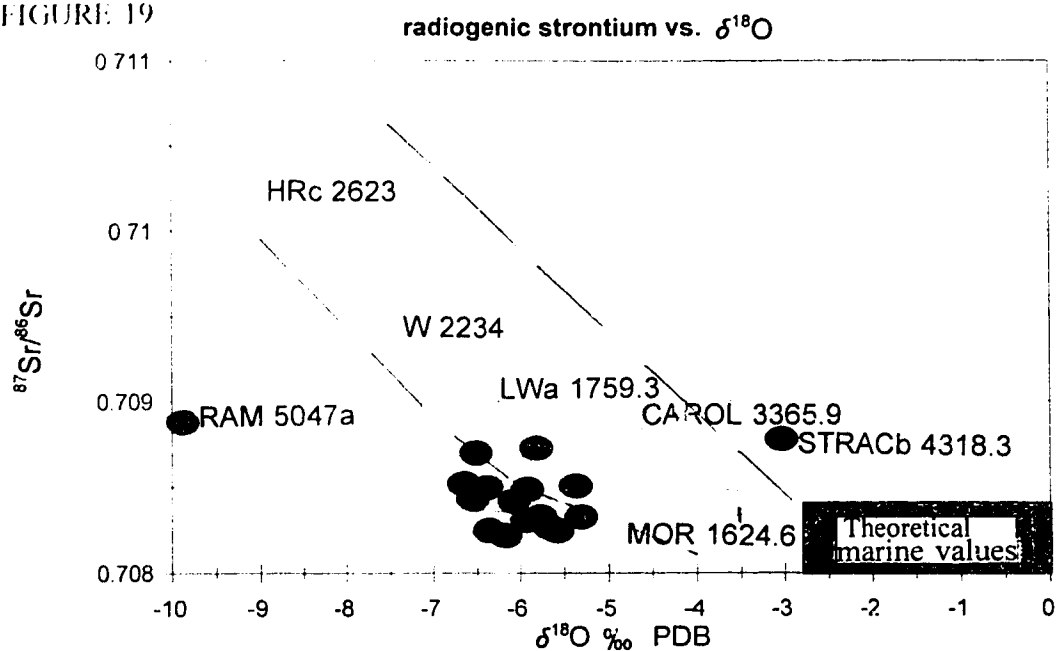
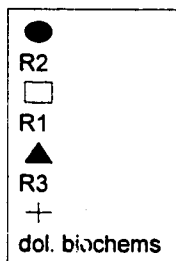
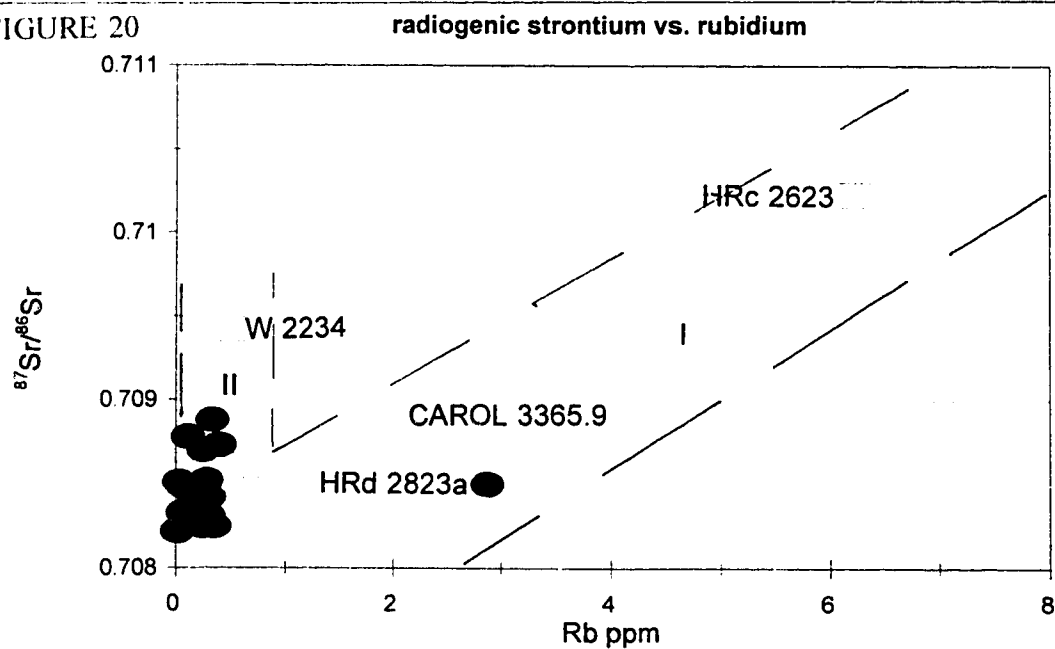


FIGURE 20

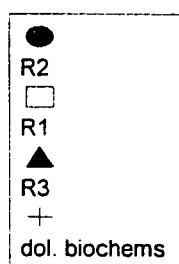
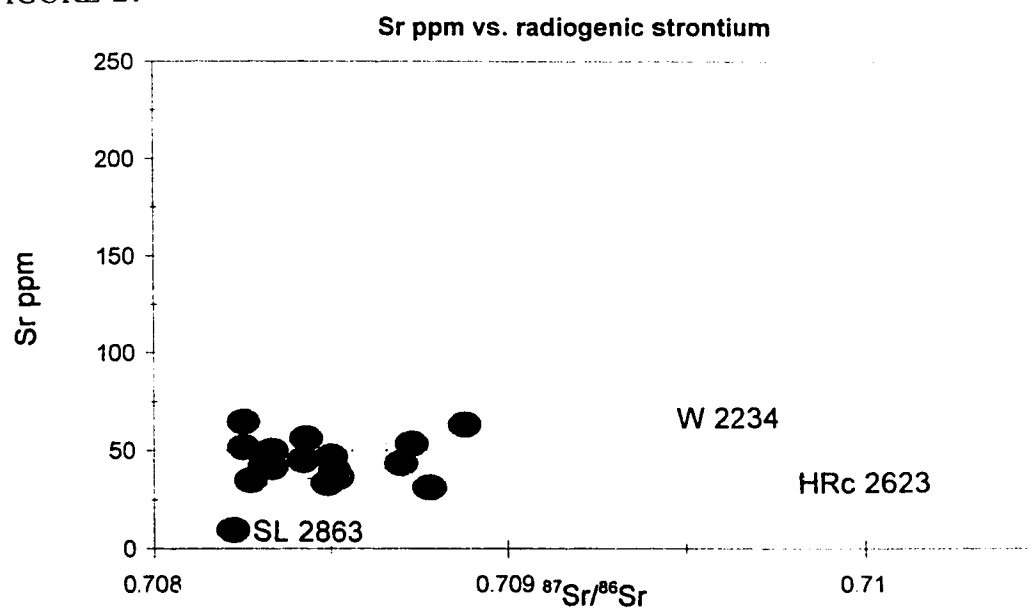


more dispersed and range upward from 0.7084 to 0.7102. There is a weak negative trend of increasing $^{87}\text{Sr}/^{86}\text{Sr}$ with decreasing $\delta^{18}\text{O}$ (increasing temperature). Such a trend would be consistent with increased *local* leaching of radiogenic strontium (^{87}Sr) from clay impurities during precipitation of R1 at higher temperatures. The R1 samples also show a correlation of $^{87}\text{Sr}/^{86}\text{Sr}$ of dolomite with the Rb content as determined by ICP analysis (Figure 20). It should be noted that the strontium isotopic compositions were determined by leaching each sample with dilute HCl (1N) at room temperature to minimize any contribution of ^{87}Sr from clay impurities. In contrast, the ICP sample solutions were prepared by a standard procedure using a strong oxidizing acid (HCl:HNO₃, 1:3); the leaching of Rb from clay minerals is a strong probability under these conditions. Results from the $^{87}\text{Sr}/^{86}\text{Sr}$ analysis and the ICP data are, thus, not directly comparable. Nevertheless, the plot of Rb (ppm) vs $^{87}\text{Sr}/^{86}\text{Sr}$ does suggest that the local (clay impurity) Rb content had an effect on the $^{87}\text{Sr}/^{86}\text{Sr}$ -ratios determined here. This is in accord with results of Banner (1995).

The strontium contents show no correlation with $^{87}\text{Sr}/^{86}\text{Sr}$ (Figure 21) indicating that this is not a simple two endmember mixing model situation. There are two possible endmembers involved in the representation of the $^{87}\text{Sr}/^{86}\text{Sr}$ -ratios, replacement dolomites and recrystallized dolomites. The relatively tight cluster of reef trend matrix R2 samples, with low Sr concentrations (< 100 ppm) and $^{87}\text{Sr}/^{86}\text{Sr}$ -ratios slightly more radiogenic than Late Devonian seawater, may represent an intermediate burial (~300-1600 m) dolomite replacement phase, as suggested by Amthor *et al.* (1993). It is possible that the one matrix R2 sample, SL 2863 (Sylvan Lake reef 10-17-37-3W5), with low Sr concentrations (9.83) ppm and a $^{87}\text{Sr}/^{86}\text{Sr}$ -ratio of 0.7082, may be representative of a thin-film recrystallization environment dolomite, *e.g.*, the Sr concentration decreased without an increase in the radiogenic strontium ratio (Banner 1995). It is also possible that the R2 samples form a relatively tight cluster (compared with R1 samples) as the result of thin-film recrystallization, decreasing the Sr content (as seen in trend II in Figure 16A) without affecting the $^{87}\text{Sr}/^{86}\text{Sr}$ -ratios. The depleted Sr concentrations of the reef trend dolomites compared with other ancient dolostones (< 100 ppm), are probably representative of burial replacement fluid conditions, because they are consistent for all analyzed matrix types.

Figure 21. Plot of trace element strontium and radiogenic strontium isotopes. This plot is used to show if variations of $^{87}\text{Sr}/^{86}\text{Sr}$ are related to the two dolomite endmembers. The majority of the reef trend samples have Sr concentrations around 50 ppm and $^{87}\text{Sr}/^{86}\text{Sr}$ -ratios around 0.7083 - 0.7085 and may represent replacement dolomite fluid strontium isotopic chemistry. One matrix R2 sample has a Sr concentration around 10 ppm and a $^{87}\text{Sr}/^{86}\text{Sr}$ -ratio around 0.7082 and may represent a sample recrystallized in the thin-film fluid environment.

FIGURE 21



CHAPTER SEVEN

EXTENT OF DOLOMITE RECRYSTALLIZATION IN THE RIMBEY- MEADOWBROOK REEF TREND

These petrographic and isotopic data along with the previous and following discussions show that the *extent* of dolomite recrystallization in the Rimbey-Meadowbrook Reef Trend is difficult to determine. Most samples may be either replacement dolomite or underwent only "insignificant recrystallization" (as defined on p. 7). This is because most of the samples analyzed display petrographic and isotopic characteristics that may result from either burial dolomitization *or* from recrystallization of "marine" dolomite, or from a combination of these two processes. Few samples have characteristics indicative of "significant recrystallization" (as defined p. 6-7), and these characteristics are defined with respect to the replacement dolomite samples, not hypothetical precursor ("marine" dolomite) characteristics.

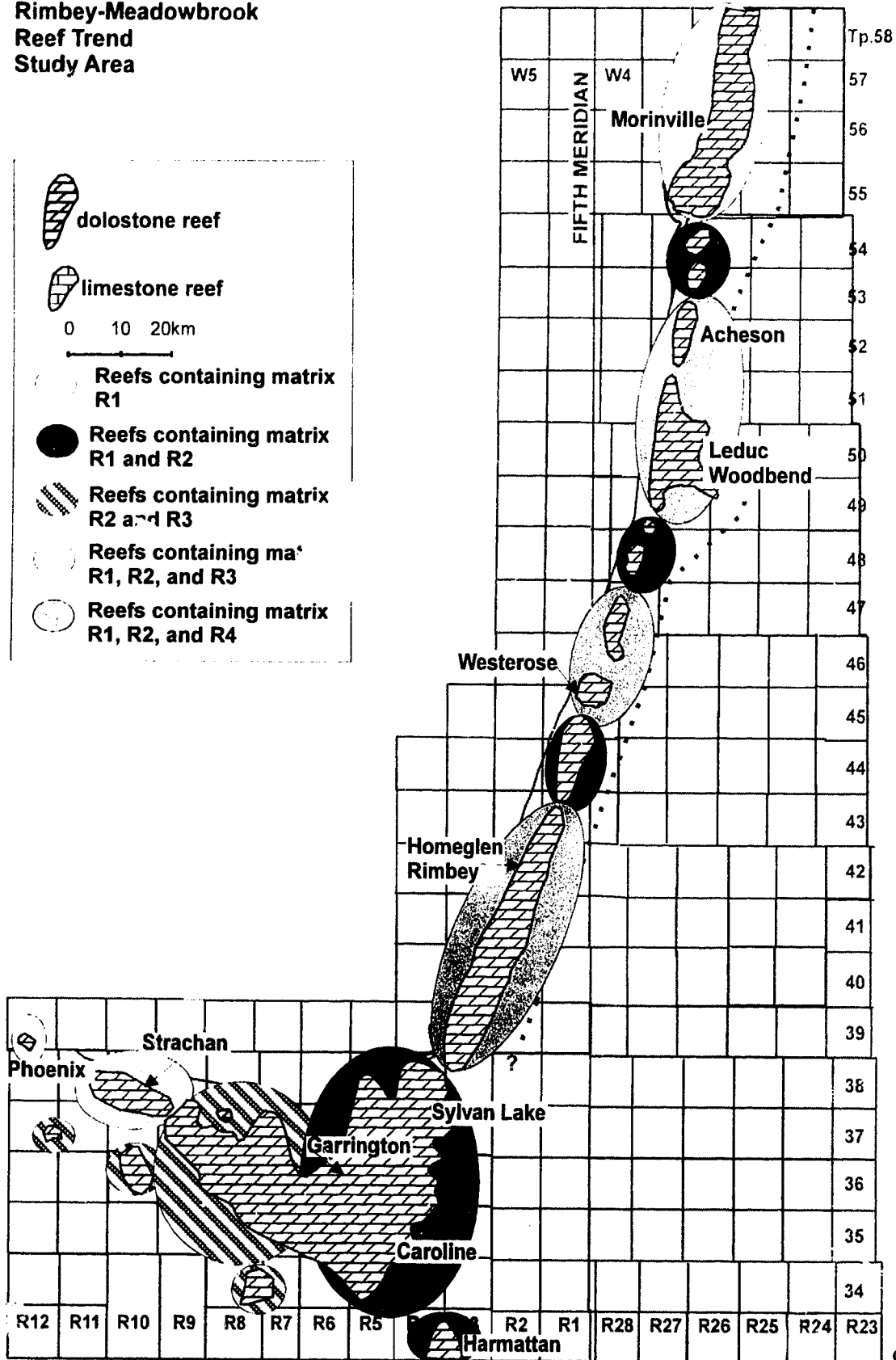
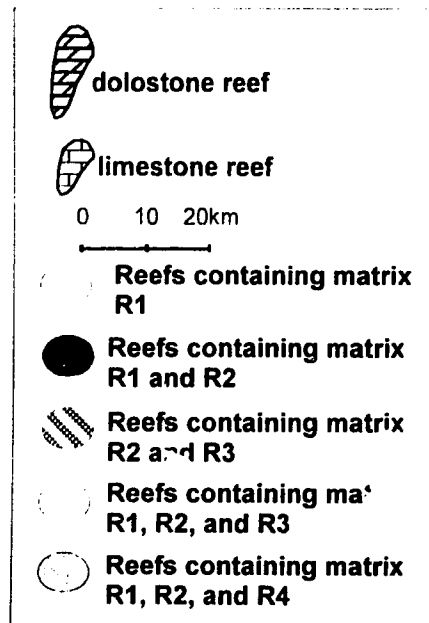
Based on the data obtained in this study, two trends are identified which may suggest that recrystallization took place along the sampled interval of the reef trend. The first trend concerns matrix type abundances, and the second trend concerns geochemical characteristics that vary between matrix types and location. In addition, the bimodal distribution of crystals found in some of the echinoderm fragments may also indicate that recrystallization has taken place. Based on the extent of recrystallized matrix dolomite and echinoderms, possible fluid sources for replacement dolomitization and dolomite recrystallization will be discussed at the end of this chapter.

PETROGRAPHIC TREND

A major objective of this thesis was to determine if there is any petrographic or geochemical trend along the sampled interval of the Rimbey-Meadowbrook Reef Trend (~75 m above underlying Cooking Lake Platform) that may reflect a diagenetic fluid pathway. There is a weak petrographic trend separating the southwestern and northeastern parts of the reef trend, based on the concentrations of matrix types in different reefs (Figure 22). Matrix type R1 is present throughout most of the northeastern reefs between

Figure 22. Distribution of the four types of matrix dolomite along the sampled interval of the Rimbey-Meadowbrook Reef Trend. A weak trend of matrix types is present in the reef trend. Matrix type R2 is the most widespread, occurring throughout the reef trend. Matrix R1 is restricted primarily to the reefs between Morinville and Homeglen-Rimbey, with rare occurrences in Strachan. The occurrence of matrix R1 in the southwestern Phoenix reef is a result of partial dolomitization of micrite matrix in this reef. The deep, southwestern area of the reef trend including the Strachan, Ricinus West, Ricinus, and Ram River reefs, is characterized by the presence of abundant matrix R3, also found in Morinville. Matrix type R4 is sparse and restricted to the Homeglen-Rimbey, Westrose, Leduc, and Acheson reefs.

**Rimbey-Meadowbrook
Reef Trend
Study Area**



Morinville and Garrington / Caroline, in the Strachan reef (one sample), and in the Phoenix reef where it replaces micrite matrix. Matrix type R2 is present throughout the entire reef trend, except for the partially dolomitized Phoenix reef. The widespread distribution of these two matrix types may indicate that they are primarily a result of replacement dolomitization of two different precursor limestone fabrics, *i.e.*, fabric controlled nucleation sites determined texture variations, via fluids at relatively high supersaturation with respect to dolomite (Gregg and Sibley 1984, Sibley and Gregg 1987). The petrographic observation that inclusions of R2 sized crystals form compromise boundaries with matrix R1 crystals in scattered samples (Plate 2A, B) may indicate that these two dolomite textures (R1 and R2) crystallized roughly simultaneously.

Matrix type R3 is abundant at the extreme ends of the reef trend, in the northeastern Morinville reef and in the Chedderville through Ram River reefs in the southwestern section of the reef trend. This distribution may be a result of nucleation sites and/or relatively low fluid supersaturation with respect to dolomite during replacement dolomitization. Both of these possibilities would form coarse, planar-c crystals that are characteristic of matrix R3 (Plate 3) (Gregg and Sibley 1984, Sibley and Gregg 1987). If the distribution of R3 is the result of widely spaced nucleation sites, then it might be expected that these sites were fabric controlled as in the other areas of the reef trend. Possible precursor fabrics would be open pore space, cements, or large grains (presumably biochems). Presumably all of the suggested precursor fabrics were present throughout the reef trend. The problems with this scenario are the lack R3 in the rest of the sample set, and the lack of R1 in the southwestern reefs. There is only one R1 sample in a partially dolomitized well in the Strachan reef, indicating that nucleation of matrix R1 was possible in this area. If the nucleation sites for R3 were not fabric controlled, the question remains why the sites were fabric controlled for R1 and R2, but not for R3.

If the distribution of R3 is the result of relatively low fluid supersaturation with respect to dolomite, it would suggest that R3 crystals precipitated after the onset of matrix R1 and R2 dolomitization (see above). The evolution of replacement dolomitization fluids from relatively high supersaturation (forming R1 and R2) to relatively low supersaturation

(forming R3) with respect to dolomite is logical during an extensive event, such as occurred to pervasively dolomitize the Rimbey-Meadowbrook Reef Trend. If the replacement fluids flowed from a southwestern origin towards the northeast (as suggested in Chapters 2 and 6), by the time they reached Morinville, they may have had only very low supersaturation with respect to dolomite, therefore forming matrix R3. It is possible that R3 in the Chedderville through Ram River reefs began to precipitate resulting from a low supersaturated fluid evolved late in the replacement dolomitization event.

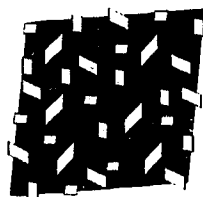
A process associated with the evolution in replacement dolomitizing fluids (as discussed in the previous paragraph) is the preferred growth of coarse crystals over fine crystals, *e.g.*, R3 growing at the *expense* of R1, *i.e.*, Ostwald-ripening. It is possible, therefore, that R3 may be a recrystallized texture after R1 through Ostwald-ripening. This could account for the rare occurrences of R1 in the southwestern reefs. In the Morinville reef where R1 is more common, Ostwald-ripening may have been a minor event. It is possible, then, that the eleven R3 samples located in the deep, southwestern reefs, and the four R3 samples located in the Morinville reef may have been locally "significantly recrystallized" through Ostwald-ripening during the later stages of the replacement dolomitization event.

It is possible that matrix R2 may also be recrystallized. There are two matrix R2 samples, H-R 2514 and H-R 2525, that exhibit mottled CL zones (Plate 2F). This mottling may have resulted from recrystallization of originally CL zoned crystals (Cander et al. 1988), although there is no evidence of CL zoned matrix R2. This texture may represent a recrystallized dolomite sample, if the recrystallized phase of dolomite overprinted original zones of the replacement phase (Figure 23). These two samples may represent an earlier, partially recrystallized phase compared to the other the R2 samples. It is possible, then, that the dull, non-luminescent, blotchy CL signature of matrix R2 represents a series of recrystallization textures. However, there is no evidence of CL zoned matrix R2, so this observation cannot prove extensive textural recrystallization of matrix R2 dolomites.

Figure 23. Illustration of possible recrystallization effects on CL zones. The zoned crystal is the first replacement dolomite phase. The small inclusions are the second dolomite recrystallization phase. The blotchy CL crystal is representative of most dolomite crystals within the Rimbey-Meadowbrook Reef Trend and may be an outcome of dolomite textural recrystallization.



Original replacement phase
CL zoned dolomite crystal.



First dolomite recrystallization
phase with small inclusions
overprinting original CL
zones. Mottled texture.



Possible result of extensive
recrystallization; blotchy CL
signature.

GEOCHEMICAL TRENDS

Inter-matrix type variations

Another objective of this thesis was to determine if the chemical and textural characteristics of the matrix represent replacement dolomitization or dolomite recrystallization characteristics. The reef trend matrix types are coarse grained and geochemically similar (Chapters 5 & 6, Figure 8). For each geochemical analysis, *i.e.*, unit cell parameters (XRD), major and trace elements (ILS and ICP, respectively), stable isotopes ($\delta^{13}\text{C}$ and $\delta^{18}\text{O}$), and radiogenic isotopes ($^{87}\text{Sr}/^{86}\text{Sr}$ -ratio), however, the data points for matrix types R2 and R3 (unit cell parameters and trace element data relevant only for R3) form relatively tight clusters, whereas the data points for matrix type R1 are dispersed (Figures 11 to 21). The tight clusters of matrix types R2 and R3, therefore, may indicate that they are "insignificantly recrystallized" (defined p. 7).

Where matrix R1 is abundant (Figure 22), the dispersed nature of the geochemical data suggests it is, for the most part, replacement dolomite (Ostwald-ripening of R1 to R3 suggested in southwest, p. 99). XRD-derived unit cell lattice parameters for R1 range from near ideal dolomite towards a more calcian composition, indicating that at least some R1 samples may not be as thermodynamically stable as matrix types R2 and R3 (Figure 11) (Land 1980). The major and trace element concentrations determined for matrix R1 probably reflect the influence of adjacent, intra- and inter-crystalline clay minerals during sample preparation (Figures 12 to 21).

The matrix R1 stable isotope ($\delta^{13}\text{C}$ vs $\delta^{18}\text{O}$) data do not vary more than ± 2 ‰ from the matrix R2 cluster (Figure 17). Matrix R1 samples form a weak negative trend with: increasing $^{87}\text{Sr}/^{86}\text{Sr}$ -ratios and decreasing $\delta^{18}\text{O}$ values (Figure 19). This trend does not directly follow sample depth, but probably indicates that these samples were affected by slightly higher temperature fluids than might be expected for theoretical Late Devonian seawater during replacement dolomitization (p. 92). This would allow for the incorporation of ^{87}Sr from adjacent clays, as suggested by the weak trend in Figure 20. These varying geochemical data points for matrix R1 (unit cell parameters, major and trace elements, stable isotopes, and radiogenic Sr isotopes) appear to represent primarily the original geochemical variability that is inherent to reef trend sediments, which might

still be present to some extent after replacement dolomitization.

Although there are slight differences in the chemical characteristics between matrix types R1 and R2, both are suggested to be replacement dolomite, or at least "insignificantly recrystallized" dolomite in the sampled interval. Matrix R1 and R2 crystals probably began to form slightly earlier than R3 (see p. 98), at a time early in the burial history of the reef trend, such as during the time span between the Late Devonian and Late Mississippian (depths of about 300 to 1500 m and temperatures of about 45° to 75°C as derived from $\delta^{18}\text{O}$ values, p.23) (Figures 24 and 25). Matrix type R3 probably began to crystallize later in the dolomitization event between approximately 600 to 1500 m intermediate burial depths (Figures 24 and 25) (Drivet 1993). Temperatures and depths at this paragenetic interval correspond with previous studies and $\delta^{18}\text{O}$ data for matrix R2 (Amthor *et al.* 1993, Drivet 1993, Mountjoy and Amthor 1994, Marquez 1994).

This temperature and time frame could also explain the tight grouping of $^{87}\text{Sr}/^{86}\text{Sr}$ ratios (between 0.7082 and 0.7089) for matrix R2 (as opposed to the higher, clay enriched radiogenic ratios of matrix R1, p. 101), which were derived from a fluid source hotter and more radiogenic than theoretical Late Devonian seawater (Figure 19). These matrix R2 strontium ratios therefore may have been derived from the replacement dolomitization fluids (modified Late Devonian seawater), which in turn were probably partly derived from compaction fluids from the shale basin surrounding the Rimbey-Meadowbrook Reef Trend and farther southwest, as suggested by Illing (1959), Barfoot and Ko (1987), Machel and Mountjoy (1987), and Amthor *et al.* (1993).

There is only one sample in the sampled interval, matrix R2 (Ram 5047a), which has a depleted $\delta^{18}\text{O}$ value (-9.9‰ PDB) suggesting that it may be "significantly recrystallized" because it falls outside the observed range for matrix dolomites analyzed both in this study and in previous studies (Amthor *et al.* 1993, Drivet 1993, and Marquez 1994) (Figure 8). It is possible that this sample was locally exposed to a fluid with a higher temperature than the replacement dolomitization fluid during a localized recrystallization event creating the depleted $\delta^{18}\text{O}$ value. Why only one sample was affected is a matter of speculation. It is possible that a hot fluid, calculated to be roughly 98°C from $\delta^{18}\text{O}$ (see p. 23), may have been expelled at deepest burial via the late

Figure 24. Revised burial history diagram for the Rimbey-Meadowbrook Reef Trend. The two curves represent the shallow northeast (Leduc) and the deep southwest (Strachan) areas of the reef trend. Based on Amthor *et al.* (1993) and Marquez (1994). Included are interpreted time and temperature ranges for replacement dolomitization and dolomite recrystallization. Assumed 30°C/Km geothermal gradient.

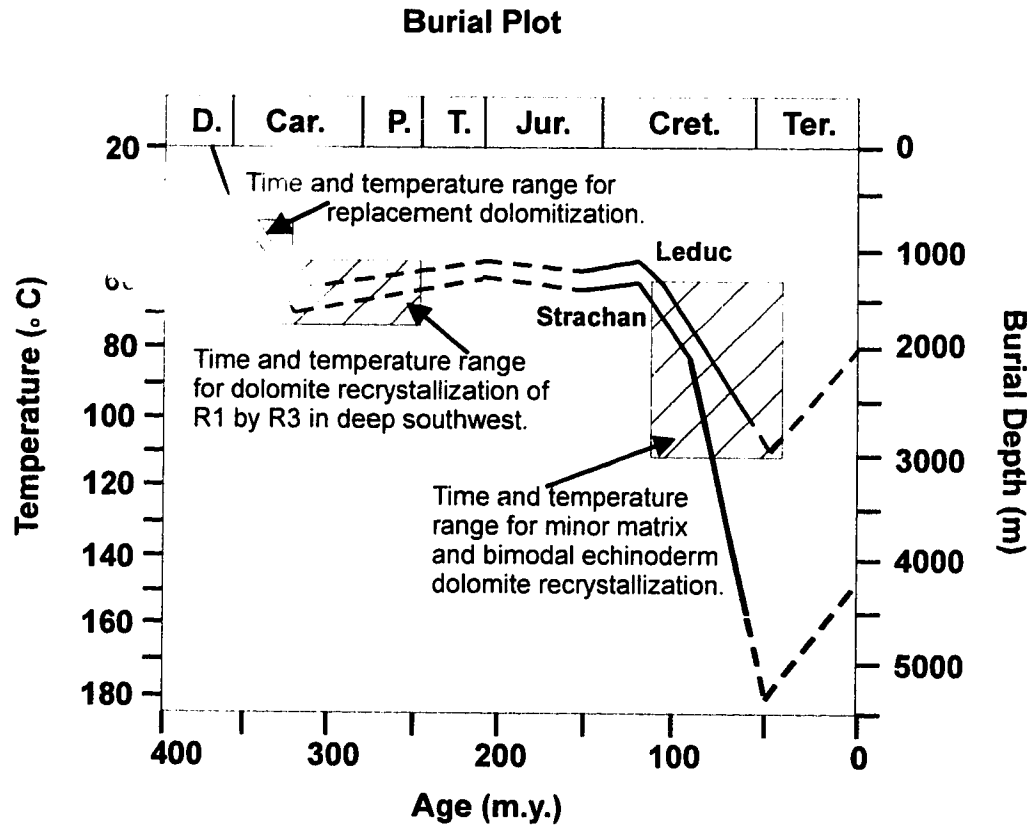


Figure 25. Paragenetic sequence of the Rimbey-Meadowbrook Reef Trend as a result of this study. Most diagenetic features have not been altered from previous studies (Amthor et al. 1993, Drivet 1993). The timing of recrystallization of matrix types R1, R2, and R3, and echinoderm fragments, is interpreted as occurring in two stages, at the end of replacement dolomitization, and during and after the second onset of stylolitization and bitumen emplacement at the time of the deep burial of the reef trend in the Late Cretaceous / Early Tertiary (Figure 23).

Paragenetic sequence of reef trend dolostones

Diagenetic Event	Early → Late		
	Early		Late
Isopachous calcite cementation	██████████		
Submarine cementation	██████████		
Stylolitization		██████████	██████████
Replacement dolomitization		██████████	
Dolomite recrystallization		██████████	██████████
Dolomite cementation			██████████
Anhydrite cementation and replacement			██████████
Calcite cementation			██████████
Quartz cementation			██████████
Bitumen emplacement			██████████
Sulfur and sulphide emplacement			██████████

Sea Floor Shallow Burial (< 500 m) Intermediate Burial (500 - 2000 m) Deep Burial (> 2000 m)

formation of wispy stylolites, allowing for this localized occurrence (Figures 24 and 25).

One of the driving forces for recrystallization is thermodynamic instability at higher temperatures and pressures associated with burial depths. The major result is usually larger grain sizes through Ostwald-ripening, and nonplanar textures when the recrystallizing fluid is above the CRT (Gregg and Sibley 1984, Sibley and Gregg 1987). The thermodynamic instability of R1 (XRD data discussed above), may have made this matrix type more susceptible to recrystallization through Ostwald-ripening in the southwestern reefs where it is rare (as discussed previously p. 99).

There are twelve samples from the southwestern reefs in this study suggested to be "significantly recrystallized" because they are different from the rest of the dolomite in the sampled interval (p. 99 & 102). Due to the paucity of evidence for this interpretation, it is not possible to determine the extent and number of recrystallization events affecting this southwestern area. As for the four "significantly recrystallized" samples in the Morinville reef, R3 may represent a minor recrystallization event through Ostwald-ripening (p. 99). If the fifteen R3 samples from the Morinville and the southwestern reefs in the sampled interval are recrystallization textures, the event may have occurred at the end of replacement dolomitization (Figures 24 and 25).

Variations with location

In the deep, southwestern part of the reef trend, one matrix R1 sample (Strachan 4085.2), three matrix R2 samples (Strachan 4318.3, Ram River 5047, and Ram River 5067), and four R3 samples (Ricinus West 4545.4, Ricinus West 4563.9, Ricinus West 4397.9, and Ram River 5047) have high Mn contents but low Fe contents (Figure 15, trend II). The incorporation of reduced Mn into the dolomite lattices of all three geochemically analyzed matrix types, R1, R2, and R3 is an indication that reducing conditions were present during replacement dolomitization in this southwestern area of the reef trend.

The interpretation that R1 and R2 were the first matrix types to form in the reef trend, followed by R3 (p. 98 & 102) which may be a recrystallization texture after R1 in the southwest reefs, where all analyzed samples have elevated Mn concentrations suggests

three possible fluid characteristics. First, this reducing fluid may have been present throughout the entire replacement dolomitization process in the deep, southwestern reefs (in order to incorporate reduced Mn into matrix types R1, R2 and R3). Second, this reducing fluid either oxidized or lost Mn concentrations as it flowed to the northeast. Third, the combination of the previous two points suggests that the deep, southwestern reefs coincide with the entrance of the replacement dolomitization fluids into the reef trend which then flowed in a northeasterly direction. This flow pattern corresponds with Bachu's (1995) hydrogeologic flow regime for the Rimbey-Meadowbrook Reef Trend (p. 20).

There is only one shallow matrix R2 sample that contains elevated Mn concentrations, Ach 1547.4. It is possible that the location of this one sample might be further evidence for migration of the reducing fluids from the deeper, southwestern portion of the reef trend towards the northeast (Figures 2 and 9). If the dolomitizing fluid did enter the reef trend in the area of the deep, southwestern reefs as suggested by Mn data, this would back up the petrographic and geochemical interpretations that suggest matrix R3 recrystallized R1 through Ostwald-ripening in the later stages of replacement dolomitization, if the later fluids had lower supersaturation with respect to dolomite.

BIMODAL CRYSTAL ECHINODERM FRAGMENTS

There are several dolomitized echinoderm fragments scattered throughout the sampled interval of the reef trend. There is only one example, however, of partial echinoderm microdolomitization in a partially dolomitized sample in Phoenix 4739.9. This partially dolomitized limestone sample contains an echinoderm fragment with small crystals of dolomite scattered throughout its stereom (Plate 5A-D). The microdolomite in this stereom probably originates from the dissolution-reprecipitation of HMC within the echinoderm fragment during early diagenesis, to form microdolomite crystals, either before or during the transformation of the HMC stereom to LMC (Lohmann and Meyers 1977, Blake *et al.* 1982, Richter 1985, Bruckschen *et al.* 1990).

With further burial and time, scattered crystals in this stereom may have recrystallized into more stoichiometric and better ordered crystals that are optically

continuous and unimodal (Blake *et al.* 1982, Fagerstrom 1983, Sibley 1982, Gregg and Sibley 1984, Sibley and Gregg 1987, Bruckschen 1990, Brand 1990). The fully dolomitized echinoderm fragments in the Rimbey-Meadowbrook Reef Trend, however, are not unimodal. Each stereom is primarily optically continuous with fine dolomite crystals (Plates 7 and 8), but they have distinct areas of optically discontinuous larger dolomite crystals inside the fragments (Plate 7A, 7B).

These larger and optically discontinuous crystals in the fragments occur primarily in the interior of the granis, adjacent to at least on edge, the location of which may indicate a possible fluid pathway into the fragment after pervasive dolomitization. These pathways may indicate that the fragments were still porous after pervasive dolomitization, in opposition to previous suggestions by Fagerstrom (1983) and Brand (1990) (p. 25). There is always at least one observable zone in the interior of a fragment where the large crystal fraction is concentrated. One fragment even shows a "flame"-like structure (II-R 2629.8, Plate 7C) which surrounds several large crystals in the bimodal fragment. This "flame" indicates a possible fluid pathway precipitating the larger crystal fraction in the already pervasively dolomitized fragment. The larger crystal fraction in the bimodal crystal echinoderm fragments of the reef trend may, therefore, be a later recrystallization phase than the fine crystal fraction of the fragments. This type of recrystallization is described as Ostwald-ripening, therefore, the bimodal crystal echinoderm fragments are here interpreted as being "significantly recrystallized."

The presence of the large "significantly recrystallized" dolomite crystal fraction may indicate that the echinoderm fragments remained relatively porous during replacement dolomitization, keeping them open to recrystallizing fluids. The porous structure of the fragments is petrographically evident in this study, not only from the observation of the larger, optically discontinuous recrystallized crystals and their fluid pathways, but from the occurrence of bitumen in the axial canals within the dolomitized stereoms, patches of the original stereom structure, and the vuggy appearance under SEM (Plates 7B, 8, and 9A).

POSSIBLE FLUID SOURCES

Matrix

A fluid with a great volume and large amount of Mg^{2+} is required to pervasively dolomitize the reef trend and locally recrystallize the proposed "significantly recrystallized" matrix samples in the Morinville reef and the southwestern reefs. Calculations derived from Machel and Anderson (1989) and Amthor *et al.* (1993) utilizing the area of the reef trend, the proposed porosity of 10%, and the transformation of dolomite to calcite, determined that 1.6×10^{15} moles of Mg are required to dolomitize a distance of about 560 km of original limestone (with an average width of 10 km and a height of 200 m) in the Rimbey-Meadowbrook Reef Trend. The maximum amount of Mg derived from compaction fluids, calculated by Amthor *et al.* (1993), is only 1.1×10^{14} moles. So, as Amthor *et al.* (1993) suggested, an additional Mg source is required for the pervasive replacement dolomitization event of the Rimbey-Meadowbrook Reef Trend matrix dolomites. Two additional Mg sources to the reef trend during replacement dolomitization are suggested to be (1) early wispy stylolitization, through the dissolution of calcite, and (2) undefined fluids derived through cross-formational flow from the area southeast of the reef trend (Rostron 1995).

The process of cross-formational flow has not been identified in the Rimbey-Meadowbrook Reef Trend. Rostron (1995), however, suggested that it may have occurred in the deep, southwestern area of the reef trend because cross-formational flow is suggested to occur in the adjacent Bashaw Complex (Figures 1 and 2). If cross-formational flow did occur in this area, this could be the source of both replacement dolomite and dolomite recrystallization fluids, as yet unidentified. If this flow decreased at the end of the dolomitization event, this could explain the local occurrence of "significantly recrystallized" matrix R3 dolomite in the southwestern reefs.

A later, minor recrystallization event possibly occurred locally in the southwestern Ram River reef during the Late Cretaceous/ Early Tertiary late stage stylolitization event (Figures 24 and 25). This time frame (Laramide Orogeny) would correspond with the proposed recrystallization fluid temperatures of about 98°C, calculated from the depleted $\delta^{18}\text{O}$ value of the one "significantly recrystallized" matrix R2 sample Ram 5047a (p. 102).

Echinoderm Fragments

The timing of recrystallization of the observed bimodal crystal echinoderm fragments is unable to be constrained by this study. If the fragments were porous after replacement dolomitization, they may have lost that porosity during recrystallization, inhibiting emplacement of bitumen. Bitumen may have been emplaced prior to recrystallization indicating the possibility that these fragments were recrystallized after this event. In this scenario, relatively hot fluids associated with deepest burial of the reef trend during the Late Cretaceous/ Early Tertiary Laramide orogeny and the onset of late stage stylolitization (Figures 24 and 25) may be the fluids that "significantly recrystallized" the echinoderm fragments. This timing would correspond with the minor, local recrystallization event described in the previous paragraph, and the stylolites associated with the fragments (Plate 9). Because there is very little evidence to support this hypothesis, there is no timing defined for the recrystallization of these fragments.

CHAPTER EIGHT

CONCLUSIONS

The Upper Devonian Rimbey-Meadowbrook Reef Trend and the margin of the underlying Cooking Lake Platform are parts of a pervasively dolomitized aquifer in the Western Canada Sedimentary Basin. This study was undertaken in order to examine one interval along the entire reef trend to define whether or not matrix dolomites have been recrystallized. This objective was obtained by integrating matrix dolomite crystal structures, major and trace element concentrations, carbon, oxygen, and strontium isotopic compositions, and crystal textures. This study led to six major conclusions.

1) The analyzed reef trend matrix dolomite samples are petrographically and geochemically similar to each other. Even in this small sample set, fine grained matrix type R1 is more abundant than suggested in previous studies of the reef trend.

2) Matrix R1 consistently contains higher Al, Si, and Fe concentrations than most of the reef trend matrix R2 and R3 dolomites, which is consistent with relatively high amounts of clays present in these matrix R1 samples. These clays probably contributed ^{87}Sr to matrix R1 during replacement dolomitization, creating the high radiogenic $^{87}\text{Sr}/^{86}\text{Sr}$ ratios in matrix R1 samples.

3) Matrix types R1 and R2 may have formed prior to R3 during replacement dolomitization from fluids at relatively high supersaturation with respect to dolomite, probably between approximately 300 and 1500 m in the Late Devonian to Mississippian in a shallow to intermediate burial environment. Replacement dolomitization fluids may have been derived from one or a combination of (a) fluids derived from basinal shales during early compaction, (b) fluids derived from late stage stylolitization, and (c) fluids derived from cross-formational flow. The temperature range for the replacement dolomitization event for both matrix types was calculated to be between about 45 and 75°C.

4) The dolomitizing fluids may have entered into the reef trend in the deep, southwestern area, as suggested by elevated Mn concentrations in matrix types R1, R2, and R3 in the deep southwestern reefs. Mn concentrations are drastically lower in the

northeastern areas of the reef trend, suggesting the direction of fluid flow may have been northeasterly during replacement dolomitization.

5) There may have been two minor recrystallization events that affected the reef trend. The first event may have "significantly recrystallized" roughly fifteen matrix R3 samples in the deep, southwestern reefs and the Morinville reef through Ostwald-ripening of matrix R1. This event may have taken place at the end of replacement dolomitization during intermediate burial, approximately 600 to 1500 m in the Late Devonian to Mississippian, by a fluid with relatively low supersaturation with respect to dolomite. The second event may have "significantly recrystallized" one matrix R2 sample in the deep, southwestern Ram River reef with respect to $\delta^{18}\text{O}$ values, which calculated a fluid temperature of about 98°C. This relatively hot fluid may have been expelled during late stage stylolitization, during the Laramide Orogeny when the reef trend was near deepest burial. It was not possible in this study to determine the "significant recrystallization" timing of bimodal crystal echinoderm fragments.

6) The majority of reef trend matrix dolomites are suggested to be burial replacement dolomites. Although "significant recrystallization" is suggested to have occurred, the small data set can only suggest a minor event that is *not* extensive in the Rimbey-Meadowbrook Reef Trend.

REFERENCES

- Allan, J., and Creaney, S., 1991, Oil families of the Western Canada Basin. Canadian Petroleum Geology Bulletin. 39: 107-122.
- Amthor, J.E., Mountjoy, E.W., and Machel, H.G., 1993, Subsurface dolomites in Upper Devonian Leduc Formation buildups, central part of Rimbey-Meadowbrook reef trend, Alberta, Canada. Canadian Petroleum Geology Bulletin. 41: 164-185.
- Amthor, J.E., Mountjoy, E.W., and Machel, H.G., 1994, Regional-scale porosity and permeability variations in Upper Devonian Leduc Buildups: implications for reservoir development and prediction in carbonates. American. Association of Petroleum Geology Bulletin. 78: 1541-1559.
- Andrichuck, J.M., 1958, Stratigraphy and facies analysis of Upper Devonian reefs in Leduc, Stettler, and Redwater areas, Alberta. American. Association of Petroleum Geology Bulletin. 42: 1-93.
- Bachu, S., 1995, Synthesis and model of formation-water flow, Alberta Basin, Canada. American. Association of Petroleum Geology Bulletin. 79: 1159-1178.
- Baker, P.A. and Kastner, M., 1981, Constraints on the formation of sedimentary dolomite. Science. 213: 214-216.
- Banner J.L., 1995, Application of the trace element and isotope geochemistry of strontium to studies of carbonate diagenesis. Sedimentology. 42: 805-824.
- Banner, J.L., Hanson, G.N., and Meyers, W.J., 1988, Water-rock interaction history of regionally extensive dolomites of the Burlington-Keokuk Formation (Mississippian): isotopic evidence. *in* Shukla, V. and Baker, P.A. (eds.) Sedimentology and Geochemistry of Dolostones, Society of Economic Paleontology and Mineralogy Special Publication. 43: 97-113.
- Barfoot, G.L. and Ko, S.C.M., 1987, Assessing, and compensating for, the impact of the Leduc D-3A gas cap blowdown on the other Golden Trend pools. Journal of Canadian Petroleum Technology. May-June: 41-46.
- Benoit, P., 1988, Xeditor, The Appleman and Evans X-ray editor, Version 2.2.
- Blake, D.F., Peacor, D.R., and Wilkinson, B.H., 1982, The sequence and mechanism of low-temperature dolomite formation: calcian dolomites in a Pennsylvanian

- echinoderm. *Journal of Sedimentary Petrology*. 52: 59-70.
- Brand, U., 1990, Chemical diagenesis and dolomitization of Paleozoic high-Mg calcite crinoids. *Carbonates and Evaporites*. 5: 179-195.
- Bruckschen, P., Noeth, S., and Richter, D.K., 1990, Tempered microdolomites in crinoids: a new criterion for high-grade diagenesis. *Carbonates and Evaporites*. 5: 197-207.
- Burns, S.L., Baker, P.A. and Showers, W.J., 1988, The factors controlling the formation and chemistry of dolomite in organic-rich sediments: Miocene Drakes Bay Formation, California *in* Shukla, V. and Baker, P.A. (eds.) *Sedimentology and Geochemistry of Dolostones*, Society of Economic Paleontology and Mineralogy Special Publication. 43: 41-52.
- Cander, H.S., Kaufman, L., Daniels, L.D., Meyers, W.J., 1988, Regional dolomitization of shelf carbonates in the Burlington-Keokuk Formation (Mississippian), Illinois and Missouri: constraints from cathodoluminescent zonal stratigraphy. *in* Shukla, V. and Baker, P.A. (eds.) *Sedimentology and Geochemistry of Dolostones*, Society of Economic Paleontology and Mineralogy Special Publication. 43: 129-144.
- Corballo, J.D., Land, L.S., and Miser, D., 1987, Holocene dolomitization of supratidal sediments by active tidal pumping, Sugarloaf, Key, Florida. *Journal of Sedimentary Petrology*. 57: 153-165.
- Claypool, G.E. and Kaplan, I.R., 1974, The origin and distribution of methane in marine sediments: *in* Kaplan, I. (ed.) *Natural Gases in Marine Sediments*, Plenum Press: 99-140.
- Compton J.S., 1988, Sediment composition and precipitation of dolomite and pyrite in the Neogene Monterey and Sisquoc Formations, Santa Maria Basin area, California *in* Shukla, V. and Baker, P.A. (eds.) *Sedimentology and Geochemistry of Dolostones*, Society of Economic Paleontology and Mineralogy Special Publication. 43: 53-64.
- Coniglio, M., James, N.P., and Aissazoui, D.M., 1988, Dolomitization of Miocene carbonates, Gulf of Suez, Egypt. *Journal of Sedimentary Petrology*. 58: 100-119.
- Connolly, C.A., Walter, L.M., Baadsgaard, H., and Longstaffe, F.J., 1990, Origin and

- evolution of formation waters, Alberta Basin, Western Canada Sedimentary Basin. 1. Chemistry. *Applied Geochemistry*. 5: 375-395.
- _____. 1990. Origin and evolution of formation waters. Alberta Basin, Western Canada Sedimentary Basin. 2. Isotope systematics and water mixing. *Applied Geochemistry*. 5: 397-413.
- Curtis, C., Petrowski, C., and Oertel, G., 1972, Stable carbon isotope ratios within carbonate concretions: a clue to the place and time of formation. *Nature*. 235: 98-100.
- Dravis, J.J. and Yurewicz, D.A., 1985. Enhanced carbonate petrography using fluorescence microscopy. *Journal of Sedimentary Petrology*. 55: 795-804.
- Drivet, E., 1993, Diagenesis and reservoir characteristics of Upper Devonian Leduc dolostones, southern Rimbey-Meadowbrook reef trend, central Alberta. unpub. Msc. thesis McGill University, Montreal, Quebec: 115p.
- Dunham, R.J., 1962, Classification of carbonate rocks according to depositional texture. *in* Ham, W.E. (ed.) *Classification of Carbonate Rocks*. American Association of Petroleum Geology Memoir. 1: 108-121.
- Eaton, D.W., Milkereit, B., Ross, G.M., Kanasewich, E.R., Geis, W., Edwards, D.J., Kelsch, L., and Varsek, J., 1995, Lithoprobe basin-scale seismic profiling in central Alberta: influence of basement on the sedimentary cover. *Canadian Petroleum Geology Bulletin*. 43: 65-77.
- Embry, A. F., III and Klovan, J.E., 1972, Absolute water depths of Late Devonian paleoecological zones. *Geologische Rundschau* 61: 672-686.
- Fagerstrom, J.A., 1983, Petrology and regional significance of a Devonian carbonate / evaporite complex, eastern Michigan Basin. *Journal of Sedimentary Petrology*. 53: 295-317.
- Flügel, E., 1982, *Microfacies Analysis of Limestones*, Springer: 453p.
- Folk, R.L., 1964, Some aspects of recrystallization of ancient limestones. *American Association of Petroleum Geology Bulletin*. Abstract. 48: 525.
- Folk, R.L. 1965, Some aspects of recrystallization in ancient limestones. *in* Pray, L.C. and Murray R.C. (eds) *Dolomitization and Limestone Diagenesis*. Society of

- Economic Paleontology and Mineralogy Special Publication. 13: 14-48.
- Friedman, I. and O'Neil, J.R., 1977, Data of geochemistry, 6th edition, Chapter KK. Compilation of stable isotope fractionation factors of geochemical interest, US Geological Survey Professional Paper. 440-KK: 1-12.
- Gao, G., 1990 Geochemical and isotopic constraints on the diagenetic history of a massive stratal, late Cambrian (Royer) dolomite, Lower Arbuckle Group, Slick Hills, SW Oklahoma, USA. *Geochimica et Cosmochimica Acta*. 54: 1979-1989.
- Gao, G. and Land, L.S., 1991, Early Ordovician Cool Creek Dolomite, Middle Arbuckle Group, Slick Hills, SW Oklahoma, U.S.A.: origin and modification. *Journal of Sedimentary Petrology*. 61: 161-173.
- Goldsmith, J.R. and Graf, D.L., 1958, Relation between lattice constants and composition of the Ca-Mg carbonates. *American Mineralogist*. 43: 84-101.
- Gregg, J.M., Howard, S.A., and Mazzullo, S.J., 1992, Early diagenetic recrystallization of Holocene (<3000 years old) peritidal dolomites, Ambergris Cay, Belize. *Sedimentology*. 39: 143-160.
- Gregg, J.M., and Sibley, D.F., 1984, Epigenetic dolomitization and the origin of xenotopic dolomite texture. *Journal of Sedimentary Petrology*. 54: 908-931.
- Gregg, J.M. and Shelton, K.L., 1990, Dolomitization and dolomite neomorphism in the back reef facies of the Bonnetterre and Davis Formations (Cambrian), Southeastern Missouri. *Journal of Sedimentary Petrology*. 60: 549-562.
- Gussow, W.C., 1968, Migration of reservoir fluids. *Journal of Petroleum Geology*. *Journal of Petroleum Technology*: 353-363.
- Halbertsma, H.L., 1994, Chapter 13 - Devonian Wabamun Group of the Western Canada Sedimentary Basin. *in Geological Atlas of the WCSB*. compiled by Mossop, G. and Shetsen, I., Canadian Society of Petroleum Geology and American Research Council in association with Alberta Department of Energy and Geological Society of Canada.: 203-220.
- Hardy, R.G. and Tucker, M.E., 1989, X-ray powder diffraction of sediments, Chapter 7. *in Tucker, M.E. (ed.) Techniques in Sedimentology*, Blackwell Scientific Publications: 191-228.

- Hennessy, J. and Knauth, L.P., 1986, Isotopic variations in dolomite concretions from the Monterey Formation, California. *Journal of Sedimentary Petrology*. 55: 120-130.
- Hitchon, B., 1969, Fluid flow in the Western Canada Sedimentary Basin. 1. Effect of topography. *Water Resources Research*. 5: 186-195.
- _____, 1969, Fluid flow in the Western Canada Sedimentary Basin. 2. Effect of Geology. *Water Resources Research*. 5: 460-469.
- Hitchon, B., Billings, G.K., and Klován, J.E., 1971. Geochemistry and origin of formation waters in the Western Canada Sedimentary Basin. 3. Factors controlling chemical composition. *Geochimica et Cosmochimica Acta*. 35: 567-598.
- Hitchon, B. and Friedman, I., 1969, Geochemistry and origin of formation waters in the Western Canada Sedimentary Basin. 1. Stable isotopes of hydrogen and oxygen. *Geochimica et Cosmochimica Acta*. 33: 1321-1349.
- Hugo, K., 1990, Mechanisms of groundwater flow and oil migration associated with Leduc reefs. *Canadian Petroleum Geology Bulletin*. 38: 307-319.
- Illing, L.V., 1959, Deposition and diagenesis of some Upper Paleozoic carbonate sediments in western Canada. *Proceedings of the 5th World Petroleum Congress*, N.Y. section. 1: 23-52.
- Irwin, H., Curtis, C., and Coleman, M., 1977, Isotopic evidence for source of diagenetic carbonates formed during burial of organic rich sediments. *Nature*. 269: 209-213.
- James, N.P., 1983, Reef environment. *in* Scholle, P.A., Bebout, D.G., and Moore, D.H. (eds.) *Carbonate Depositional Environments*. American Association of Petroleum Geology Memoir. 33: 345-440.
- James, N.P. and Bourque, P.-A., 1992, Reefs and mounds. *in* Walker, R.G. and James, N.P. (eds.) *Facies Models: Response to Sea Level Change*. Geological Association of Canada, St. Johns.: 323-347.
- Jones, F.W., and Majorowicz, J.A., 1987, Some aspects of the thermal regime and hydrodynamics of the Western Canada Sedimentary Basin. *in* Goff, J.C., and Williams, B.P.J. (eds), *Fluid Flow in Sedimentary Basins and Aquifers*, Geological Society Special Publication. 34: 79-85.

- Kruger, J.M. and Simo, J.A., 1994, Pervasive dolomitization of a subtidal carbonate ramp, Silurian and Devonian, Illinois Basin, USA *in* Dolomites: A volume in Honour of Dolomieu. Purser, B., Tucker, M., Zenger, D (eds.). International Association of Sedimentology Special Publication. 21. Blackwell Scientific Publications: 387-405.
- Kupecz, J.A. and Land, L.S., 1994, Progressive recrystallization and stabilization of early stage dolomite: Lower Ordovician Ellenburger Group, West Texas *in* Dolomites: A volume in Honour of Dolomieu. Purser, B., Tucker, M., Zenger, D (eds.). International Association of Sedimentology Special Publication. 21. Blackwell Scientific Publications: 255-279.
- Land, L.S., 1980, The isotopic and trace element geochemistry of dolomite: the state of the art. *in* Zenger, D.H., Dunham, J.B., and Ethington, R.L. (eds.) Concepts and Models of Dolomitization. Society of Economic Paleontology and Mineralogy Special Publication. 28: 87-110.
- Land, L.S., 1982, Dolomitization. American. Association of Petroleum Geology Bulletin. Education Course Note Series 24: 1-20.
- Land, L.S., 1985, The origin of massive dolomite. *Journal of Geological Education* 33: 112-125.
- Lohmann, K.C. and Meyers, W.J., 1977, Microdolomite inclusions in cloudy prismatic calcites: a proposed criterion for former high-magnesium calcites. *Society of Economic Paleontology and Mineralogy Bulletin.* : 1078-1088.
- Lumsden, D.N., 1979, Discrepancy between thin-section and X-ray estimates of dolomite in limestone. *Journal of Sedimentary Petrology.* 49: 429-436.
- Machel, H.G., 1988, Fluid flow direction during dolomite formation as deduced from trace element trends. *in* Shukla, V. and Baker, P.A. (eds.) *Sedimentology and Geochemistry of Dolostones*, Society of Economic Paleontology and Mineralogy Special Publication. 43: 115-125.
- Machel, H.G., 1990, Dolomitization, reservoir development, and dolostone reservoirs in Western Canada. *in* Bloy, G.R., and Hadley, M.G. (eds.), *The development of porosity in carbonate reservoirs.* Canadian Society of Petroleum Geology Short

Course Notes.: 3-1 to 3-30.

- Machel, H.G., Cavell, P.A., Patey, K.S., 1996, Isotopic evidence for carbonate cementation and recrystallization, and for tectonic expulsion of fluids into the Western Canada Sedimentary Basin. *Geological Society of America Bulletin*. 108: 1108-1119.
- Machel, H.G. and Hunter, I.G., 1994, Facies models for Middle to Late Devonian shallow-marine carbonates with comparisons to modern reefs: a guide for facies analysis. *Facies*. 30: 155-176.
- Machel, H.G. and Mountjoy, E.W., 1986, Chemistry and environments of dolomitization-a reappraisal. *Earth Science Review*. 23: 175-222.
- _____, 1987, General constraints on extensive pervasive dolomitization-and their application to the Devonian carbonates of Western Canada. *Canadian Petroleum Geology Bulletin*. 35: 143-158.
- Machel, H.G., Mountjoy, E.W., and Amthor, J.E., 1993, Dolomitization of Devonian reef and platform carbonates in Western Canada. *Zentralblatt für Geologie und Paläontologie*. 7/8: 941-957.
- Malone, M.J., Baker, P.J., and Burns, S.J., 1994, Recrystallization of dolomite: evidence from the Monterey Formation (Miocene), California. *Sedimentology*. 41: 1223-1239.
- Marquez, X.M., 1994, Reservoir geology of Upper Devonian Leduc buildups deep Alberta basin. unpublished Ph.D. thesis McGill University, Montreal Quebec: 281 p.
- Mattes, B.W. & Mountjoy, E.W., 1980, Burial dolomitization of the Upper Devonian Miette Buildup, Jasper National Park, Alberta. *in* Zenger, D.H., Cunham, J.B., Ethington, R.L. eds., *Concepts and Models of Dolomitization*, Society of Economic Paleontology and Mineralogy Special Publication. 28: 259-297.
- Mazzullo, S.J., 1992, Geochemical and neomorphic alteration of dolomite: a review. *Carbonates and Evaporites*. 7: 21-37.
- McKenzie, J.A., 1981, Holocene dolomitization of calcium carbonate sediments from coastal sabkhas of Abu Dhabi, U.A.E.: a stable isotopic study. *Journal of Geology*.

89: 185-198.

- McLean, D.J., 1992, Upper Devonian buildup development in the southern Canadian Rocky Mountains: a sequence stratigraphic approach. Unpublished Ph.D. thesis, McGill University, 245p.
- McLean, D.J. and Mountjoy, E.W., 1993a, Stratigraphy and depositional history of the Burnt Timber Embayment, Fairhome Complex, Alberta. Canadian Petroleum Geology Bulletin. 41: 290-306.
- McLean, D.J. and Mountjoy, E.W., 1993b, Upper Devonian buildup-margin and slope development in the southern Canadian Rocky Mountains. Geological Society of America Bulletin. 39: 332-351.
- McNamara, L.B. and Wardlaw, N.C., 1991, Geological and statistical description of the Westrose Reservoir, Alberta. Canadian Petroleum Geology Bulletin. 39: 332-351.
- Morrow, D.W., 1982, Diagenesis 1. Dolomite - Part 1: The chemistry of dolomitization and dolomite precipitation. Geoscience Canada. 9: 5-13.
- Morrow, D.W., 1982, Diagenesis 2. Dolomite - Part 2: Dolomitization models and ancient dolostones. Geoscience Canada. 9: 95-107.
- Morrow, D.W. and Mayers, I.R., 1978, Simulation of limestone diagenesis - a model based on strontium depletion. Canadian Journal of Earth Science. 15: 376-396.
- Mountjoy, E.W., and Amthor, J.E., 1994, Has burial dolomitization come of age? Some answers from the Western Canada Sedimentary Basin. International Association of Sedimentology Special Publication. 21 Blackwell Scientific Publications: 203-229.
- Montanez, I.P. and Read, J.F., 1992, Eustatic control on early dolomitization of cyclic peritidal carbonates: Evidence from the Early Ordovician Upper Knox Group, Appalachians. Geological Society of America Bulletin.: 104: 872-886.
- Montanez, I.P. and Read, J.F., 1992, Fluid-rock interaction history during stabilization of early dolomites, Upper Knox Group (Lower Ordovician), U.S. Appalachians. Journal of Sedimentary Petrology. 62: 753-778.
- Moore, P.F., 1989, Chapter 9. The Kaskaskia Sequence: Reefs, platforms and foredeeps

- The Lower Kaskaskia Sequence - Devonian *in* Ricketts, B.D. (ed.) Western Canada Sedimentary Basin: A Case History, Canadian Society Petroleum Geology: 139-164.
- Mumme, W.G., Tsambouakis, G., Madsen, I. C., and Hill, R.J., 1996, Improved petrological modal analyses from X-ray powder diffraction data by use of the rietveld method. Part II. Selected sedimentary rocks. *Journal of Sedimentary Research* 66: 132-138.
- Nordeng S.H., and Sibley, D.F., 1994, Dolomite stoichiometry and Ostwald's Step Rule. *Geochimica et Cosmochimica Acta* 58:191-196.
- Paul, D., 1994, Hydrogeology of the Devonian Rimbey-Meadowbrook reef trend of central Alberta. unpublished Msc. thesis University of Alberta: 152p.
- Pingitore, N.E. Jr., 1982, The role of diffusion during carbonate diagenesis. *Journal of Sedimentary Petrology*. 52: 27-39.
- Porter, J.W., Price, R.A., and McCrossan, R.G., 1982, The Western Canada Sedimentary Basin. *Phil. Trans. Reservoir Society London A* 305: 169-192.
- Purser, B., Tucker, M., Zenger, D., 1994, Problems, progress, and future research concerning dolomites and dolomitization *in* Dolomites: A volume in Honour of Dolomieu. Purser, B., Tucker, M., Zenger, D. (eds.). International Association of Sedimentology Special Publication. 21. Blackwell Scientific Publications: 3-20.
- Richter, D.K., 1985, Microdolomites in crinoids of the Trochitenkalk formation (Middle Triassic) and the thermal anomaly of Vlotho (Lower Saxonian Mountains). *Neues Jahrbuch für Geologie Paläontologie*. 11: 681-690.
- Rostron, B.J., 1995, Cross-formational fluid flow in Upper Devonian to Lower Cretaceous Strata, West-Central Alberta, Canada. Unpublished Ph.D. Thesis, University of Alberta: 125p.
- Saller, A.H. and Koepnick, R.B., 1990, Eocene to early Miocene growth of Enewetak Atoll: insight from strontium-isotopic data. *Geological Society of America Bulletin*. 102: 381-390.
- Sharma, T. and Clayton, R.N., 1965, Measurement of O^{18}/O^{16} ratios of total oxygen of carbonates. *Geochimica et Cosmochimica Acta*. 29: 1347-1353.

- Shields, M.J., and Geldstzer, H.H.J., 1992, The MacKenzie margin, Southesk-Cairn carbonate complex: depositional history, stratal geometry and comparison with other Late Devonian platform-margins. *Canadian Petroleum Geology Bulletin*. 40: 274-293.
- Sibley, D.F., 1991, Secular changes in the amount and texture of dolomite. *Geology*. 19: 151-154.
- Sibley, D.F., 1982, The origin of common dolomite fabrics: clues from the Pliocene. *Journal of Sedimentary Petrology*. 52: 1087-1100.
- Sibley, D.F., 1990, Unstable to stable transformations during dolomitization. *Journal of Geology*. 98:739-748.
- Sibley, D.F., and Gregg, J.M., 1987, Classification of dolomite rock textures. *Journal of Sedimentary Petrology*. 57: 967-975.
- Simo, J.A., Johnson, C.M., Vandry, M.R., Brown, P.E., Castrogiovanni, E., Drzewiecki, P.E., Valley, J.W., Boyer, J., 1994, Burial dolomitization of the Middle Ordovician Glenwood Formation by evaporitic brines, Michigan Basin *in* Dolomites: A volume in Honour of Dolomieu. Purser, B., Tucker, M., Zenger, D (eds.). International Association of Sedimentology Special Publication. 21. Blackwell Scientific Publications: 169-186.
- Smalley, P.C., Higgins, A.C., Howarth, R.J., Nicholson, H., Jones, C.E., Swinburne, N.H.M., and Bessa, J., 1994, Seawater Sr isotope variations through time: a procedure for constructing a reference curve to date and correlate marine sedimentary rocks. *Geology*. 22: 431-434.
- Smith, T.D. and Dorobek, S.L., 1993, Alteration of early-formed dolomite during shallow to deep burial: Mississippian Mission Canyon Formation, central to southwestern Montana. *Geological Society of America Bulletin*. 105: 1389-1399.
- Sperber, C.M., Wilkinson, B.H., and Peacor, D.R., 1984, Rock composition, dolomite stoichiometry, and rock / water reactions in dolomitic carbonate rocks. *Journal of Geology*. 92: 609-622.
- Stearn, C.W., 1984, Growth forms and macrostructural elements of the coralline sponges. *Palaeontographica Americana*. 54: 315-325.

- Switzer, J.B., Holland, W.G., Christie, D.S., Graf, G.C., Hedinger, A.S., McAuley, R.J., Wierzbicki, R.A., Packard, J.J., 1994, Chapter 12 - Devonian Woodbend-Winterburn strata of the Western Canada Sedimentary Basin. *in* Geological Atlas of the WCSB. compiled by Mossop, G. and Shetsen, I., Canadian Society of Petroleum Geology and American Research Council in association with Alberta Department of Energy and Geological Society of Canada.: 165-202.
- Tan, F.C. and Hudson, J.D., 1971, Carbon and oxygen isotopic relationships of dolomites and co-existing calcites, Great Estuarine Series (Jurassic), Scotland. *Geochimica et Cosmochimica Acta* 35: 755-767.
- Undershultz, J.R., and Erdmer, P., 1991, Tectonic loading in the Canadian Cordillera as recorded by mass accumulation in the foreland basin. *Tectonics*. 10: 367-380.
- Vahrenkamp, V.C. and Swart, P.K., 1990, New distribution coefficient for the incorporation of strontium into dolomite and its implications for the formation of ancient dolomites. *Geology*. 18: 387-391.
- Veizer, J., 1978, Simulation of limestone diagenesis - a model based on strontium depletion: Discussion. *Canadian Journal of Earth Science* 15: 1683-1685.
- Weissenberger, J.A.W., 1994, Frasnian reef and basinal strata of West Central Alberta: a combined sedimentological and biostratigraphic analysis. *Canadian Petroleum Geology Bulletin*. 42: 1-25.
- Wendte, J.C., 1994, Cooking Lake platform evolution and its control on Late Devonian Leduc reef inception and localization, Redwater, Alberta. *Canadian Petroleum Geology Bulletin*. 42: 499-528.
- Wilson, J.L., 1975, Carbonate Facies in Geologic History. Springer: 471p.
- Woody, R.E., Gregg, J.M., and Koederitz, L.D., 1996, Effect of texture on petrophysical properties of dolomite : evidence from the Cambrian-Ordovician of Southeastern Missouri. *American Association of Petroleum Geology Bulletin*. 80: 119-132.
- Wright, G.N., McMechan, M.E., Potter, D.E.G., 1994, Chapter 3 - Structure and architecture of the Western Canada Sedimentary Basin. *in* Geological Atlas of the WCSB. compiled by Mossop, G. and Shetsen, I., Canadian Society of Petroleum Geology and American Research Council in association with Alberta Department

of Energy and Geological Society of Canada.: 25-40.

Zenger, D.H. and Dunham, J.B., 1988, Dolomitization of Siluro-Devonian limestones in a deep core (5,350 m), Southwestern New Mexico. *in* Shukla, V. and Baker, P.A. (eds.) *Sedimentology and Geochemistry of Dolostones*, Society of Economic Paleontology and Mineralogy Special Publication. 43: 161-173.

APPENDIX A

Analytical procedure for ICP-MS (trace elements):

Dolomite samples were run on a Fisons inductively coupled mass spectrometer, using the conditions listed in Table A1. The samples were run in two sets with a combination of standard addition, external standard calibration, and surrogate calibration to give quantitative results, using a method developed by Rui Feng. External (STDA and STDB) and internal (spike C) standards were used in the analysis. The first set of samples was run with standards listed and defined in table A2a; the second, with standards listed and defined in table A2b. Fifty three trace elements were determined. STDA contains 38 elements, STDB contains 20 with an overlap for 5 elements. The internal (spike C) solution contains 25 elements. The elemental concentrations of the two external (STDA and STDB) and internal (spike C) standard sets are listed in Table A2.

A sequence of STDA, STDB, a flush (deionized water), a blank, sample 1, sample 1 + spike, flush, sample2, sample 2 + spike, flush, sample 3, and sample 3 + spike was repeated, in triplicate, until all the samples were run. The results, in ppm, are listed in Table A3. The blanks were used to determine the detection limits for each set of calculated results, with 3x the deviation of the blank for each element being taken as the detection limit (D.L.).

The data reported have all been compared to the detection limit for that part of the sample run, listed at the bottom of Table A3, and any data values <D.L. have been reported as "<D.L." in the major and trace element tables included in the text. In Table A3, the data values <D.L. were left blank. Any sample values that are >10 x D.L. may be considered to be reliable to within 10% of the real value. Any results closer than one order of magnitude (10x) of the detection limit are probably not reliable. This can give an estimate of the reliability of the sample data when it is compared to the average detection limit.

TABLE A1:

Instrument: PQ2 with laser probe (LA-ICP-MS_ and electrothermal vaporizer (GF-ICP-MS) from Fisons (VG Elemental), Ion Path Road Three, Winsford, Cheshire, U.K.

ICP-MS

Autosampler:	Gilson, Model 222	
Dilutor:	Gilson, Model 401	
Flow injector:	Fisons, Model VGS 100	
Plasma Power:	Forward	1348 watts
	Reflected	<3 watts
Gas flow:	Coolant	14.0 L/min
	Auxiliary	0.6 L/min
	Nebulizer	1.0 L/min
Sample cone:	Nickel, 1.0 mm diameter	
Skimmer cone:	Nickel, 0.7 mm diameter	
Acquisition time:	60 s/repeat	
Channels per amu:	20	
Swell time:	Pulse count:	320 us/channel/sweep
	Analogue:	160 us/channel/sweep
Detector:	Channeltron, in pulse-count and analogue mode	
Tunning:	on ^{115}In	

Table A2a. Concentration of standards used for external (STDA, STDB) and internal (Spike C) calibration, for first sample and blank set. Abundance column lists element abundances. Values in STDA, STDB, and spike C columns in ppm.

Element	Mass	STDA	STDB	Spike C	Abundance	Element	Mass	STDA	STDB	Spike C	Abundance
Li	7	44.62087	0	111.5751	0.926	Ag	107	26.7067	0	53.79798	0.5135
Be	9	48.25035	45.95192	127.8782	1	Cd	111	24.22458	0	114.5333	0.128
B	11	42.13733	0	100.7678	0.802	Sn	120	41.01868	0	0	0.3297
Na	23	0	3454.931	0	1	Ab	121	47.21427	0	0	0.573
Mg	26	2284.783	0	0	0.11	Cs	133	45.08451	38.47759	105.5292	1
Al	27	0	3920.987	0	1	Ba	137	42.39295	0	0	0.113
Si	28	8779.489	0	0	0.922	La	139	43.23546	0	107.8248	0.999
K	39	0	3485.097	0	0.933	Ce	140	45.39018	36.69942	0	0.885
Ca	44	0	3540.335	0	0.0014	Pr	141	41.6433	0	110.0235	1
Sc	45	0	40.3484	113.9923	1	Nd	146	0	39.11862	99.89299	0.176
V	51	44.77777	0	110.313	0.998	Sm	147	0	39.53488	106.7467	0.15
Cr	52	84.26435	0	0	0.838	Eu	151	0	36.60577	0	0.478
Mn	55	237.2061	0	0	1	Gd	157	0	35.91739	0	0.157
Fe	57	614.1258	0	0	0.022	Tb	159	19.65716	0	0	1
Co	59	64.23831	0	105.5385	1	Dy	163	44.42247	0	0	0.25
Ni	60	41.44163	0	99.79338	0.261	Ho	165	44.7576	0	0	1
Cu	65	40.48922	0	106.4533	0.308	Er	167	41.85676	0	112.8312	0.229
Zn	68	0	36.7523	101.3464	0.188	Tm	169	20.59214	0	108.1678	1
Ga	69	0	39.31723	111.2324	0.602	Yb	173	42.4157	0	0	0.218
As	75	43.93296	0	0	1	Lu	175	0	34.55987	0	0.974
Br	81	0	2443.752	0	0.493	Hf	177	0	42.52916	0	0.185
Se	82	46.51195	0	0	0.497	Ta	181	0	32.81693	0	1
Rb	85	48.71786	43.25705	120.3361	0.722	Tl	205	21.77163	0	113.5107	0.705
Sr	86	89.36308	0	0	0.099	Pb	206	43.05773	0	0	0.985
Y	89	39.95153	0	0	1	Bi	209	42.52123	0	104.7347	1
Zr	90	66.95829	0	116.6763	0.515	Th	232	41.90285	35.31613	109.6999	1
Nb	93	0	0	0	1	U	238	33.31412	0	94.56112	0.993

Table A2b. Concentration of standards used for external (STDA, STDB) and internal (Spike C) calibration, for second sample and blank set. Abundance column lists element abundances. Values in STDA, STDB, and spike C columns in ppm.

Element	Mass	STDA	STDB	Spike C	Abundance	Element	Mass	STDA	STDB	Spike C	Abundance
Li	7	55.91814	0	111.5751	0.926	Ag	107	33.4684	0	53.79798	0.5135
Be	9	60.46654	45.95192	127.8782	1	Cd	111	30.35784	0	114.5333	0.128
B	11	52.8058	0	100.7678	0.802	Sn	120	51.40392	0	0	0.3297
Na	23	0	3454.931	0	1	Ab	121	59.16814	0	0	0.573
Mg	26	2863.253	0	0	0.11	Cs	133	56.49916	38.47759	105.5292	1
Al	27	0	3920.987	0	1	Ba	137	53.12614	0	0	0.113
Si	28	11002.31	0	0	0.922	La	139	54.18196	0	107.8248	0.999
K	39	0	3485.097	0	0.933	Ce	140	56.88223	36.69942	0	0.885
Ca	44	0	3540.335	0	0.0014	Pr	141	52.1867	0	110.0235	1
Sc	45	0	40.3484	113.9923	1	Nd	146	0	39.11862	99.89299	0.176
V	51	56.11476	0	110.313	0.998	Sm	147	0	39.53488	106.7467	0.15
Cr	52	105.5987	0	0	0.838	Eu	151	0	36.60577	0	0.478
Mn	55	297.2627	0	0	1	Gd	157	0	35.91739	0	0.157
Fe	57	769.6123	0	0	0.022	Tb	159	24.63403	0	0	1
Co	59	80.50239	0	105.5385	1	Dy	163	55.6695	0	0	0.25
Ni	60	51.93396	0	99.79338	0.261	Ho	165	56.08949	0	0	1
Cu	65	50.74042	0	106.4533	0.308	Er	167	52.45419	0	112.8312	0.229
Zn	68	0	36.7523	101.3464	0.188	Tm	169	25.80573	0	108.1678	1
Ga	69	0	39.31723	111.2324	0.602	Yb	173	53.15466	0	0	0.218
As	75	55.05605	0	0	1	Lu	175	0	34.55987	0	0.974
Br	81	0	2443.752	0	0.493	Hf	177	0	42.52916	0	0.185
Se	82	58.28801	0	0	0.497	Ta	181	0	32.81693	0	1
Rb	85	61.05242	43.25705	120.3361	0.722	Tl	205	27.28385	0	113.5107	0.705
Sr	86	111.9883	0	0	0.099	Pb	206	53.95923	0	0	0.985
Y	89	50.06659	0	0	1	Bi	209	53.2869	0	104.7347	1
Zr	90	83.91102	0	116.6763	1.515	Th	232	52.51195	35.31613	109.6999	1
Nb	93	0	0	0	1	U	238	41.7487	0	94.56112	0.993

Table A3. Major and trace element concentrations in ppm for all elements analysed.

#	Sample	Depth (m)	Type	Li	Be	B	Na	wt%Mg	Al
1	3-21-57-24W4	1229.6	R2	1.58		19.05	584.40	15.42	113.76
2	3-21-57-24W4	1229.6	R1	1.32		8.39	364.89	13.13	256.88
3	7-15-55-25W4	1358.8	R3	0.68		7.93	233.82	11.40	12.58
4	7-15-55-25W4	1358.8	R2	0.85		4.98	396.71	12.69	17.71
5	6-22-55-26W4	1562.25	R2	1.73		15.73	462.53	14.50	124.26
6	6-22-55-26W4	1654.2	R2	0.41		2.79	258.89	8.12	1.64
7	2-14-53-26W4	1545.1	R2	0.96		8.11	658.13	11.25	75.91
8	15-23-52-26W4	1547.4	biochem	0.17		1.76	146.47	4.47	21.96
9	15-23-52-26W4	1547.4	R2	1.07		13.03	232.15	11.80	9.76
10	8-17-50-26W4	1704.4	R2	1.06		8.84	264.80	10.33	85.91
11	8-17-50-26W4	1704.4	R2	1.17		13.41	621.46	12.48	82.41
12	8-17-50-26W4	1704.4	R2	2.14	0.13	33.49	496.36	9.02	174.40
13	8-17-50-26W4	1936.7	R1	1.07	0.14	3.13	329.75	14.43	175.55
14	3-22-48-27W4	1994.37	R2	1.78		12.22	391.41	14.17	74.34
15	3-22-48-27W4	2020.5	R2	2.13	0.01	13.76	355.95	14.63	191.62
16	3-22-48-27W4	2020.5	biochem	0.71		6.12	202.94	7.73	22.62
17	3-20-47-27W4	1998.9	R4	0.62		3.78	173.86	17.51	
18	8-4-46-28W4	2207	R2	1.46		10.28	461.76	16.33	379.77
19	8-4-46-28W4	2207	biochem	0.53		4.67	326.89	12.46	28.44
20	8-4-46-28W4	2207	R1	1.48	0.05	8.43	343.00	13.67	506.06
21	8-4-46-28W4	2234	R1	1.62	0.04	13.46	367.06	15.79	188.46
22	16-33-45-28W4	2121	R2	0.60		3.29	265.48	14.71	
23	11-7-43-1W5	2390	R2	0.51		4.44	231.39	8.27	68.52
24	7-22-42-2W5	2402.5	R2	0.63		5.30	124.33	14.39	
25	7-22-42-2W5	2402.5	R2cr	0.67		5.26	267.94	12.90	47.38
26	14-5-41-2W5	2514	R2	0.76	0.05	4.97	516.02	12.74	50.92
27	14-5-41-2W5	2525	R2	0.70	0.09	2.72	252.42	14.27	37.84
28	14-5-41-2W5	2525	R2	0.49	0.00	2.68	193.20	8.26	111.41
29	10-7-40-2W5	2615.1	R1	15.37	0.43	18.70	549.67	8.13	7166.85
30	10-7-40-2W5	2623	R1	3.79	0.15	13.49	224.50	4.83	1558.59
31	14-28-39-3W5	2823	R2	1.77	0.03	19.99	148.06	10.74	1239.22
32	14-28-39-3W5	2823	R2	1.09		15.40	130.56	9.85	
33	14-28-39-3W5	2823	R2	1.34	0.01	23.26	234.10	9.88	66.03
34	14-28-39-3W5	2823	R2	4.36	0.35	58.23	421.74	12.42	109.40
35	16-11-38-5W5	3071	R1	0.85		8.62	245.74	12.52	32.28
36	10-17-37-3W5	2863	R2	0.05		0.38	24.90	7.23	1.95
37	16-32-37-3W5	2982	R2	0.75		6.21	247.44	9.66	22.90
38	11-10-35-5W5	3360.1	R1	2.33	0.11	10.19	493.76	11.38	1280.54
39	11-10-35-5W5	3360.1	biochem	2.24	0.14	8.36	417.07	11.44	1194.24
40	11-10-35-5W5	3365.9	R1	2.58	0.11	11.16	502.56	14.10	1509.45
41	13-9-33-4W5	3467	R2	0.65		5.50	311.40	15.11	
42	10-31-37-9W5	4318.3	R2	0.29		1.63	199.65	13.67	9.06
43	7-32-37-9W5	4085.2	R2	0.72		8.18	434.69	13.63	
44	7-32-37-9W5	4085.2	R1	0.48	0.12	2.26	280.99	13.07	31.36
45	15-23-36-10W5	4592.5	biochem	0.54		15.30	114.32	5.52	
46	10-33-36-10W5	4563.9	R3	0.61		5.96	205.03	12.69	53.95
47	10-33-36-10W5	4563.9	R2	0.76		8.28	214.86	12.03	60.31
48	10-33-36-10W5	4577.4	R3	0.20		4.02	81.12	5.18	12.25
49	10-33-36-10W5	4661	R2	0.77	0.06	9.39	160.77	11.24	28.27
50	11-27-36-10W5	4489.9	R2	0.73		5.91	195.73	14.96	176.92
51	7-26-36-10W5	4397.9	R3	0.63		5.27	295.95	14.79	
52	6-24-34-8W5	4379.9	biochem	1.10	0.11	21.41	184.19	13.91	7.20
53	6-14-34-8W5	4285.2	R2	0.63	0.02	7.52	164.85	10.03	7.32
54	6-14-34-8W5	4286.9	R2	0.63		4.90	327.26	11.49	
55	5-13-37-7W5	5047	R2	0.93	0.05	2.86	539.64	14.58	200.93
56	5-13-37-7W5	5047	R3	0.61	0.03	3.76	596.88	14.44	42.27
57	5-13-37-7W5	5067	R2	0.39	0.00	1.86	315.42	14.51	66.68
	LOD ppm (ave)			0.0028	0.0037	0.0280	1.3170		1.0880

Table A3 cont. Major and trace element concentrations in ppm for all elements analysed.

#	Si	K	wt%Ca	Sc	V	Cr	Mn	Fe	Co	Ni
1	14.73	150.90	22.06		7.32	1.16	93.10	537.17		
2	96.70	245.79	20.05	0.19	6.84	1.49	77.23	926.49		
3	27.59	59.54	17.41	0.07	11.80	0.42	67.88	606.76		
4	18.00	54.72	19.61		12.59	0.43	73.58	590.21		
5	75.45	144.41	21.14	0.42	7.53	1.11	90.18	1311.63		
6	7.54	57.88	15.23		8.12	0.23	56.31	545.01		
7	98.60	267.84	15.00	0.77	12.72	1.01	67.93	680.48		
8	117.96	86.04	9.31	0.61	12.50	0.75	56.50	427.47		
9	16.18	26.36	18.23		14.93	1.10	158.84	1613.72		
10	106.01	153.10	16.30	0.55	12.08	1.21	61.76	948.61		
11	90.66	212.99	16.93	0.66	11.81	1.60	73.30	647.26		
12	55.04	218.95	14.97	0.08	10.37	1.76	95.21	2019.80		
13	125.79	220.94	28.21		30.77	0.47	217.15	8191.53		
14	78.29	184.48	21.55	0.40	16.50	1.11	88.52	1242.92		
15	127.59	213.60	21.66	0.61	18.91	1.62	89.39	1360.37		
16	46.97	106.97	15.67	0.30	13.67	0.54	44.33	368.91		
17			24.66		31.65		94.78	603.46		
18	151.46	423.03	23.14	0.39	22.52	2.62	91.29	3028.21		
19	79.31	142.37	18.09	0.48	13.51	1.02	59.96	714.05		
20	134.84	567.30	19.95	0.67	17.59	2.60	73.17	1816.30		
21	175.00	257.30	22.92	0.58	23.05	1.62	87.33	2159.61		
22	13.57	26.14	20.67		25.67		69.15	468.45		
23	51.53	126.08	13.08	0.53	31.20	1.03	57.24	1287.50		
24	32.54		20.33		29.46	0.92	82.16	1698.44		
25	79.90	103.79	18.36	0.53	15.32	4.75	88.00	1438.41		
26	50.12	159.27	17.76	0.61	31.03	1.22	88.17	1637.98		
27	55.04	99.81	20.00	0.45	33.34	1.78	80.85	1384.03		
28	60.80	118.11	10.78	0.79	26.81	59.22	55.77	1067.19		
29	227.00	3599.42	11.48	2.50	15.96	13.76	315.53	14189.14	7.38	
30	326.42	1322.28	7.88	1.45	34.83	4.29	174.48	5567.19	0.08	
31	211.44	889.34	15.46	1.07	41.80	7.41	69.15	2409.45		
32	183.92	39.19	14.56		28.56	0.47	53.55	1459.10		
33	73.82	133.13	14.78	0.83	28.47	1.60	57.45	1018.08		
34	655.77	348.88	17.82	0.74	91.70	3.12	232.67	7699.39	0.95	
35	254.31	72.51	17.65		35.32	0.89	58.73	828.53		
36	5.52	14.49	13.46	0.07	3.43	103.00	4.17	88.08		
37	7.42		15.90		5.69	0.33	66.76	50.78		
38	236.99	1433.34	17.38	1.46	15.09	3.67	77.08	3727.98	1.15	
39	156.68	1238.02	17.61	1.44	13.93	3.74	79.75	4203.08	1.81	
40	206.78	1182.44	20.68	1.21	29.24	2.79	72.53	1979.69		
41	71.95	52.24	21.34		30.30	0.16	93.20	917.67		
42	40.35	71.23	19.38	0.57	29.51	1.02	162.15	1721.03		
43	57.03	122.98	20.16	0.51	11.22	0.57	80.74	770.55		
44	95.50	132.56	19.23	1.00	29.14	16.57	152.05	1696.56		
45	29.76	28.60	10.48	0.11	29.68	0.25	66.76	470.85		
46	42.50	38.44	18.76		6.46	0.82	155.58	919.55		
47	56.23	123.56	18.21	0.31	44.55	1.29	102.26	1433.04		
48	75.14	96.86	8.92	0.77	28.32	0.79	44.43	663.37		
49	32.10	43.05	17.49	0.02	7.43	1.17	97.46	510.57		
50	164.01	185.23	21.02		31.13	0.71	95.45	1139.97		
51	81.29	38.07	20.89		27.34	0.47	125.53	1350.30		
52	18.31	31.43	20.55	0.02	5.91	0.72	66.42			
53	49.87	88.15	19.87	0.69	33.70	3.48	72.14	1019.15		
54	34.43	87.91	17.23	0.30	34.54	0.73	71.12	1046.80		
55	103.10	202.08	21.54	0.92	26.32	1.85	347.17	2832.96		
56	52.17	144.14	21.35	0.76	28.43	2.50	287.94	2099.99		
57	102.90	126.25	21.13	0.87	25.33	1.53	284.82	2474.80		
	0.9375	2.7020		0.0230	0.0134	0.0215	0.0105	1.2830	0.0029	0.0165

Table A3 cont. Major and trace element concentrations in ppm for all elements analysed.

#	Cu	Zn	Ga	As	Se	Rb	Sr	Y	Zr	Nb	Ag
1	0.05	4.17	0.16	1.18	0.02	0.35	65.01	1.05	0.09	0.01	0.44
2	2.05	106.79	0.44	1.33	0.01	0.87	54.98	0.82	0.30	0.02	0.49
3	1.32	3.41	0.30	1.09	0.01	0.03	40.43	1.81	0.13	0.02	0.33
4	4.40	6.18	0.16	1.30	0.02	0.07	50.07	2.40	0.07	0.00	0.53
5	6.30	4.67	0.20	1.70	0.02	0.59	81.19	2.33	0.35	0.01	0.55
6	0.87	283.36	0.41	0.75	0.01	0.03	39.89	0.75		0.01	0.30
7	2.83	5.41	0.64	1.50		0.28	37.02	0.68	0.23	0.01	0.33
8	0.53	3.98	0.10	1.16		0.02	10.00	0.41	0.24	0.01	0.39
9	2.50	3.38	0.02	0.83	0.01	0.06	33.85	1.32	0.15	0.01	0.35
10	1.11	3.29	0.15	1.80		0.31	45.44	0.97	0.18	0.01	0.38
11	4.17	4.13	0.14	1.68		0.30	42.95	1.28	0.25	0.02	0.44
12	1.07	3.75	0.12	0.90	0.02	0.46	53.46	1.15	0.27	0.00	0.40
13	0.86	6.16	0.52	5.01		0.61	47.63	1.51	0.22	0.01	0.36
14	3.07	4.33	0.11	1.95		0.25	52.12	2.26	0.21	0.01	0.42
15	3.03	5.11	0.30	2.21		0.55	81.16	2.64	0.35	0.01	2.61
16	1.12	4.40	0.09	1.40		0.06	47.16	1.00	0.20	0.01	0.24
17	0.19	3.32	0.09	5.02			39.99	1.36		0.00	0.30
18	4.43	4.93	0.16	5.04		1.26	51.10	3.09	0.50	0.05	0.58
19	2.98	4.88	0.13	1.84		0.14	33.49	1.27	0.20	0.02	0.45
20	2.56	4.18	0.38	2.11		1.71	32.85	1.65	0.34	0.02	0.43
21	2.06	3.61	0.18	4.04		0.47	66.45	2.57	0.45	0.04	0.54
22	2.46	5.11	0.15	3.99			35.25	0.54		0.01	0.26
23	3.95	4.44	0.32	4.20		0.18	22.27	0.53	0.25	0.02	0.28
24		3.22	0.46	4.67		0.01	40.43	1.60		0.01	0.41
25	3.03	9.84	7.24	2.68	0.02	0.16	56.63	2.16	0.34	0.02	0.79
26	1.73	6.66	3.12	6.48		0.26	45.11	1.50	0.55	0.03	0.55
27	2.42	12.86	11.01	7.47		0.40	53.80	1.11	0.63	0.04	0.75
28	5.87	12.42	5.99	3.87		0.25	43.75	0.81	0.91	0.08	0.34
29	4.89	17.28	3.53	1.93	0.01	13.22	45.65	5.56	1.14	0.04	0.45
30	5.18	8.28	2.02	4.71		6.22	34.41	2.07	0.51	0.03	0.32
31	5.76	7.52	0.92	6.49		2.87	47.12	4.54	0.51	0.02	0.61
32	3.21	3.65	0.21	4.09		0.13	38.19	2.71		0.01	0.36
33	8.58	3.92	0.28	4.86		0.24	50.80	3.11	0.49	0.04	0.45
34	8.15	3.80	0.47	6.33		0.64	58.92	3.30	0.55	0.03	0.45
35	2.08	4.40	0.27	5.87		0.24	29.42	0.96	0.25	0.02	0.38
36	0.40	0.76	0.03	0.59		0.01	9.83	0.05	0.04	0.00	0.04
37	0.73	2.80	0.29	0.67	0.02	0.06	50.05	0.62	0.16	0.01	0.33
38	5.76	4.96	1.01	3.37		5.34	55.39	2.56	0.49	0.01	0.46
39	6.28	5.43	1.13	3.90		5.25	58.39	2.74	0.37	0.01	0.50
40	2.01	5.54	0.92	6.02		4.16	58.97	1.52	0.73	0.05	0.47
41	1.10	3.45	0.25	6.13		0.15	41.85	1.44		0.01	0.37
42	2.24	16.10	38.40	7.11		0.11	31.51	2.09	0.39	0.04	0.69
43	1.85	4.27	0.11	1.48		0.04	33.60	0.85	0.12	0.01	0.43
44	2.54	6.54	0.39	5.38		0.22	24.41	1.61	0.55	0.05	0.62
45		4.39	0.80	4.66			43.25	0.92	0.06	0.01	0.19
46	1.66	4.00	0.52	0.99	0.02	0.21	32.70	0.87	0.36	0.01	0.43
47	3.63	7.26	12.37	12.66		0.47	54.36	1.04	0.48	0.05	0.66
48	1.03	3.90	0.18	3.19		0.08	15.30	0.91	0.25	0.02	0.17
49	0.64	4.47	21.54	1.29	0.02	0.17	49.92	1.10	0.27	0.02	0.45
50		3.91	1.47	5.06		0.95	28.88	0.76	0.03	0.01	0.32
51	2.59	4.61	1.89	4.76		0.07	30.93	0.93	0.10	0.02	0.43
52	1.89	2.89	0.93	0.87	0.01	0.18	63.06	0.60	0.25	0.01	0.52
53	1.46	11.06	2.12	11.51		0.09	236.03	1.42	0.69	0.04	0.94
54	0.63	3.74	0.35	5.52		0.07	28.48	0.64	0.24	0.02	0.38
55	2.31	6.90	12.87	5.13		0.33	63.54	1.42	0.54	0.04	0.67
56	2.46	3.27	40.37	5.42		0.25	82.02	1.63	0.52	0.07	0.70
57	2.25	6.60	2.69	4.92		0.16	33.24	1.37	0.60	0.04	0.61
	0.0395	0.0130	0.0030	0.0027	0.0205	0.0034	0.0055	0.0008	0.0075	0.0003	0.0011

Table A3 cont. Major and trace element concentrations in ppm for all elements analysed.

#	Cd	Sn	Sb	Cs	Ba	La	Ce	Pr	Nd	Sm
1					1.84	0.82	1.02	0.10	0.53	0.05
2	2.37			0.03	5.47	0.65	0.91	0.09	0.49	0.05
3					4.90	0.76	0.89	0.12	0.64	0.13
4					2.05	0.98	1.10	0.16	0.73	0.14
5		0.05		0.05	2.88	2.11	1.84	0.30	1.06	0.29
6	0.68				4.07	0.33	0.36	0.03	0.25	0.03
7		0.34		0.00	7.97	0.52	0.50	0.07	0.28	0.06
8	0.07	0.19	0.01		0.92	0.24	0.24	0.02	0.14	0.00
9			0.00		0.77	0.64	0.72	0.09	0.41	0.09
10					0.88	0.54	0.75	0.09	0.40	0.10
11		0.27		0.03	1.18	0.90	0.99	0.14	0.53	0.14
12				0.09	1.49	1.03	0.96	0.20	0.51	0.12
13				0.05	2.29	1.50	2.19	0.32	1.08	0.20
14					1.22	1.46	1.46	0.21	1.04	0.20
15	1.63	0.04		0.02	2.43	1.29	1.12	0.20	0.95	0.18
16					0.87	0.55	0.39	0.06	0.38	0.05
17					0.67	0.72	0.67	0.05	0.43	0.04
18	0.03	8.88	0.11	0.07	2.84	1.65	2.17	0.32	1.36	0.29
19		0.16			1.09	0.66	0.79	0.11	0.48	0.09
20		0.04	0.00	0.12	2.98	0.88	1.16	0.20	0.73	0.18
21	0.05	6.11	0.05	0.02	1.76	2.24	2.46	0.32	1.20	0.21
22					0.78	0.29	0.25		0.13	
23					1.04	0.23	0.35	0.04	0.23	0.04
24					3.29	0.71	0.74	0.07	0.51	0.05
25		0.33	0.02		107.06	0.55	0.67	0.10	0.43	0.09
26				0.05	38.36	1.20	1.01	0.17	0.58	0.14
27				0.10	111.70	0.58	0.69	0.16	0.41	0.15
28	0.02	1.50	0.03	0.04	106.51	0.56	0.78	0.10	0.40	0.08
29		0.14		0.68	24.88	7.41	18.27	2.24	9.40	2.22
30				0.27	12.39	2.17	4.63	0.55	2.35	0.44
31				0.09	4.12	2.26	3.15	0.49	2.33	0.44
32					0.96	1.61	1.88	0.25	1.23	0.22
33			0.02	0.01	1.63	2.29	2.36	0.33	1.43	0.32
34				0.05	1.70	2.11	2.12	0.36	1.43	0.28
35					1.05	0.57	0.59	0.08	0.41	0.03
36					0.09	0.03	0.03	0.00	0.02	0.00
37					4.21	0.44	0.61	0.05	0.29	0.04
38		0.05	0.07	0.23	9.35	1.11	2.94	0.40	1.99	0.65
39				0.29	12.05	1.21	3.08	0.43	1.99	0.76
40				0.19	5.86	0.83	2.00	0.28	1.26	0.27
41					1.08	0.96	0.80	0.06	0.41	0.04
42					486.19	0.81	0.68	0.15	0.66	0.13
43		0.12			0.99	0.39	0.45	0.06	0.26	0.04
44	0.16	0.54	0.06	0.16	2.41	0.94	0.70	0.23	0.55	0.22
45					5.38	0.85	0.70	0.08	0.48	0.02
46				0.03	7.83	0.58	0.61	0.10	0.42	0.12
47					126.75	0.40	0.43	0.04	0.24	0.01
48		1.90	0.04		0.54	0.44	0.68	0.09	0.40	0.07
49				0.03	347.64	0.48	0.42	0.10	0.42	0.07
50					9.82	0.48	0.82	0.07	0.44	0.03
51					16.18	0.54	0.88	0.05	0.31	0.06
52				0.11	14.05	0.40	0.44	0.16	0.34	0.15
53					21.44	0.46	0.44	0.07	0.29	0.10
54						0.44	0.36	0.05	0.20	0.04
55	0.13	3.93	0.04	0.06	319.32	0.55	0.42	0.10	0.37	0.11
56	0.12	7.14	0.12	0.09	1939.69	0.56	0.46	0.08	0.39	0.10
57	0.09	4.01	0.05		58.65	0.50	0.37	0.08	0.29	0.08
	0.0110	0.2490	0.0031	0.0031	0.0024	0.0024	0.0017	0.0023	0.0022	0.0024

Table A3 cont. Major and trace element concentrations in ppm for all elements analysed.

#	Eu	Gd	Tb	Dy	Ho	Er	Tm	Yb	Lu	Hf	Ta
1	0.01	0.11	0.01	0.09	0.01	0.03		0.01			0.05
2	0.01	0.11	0.01	0.08	0.01	0.03		0.02			
3	0.03	0.21	0.02	0.16	0.03	0.08		0.08	0.00		
4	0.03	0.25	0.03	0.25	0.04	0.16		0.12			
5	0.05	0.22	0.03	0.23	0.04	0.13	0.02	0.09	0.00		0.01
6	0.01	0.08	0.01	0.06	0.00	0.02					
7	0.00	0.07	0.01	0.06	0.01	0.04	0.01	0.02			
8	0.00	0.02	0.00	0.03	0.00	0.01		0.01			0.56
9	0.02	0.08	0.01	0.09	0.02	0.08	0.01	0.06			0.19
10	0.01	0.10	0.01	0.08	0.00	0.04		0.03			
11	0.02	0.13	0.02	0.15	0.02	0.07	0.01	0.04			
12	0.01	0.13	0.01	0.06	0.01	0.15	0.08	0.03			
13	0.03	0.13	0.03	0.20	0.03	0.15	0.06	0.06			
14	0.04	0.26	0.03	0.27	0.04	0.13	0.02	0.08	0.01		
15	0.04	0.29	0.04	0.30	0.05	0.16	0.02	0.08	0.01		
16	0.01	0.13	0.01	0.12	0.02	0.04		0.03			
17		0.05	0.00	0.08		0.01					
18	0.06	0.35	0.05	0.33	0.06	0.14	0.02	0.12	0.01		
19	0.01	0.12	0.01	0.11	0.03	0.06		0.05			
20	0.04	0.28	0.03	0.19	0.03	0.09	0.02	0.08	0.00		0.00
21	0.04	0.28	0.04	0.25	0.04	0.13	0.02	0.09	0.01		0.00
22											0.05
23	0.00	0.05	0.00	0.05		0.02		0.03			
24	0.02	0.13	0.01	0.10		0.02		0.05			0.06
25	0.03	0.11	0.01	0.11	0.02	0.06		0.03			0.05
26	0.03	0.16	0.02	0.12	0.02	0.09	0.04	0.05			0.01
27	0.03	0.10	0.02	0.08	0.01	0.11	0.06	0.05	0.00		0.05
28	0.02	0.11	0.01	0.08	0.01	0.05	0.01	0.04	0.00		0.03
29	0.48	2.11	0.29	1.59	0.24	0.72	0.06	0.41	0.04		0.07
30	0.10	0.48	0.06	0.40	0.06	0.15	0.01	0.15	0.02	0.01	0.08
31	0.09	0.57	0.07	0.43	0.06	0.16		0.13			0.00
32	0.04	0.34	0.03	0.28	0.02	0.11		0.06			0.03
33	0.07	0.37	0.04	0.30	0.06	0.18	0.01	0.13	0.01	0.01	0.07
34	0.05	0.37	0.04	0.27	0.04	0.24	0.12	0.09	0.00		
35		0.07	0.01	0.09		0.02		0.02			
36		0.00	0.00	0.00		0.00		0.00			0.01
37	0.00	0.05	0.00	0.08	0.00	0.00		0.00			0.08
38	0.14	0.68	0.10	0.59	0.09	0.26	0.02	0.18	0.01		0.07
39	0.16	0.83	0.11	0.56	0.10	0.24	0.03	0.19	0.02		
40	0.05	0.26	0.03	0.18	0.03	0.11	0.02	0.06	0.01		0.00
41		0.08	0.00	0.08				0.03			
42	0.11	0.19	0.02	0.14	0.03	0.08	0.01	0.08			
43	0.01	0.07	0.00	0.05	0.00	0.04	0.00	0.01			
44	0.02	0.14	0.02	0.13	0.03	0.17	0.10	0.10	0.01		0.00
45	0.01	0.09	0.00	0.06				0.01			0.05
46	0.01	0.09	0.02	0.07	0.01	0.06	0.04	0.02			0.03
47	0.01	0.05	0.00	0.04		0.01		0.00			
48	0.02	0.11	0.01	0.09	0.02	0.05		0.05			0.06
49	0.03	0.10	0.01	0.08	0.02	0.11	0.04	0.03			
50		0.02	0.00	0.07							
51		0.06	0.01	0.06				0.02			0.03
52	0.01	0.07	0.01	0.09	0.02	0.14	0.08	0.01	0.00		0.06
53	0.01	0.08	0.01	0.07	0.01	0.07	0.03	0.02			0.01
54		0.04	0.00	0.04		0.00		0.00			
55	0.04	0.10	0.01	0.09	0.02	0.10	0.05	0.04	0.00		
56	0.18	0.13	0.01	0.09	0.02	0.05	0.01	0.05	0.02	0.05	0.10
57	0.02	0.08	0.01	0.08	0.02	0.06	0.01	0.03	0.00		0.01
	0.0009	0.0013	0.0004	0.0011	0.0009	0.0023	0.0017	0.0008	0.0081	0.0038	0.0015

Table A3 cont. Major and trace element concentrations in ppm for all elements analysed.

#	Tl	Pb	Bi	Th	U
1		0.60	0.03		0.23
2		1.79	0.06	0.07	0.29
3		0.95			0.39
4		0.83			0.58
5	0.05	4.04	0.04	0.19	0.40
6		0.56			0.19
7	0.00	183.34	0.05	0.04	0.04
8		1.34	0.08	0.01	0.01
9		0.86		0.05	0.85
10		0.65			0.09
11	0.01	2.37	0.02	0.04	0.12
12	0.13	6.09	0.12	0.16	0.24
13	0.07	8.69	0.09	0.15	0.26
14	0.01	2.97	0.04	0.03	0.69
15	0.02	2.68	0.02	0.06	0.50
16		1.75	0.01		0.20
17		1.40			0.11
18					
19		2.01	0.01		0.49
20	0.03	2.87	0.03	0.16	0.80
21	0.03	5.03	0.02	0.09	0.33
22					0.15
23	0.02	2.16			0.10
24		0.37			0.23
25		2.24	0.00	0.02	0.18
26	0.06	2.20	0.04	0.10	0.36
27	0.07	1.21	0.05	0.13	0.15
28	0.02	1.95		0.12	0.10
29	0.05	2.42	0.10	1.74	0.16
30	0.02	0.95		0.36	0.08
31	0.02	3.13		0.36	0.41
32		0.58			0.18
33	0.02	2.10		0.23	0.29
34	0.17	1.73	0.11	0.24	0.30
35	0.03	1.56			0.32
36		0.20			0.01
37		0.47			0.12
38	0.08	7.38	0.08	0.78	0.93
39	0.16	11.10	0.06	0.84	1.03
40	0.05	2.13	0.02	0.27	0.36
41					0.01
42	0.02	2.99			0.19
43	0.01	1.21			0.59
44	0.12	1.20	0.11	0.13	0.18
45		0.21			
46	0.08	4.84	0.03	0.06	0.14
47		3.00			0.07
48		1.54			0.01
49	0.03	0.84	0.04	0.03	0.88
50					0.08
51		1.06			0.04
52	0.15	0.51	0.10	0.12	0.12
53	0.04	1.30	0.03		0.23
54		0.32			0.18
55	0.06	2.04	0.07	0.08	0.15
56	0.02	4.55	0.07	0.06	0.08
57	0.02	1.46	0.03		0.06
	0.0020	0.0100	0.0110	0.0200	0.0140

APPENDIX B

ICP-MS Dissolution conditions: Microwave conditions:

MDS-2100; CEM Corporation, Matthews, North Carolina 28106-0200

Samples dissolved in 800 μ l of HNO₃:HCl; 3:1

Conditions based on organic sample with five stages in manual

Erinntest2

Stage:	1	2	3	4	5
Power(%):	25	60	20	50	0
Pressure(psi):	20	20	20	20	0
Time(00:00):	13:00	8:00	6:00	5:00	5:00
TAP:	2:15	1:25	1:15	1:15	0

(time at psi)

No temperature (25°C)

TAP is the time at pressure (psi) specified during the microwave run (time).

Theses conditions determined by experimentation and used for both blanks and samples.

APPENDIX C

Analytical conditions of ILS (liquid chromatograph for major elements):

Cations analyzed: Magnesium, and Calcium. Analysis was performed using a Dionex 500 liquid chromatograph system with an ED40 Electrochemical Detector and Self-regenerating suppressor. Cations were separated on a Dionex IONPAC CS-12 4 mm. column with a 16 mM MSA (methanesulfonic acid) eluent at a flow rate of 1.0 ml. per min. and sample volume of 25 microliters. System was calibrated using six anions: Lithium, Sodium, Ammonium, Potassium, Magnesium, and Calcium. The concentration of the anion standards were in the range of 1 ppm to 75 ppm. Analysis for cations were run in duplicate with the average reported. The analysis was completed by B.L. Gorham.

The raw data of Mg and Ca was in ppm in solution. Values were calculated to wt.% by the equations:

x gm. sample in y gm solution.

y contains z ppm cations = $zy \cdot 10^6$ gm.

concentration of cation = $(z \cdot y) \cdot 10^6 / x \cdot 100 = \text{wt\% cation}$

Weights of sample residues from sample analysis can be used for correction of Ca and Mg values to modelled line in Figure 11 in text. The sample residues, however, were not retained and weighed due to the short time allowed and lack of laboratory space.

APPENDIX D

Procedures for $^{87}\text{Sr}/^{86}\text{Sr}$ analysis:

Unspiked Sr separation from cation columns (USP 1-6):

Resin: Bio-Rad AG50W0X8 cation resin, 200-400 mesh, H^+ form. Columns: Bio-Rad Econo-Columns (borosilicate glass and polypropylene); 15 x 0.7 cm containing 4.4 ml of wet cation resin.

Chromatography

Loading solution: Carbonates = 3 ml 0.75 N HCl

1. Centrifuge dissolved sample in loading solution (above) at full power for 5 minutes.
2. Load supernate to column using a clean disposable pipette. Put the pipette tip close to resin without touching column walls and add dropwise so as not to disturb resin.
3. Rinse glass walls with 3x1 ml new loading solution using new, clean pipette.
4. Rinse glass walls and reservoir with 3x1 ml 2.5 N HCl using new, clean pipette.
5. Wash with 24 ml of 2.5 N HCl (use plastic reservoir). Waste
6. Collect 5 ml of 2.5 N HCl. Sr

Column Washing (after sample elution)

7. 25 ml 6 N HCl (use plastic reservoir).
8. 25 ml Millipore water (use plastic reservoir).
9. 25 ml 1.5 N HCl (use plastic reservoir).

SUMMARY

<u>STEP</u>	<u>Solvent</u>	<u>Quantity</u>	<u>Purpose</u>	<u>Comments</u>
1.	0.75N HCl	3 ml	Load sample	Dropwise load
2.	0.75N HCl	3 ml	Rinse column walls	3x1 careful rinses
3.	2.5N HCl	3 ml	Remove 0.75N HCl	3x1 careful rinses
4.	2.5N HCl	24 ml	Waste	Rinse off Ca, Rb, etc.
5.	2.5N HCl	5 ml	Collect Sr	

Sr cleanup columns (CON 1-6):

Resin: Bio-Rad AG50W-X8 cation resin, 200-400 mesh, H⁺ form.

Columns: Bio-Rad Econo-Columns (borosilicate glass and polypropylene); 10x0.5 cm containing 1.7 ml of wet cation resin.

Chromatography

Loading solution: 0.25 ml oxalic acid:HCl mix (1:1 0.25M oxalic: 1N HCl)

Elution solution: Sr = 2.5 N HCl

1. Load supernate to column using a clean pipette. Put the pipette tip close to resin without touching column walls and add dropwise so as not to disturb resin.
2. Load 3x 0.25 ml new loading solution using clean pipette.
3. Rinse glass walls with 4x0.25 ml new loading solution using clean pipette.
4. Rinse walls and reservoir with 4x0.25 ml elution solution using clean pipette.
5. Wash with 5 ml of elution solution. Waste
6. Collect 4 ml of elution solution Sr

Column washing (after sample elution)

7. 15 ml 6 N HCl (use plastic reservoir).

8. 15 ml Millipore water (use plastic reservoir).

9. 15 ml 1.5 N HCl (use plastic reservoir).

SUMMARY

<u>Step</u>	<u>Solvent</u>	<u>Quantity</u>	<u>Purpose</u>	<u>Comments</u>
1.	oxalic:HCl	0.25 ml	Load sample	Dropwise load
2.	oxalic:HCl	0.75 ml	Make sample load 1 ml	3x0.25 load
3.	oxalic:HCl	1 ml	Rinse column walls	4x0.25 rinses
4.	2.5 N HCl	1 ml	Remove oxalic	4x0.25 rinses
5.	2.5 N HCl	5 ml	Waste	
6.	2.5 N HCl	4 ml	Collect Sr	